THESIS ON POWER ENGINEERING,
ELECTRICAL ENGINEERING, MINING ENGINEERING

# LC Circuit with Parallel and Series Resonance Alternation in Switch-Mode Converters

**JEVGENI SHKLOVSKI**

**TALLINN 2007**

Faculty of Power Engineering
Department of Electrical Machines and Fundamentals of Electrical Engineering
TALLINN UNIVERSITY OF TECHNOLOGY

Dissertation was accepted for the defence of the degree of Doctor of Philosophy in Power Engineering and Geotechnology on February 1, 2007

Supervisor: Professor Jaan Järvik
Department of Electrical Machines and Fundamentals of Electrical Engineering, Faculty of Power Engineering, Tallinn University of Technology

Co-supervisor: Associate Professor Kuno Janson
Head of the Department of Electrical Machines and Fundamentals of Electrical Engineering, Faculty of Power Engineering, Tallinn University of Technology

Opponents:
Professor, Dr. Manfred Sakulin, Graz Technical University, Austria

Senior Design Engineer, Doctor of Technology Juhani Tellinen, Adaptamat LTD, Finland

Professor, Vello Kukk, Tallinn University of Technology, Estonia

Oral defence: March 16, 2007. Tallinn University of Technology, room VII-422

Declaration:
*"Hereby I declare that this doctoral thesis, my original investigation and achievement, submitted for the doctoral degree at Tallinn University of Technology has not been submitted for any degree or examination".*

Jevgeni Shklovski, …….

Copyright Jevgeni Shklovski, 2007
ISSN 1406-474X
ISBN 978-9985-59-687-6

## Acknowledgments

Herewith, I would like to thank all of those people and organizations who have helped and supported me in my work.

First of all, I am very grateful to my parents for their invaluable support and care throughout the whole of my life and study. Their extensive knowledge, continuous encouragement and interest in my educational and personal development have motivated and will motivate me to continue my life-long learning.

I would like to express my sincere gratitude to my advisors, Professor Jaan Järvik and Dr. Kuno Janson, for their scientific guidance, helpful advice and encouraging attitude that made the research described in this dissertation possible.

I gratefully thank Madis Reivik for technical discussions, suggestions and help with practical implementation. I express my gratitude to Magnetics Inc and Wima GmbH for the samples and technical guidance they rendered to me.
My thanks are due to component suppliers Harry Pale from Teamtron OY and Regina Kolts from EBV Elektronik OÜ who provided me with samples and information.
I also thank Michael Schmelzer from MS Balti Trafo for the efforts to design and produce high-frequency inverter transformers needed in my research.

The financial support of my doctoral study and research activities from the TUT Development Foundation (Eesti Energia Scholarship), Estonian National Culture Foundation and the Archimedes Foundation (Kristjan Jaak Scholarship) are greatly appreciated.

I also wish to thank my present and former colleagues and friends for their contribution to my research and enjoyable discussions: Viktor Bolgov Ph.D., Mohamed Sidon M.Sc., Ants Kallaste M.Sc., Andrei Shkvorov lecturer, and many others.

Finally, I would like to thank my beautiful and loving wife Jelena, for her love, patience and support. I hope this accomplishment will be a good sign for our soon expected child.

JEVGENI SHKLOVSKI

*Tallinn, Estonia*
*December 2006*

# Table of Contents

**List of Abbreviations** ..... **6**
**List of Symbols** ..... **7**
**1. Introduction** ..... **8**
1.1 Current trends in power electronics ..... 8
1.2 Resonant switch-mode converters ..... 10
1.2.1 Resonant networks ..... 10
1.2.2 Control techniques for load-resonant converters ..... 14
1.3 Power factor correction in single-phase AC/DC converters ..... 15
1.4 PSA converter basics ..... 16
1.5 Modeling and analysis ..... 17
1.6 Purpose of the study ..... 18
**2. Mains frequency resonant converter with parametric parallel and series resonance alternation** ..... **19**
2.1 Development of a single-phase PSA converter ..... 19
2.2 Role of additional resonant inductor ..... 22
2.3 PSA converter with resonant components on the primary side ..... 23
2.4 Basics of PSA converter parameter calculation ..... 24
2.4.1 Distribution factors ..... 24
2.4.2 Defining of reactive component values ..... 25
2.5 Characteristics and peculiarities of single-phase PSA converter ..... 26
2.6 Commutations in output diode bridge rectifier ..... 27
2.7 Self-adjusting to load ..... 29
2.8 Input current distortion ..... 30
2.9 Conclusions ..... 31
**3. Switch-mode PSA converter** ..... **33**
3.1. Basics of a generalized switch-mode PSA converter ..... 33
3.1.1 Power circuit of SM-PSA and control ..... 33
3.1.2 Inverter circuit topology ..... 34
3.1.3 Switching frequency of the inverter ..... 34
3.1.3.1 Discrete reactive components ..... 35
3.1.3.2 Planar transformer and combined planar *LCT* components ..... 36
3.1.4 Conclusion ..... 37
3.2 Basic calculation procedure for resonant network of a SM-PSA converter ..... 38
3.3 Some features in the design of the inverter transformer ..... 45
3.3.1 Selection of transformer no-load voltage ..... 45
3.3.2 Distribution factor $K_E$ ..... 46
3.3.3 Leakage inductance ..... 46
3.3.4 Inductance of wires or busbars in the resonant network ..... 48
3.4 Comparison of different resonant topologies of a SM-PSA converter ..... 49
3.4.1 $L_1L_3C$ resonant network ..... 49
3.4.1.1 Output and regulation properties ..... 49
3.4.1.2 Operation in the switching cycle ..... 53
3.4.1.3 Conclusion ..... 54

3.4.2 $L_1L_2C$ resonant circuit ..... 55
3.4.2.1 Output and regulation properties ..... 55
3.4.2.2 Operation in the switching cycle ..... 58
3.4.2.3 Conclusion ..... 59
3.4.3 $L_1 L_2 L_3 C$ resonant circuit ..... 60
3.4.3.1 Output and regulation properties ..... 60
3.4.3.2 Operation in the switching cycle ..... 63
3.4.4 Summary of different SM-PSA converter *LC* topologies ..... 65
3.5 Transients during the welding process ..... 67
3.5.1 Inverter circuit ..... 67
3.5.2 Resonant network ..... 67
3.6 Alternative way of output regulation – frequency control ..... 69
3.7 Output filter design ..... 70
3.8 Experimental results ..... 71
3.8.1 Resistive load ..... 72
3.8.2 Welding ..... 74
3.8.3 Battery charging ..... 75
3.9 Conclusions ..... 76
**4. PFC in the SM-PSA converter ..... 78**
4.1 Background - reasons of poor power factor and state of art ..... 78
4.2 Properties of PSA appropriate for PFC ..... 80
4.3 Principles of operation ..... 81
4.4 Simulation of PFC SM-PSA ..... 83
4.4.1 Input current and $THD_i$ vs output voltage ..... 83
4.4.2 Converter operation in a mains cycle ..... 85
4.4.3 Converter operation in a switching cycle ..... 87
4.4.4 Conclusions ..... 89
4.5 Experimental results ..... 91
4.5.1 Resistive load ..... 91
4.5.2 Battery charging ..... 93
4.5.3 Welding ..... 94
4.6 Conclusions ..... 97
**5. Conclusions ..... 99**
5.1 Load-resonant switch-mode SM-PSA converter ..... 99
5.2 Power factor correction in the SM-PSA converter ..... 101
5.3 Plans for future studies ..... 101
**References ..... 102**
**Kokkuvõte ..... 110**
**List of Publications ..... 111**
**Intellectual property ..... 112**
**Appendix 1 ..... 113**
ELULOOKIRJELDUS ..... 113
CURRICULUM VITAE ..... 115
**Appendix 2 ..... 117**
Schematic diagram of the SM-PSA prototype converter ..... 117

## List of Abbreviations

AC – Alternating Current
DC – Direct Current
DPF – Displacement Power Factor
EMC – Electro Magnetic Compatibility
EMI – Electromagnetic Interference
FEM – Finite Element Method
IEC – International Electrotechnical Committee
IEEE – Institute of Electrical and Electronics Engineers
IGBT – Insulated Gate Bipolar Transistor
LC – Resonant circuit composed of an inductor L and a capacitor C
MMA – Metal Manual Arc
MOSFET – Metal-Oxide-Semiconductor Field-Effect Transistor
PF – Power Factor
PFC – Power Factor Correction
PRC – Parallel Resonant Converter
PSA – Parallel and Series Resonance Alternation
RMS – Root Mean Square
SMPS – Switch Mode Power Supply
SM-PSA – Switch Mode converter with Parallel and Series resonance Alternation
SRC – Series Resonant Converter
THD – Total Harmonic Distortion
ZCS – Zero Current Switching
ZVS – Zero Voltage Switching

## List of Symbols

*Inverter and resonant circuit*

$a$ – relative gating pulse width
$f_{sw}$ – switching frequency
$t_d$ – delay time between gating pulses ("dead time")
$W_1$ – primary winding of transformer
$W_2$ – one secondary winding of transformer (inductive branch)
$W_3$ – other secondary winding of transformer (capacitive branch)
$I_{tr1}$ – current in primary winding of transformer
$U_{tri1}$ –voltage on transformer primary winding
$L_1$ – inductor/inductance of main resonant inductor in inductive branch
$L_2$ – inductor/inductance of additional inductor in middle branch
$L_3$ - inductor/inductance of resonant inductor in capacitive branch
$C$ – capacitor/capacitance of resonant capacitor in capacitive circuit
$I_{L1}$ – current through the inductive branch of resonant circuit
$I_{L2}$, $I_{mb}$ – current through the middle branch
$I_C$ or $I_{L3}$ – current through the capacitive branch
$U_C$ – voltage of resonant capacitor
$K_T$ – transformer turns ratio
$K_E$ – transformer secondary windings voltage distribution factor
$K_L$ – inductance distribution factor in resonant network of PSA
$K_Q$ – reactive power distribution factor for the short-circuit mode

*Load circuit*

$C_f$ – output filter capacitor
$L_f$ – output filter inductor
$U_d$ or $U_{load}$ – load voltage
$I_d$ or $I_{load}$ – load current
$P_d$ – power delivered to load
$I_{conv}$ – converter output current before output filter

*Mains and input rectifier*

$u_S$ – input voltage of AC/DC converter
$i_S$ – input current of AC/DC converter
$U_{dc}$ – DC-link voltage after the mains rectifier

# 1. Introduction

## 1.1 Current trends in power electronics

Electrical energy, the final product of different energy kind transformations, is most widely used in modern living environment compared to other energy kinds. Rational consumption of electrical energy is not only the problem of cost reduction, but it also could prevent unreasonable energy waste and help us to solve some issues of electromagnetic ecology.
In recent decades power electronics has extended to almost any area, from low-power consumer electronics and to high-power industrial devices. Here, most of the electronic devices and equipment must be supplied with some DC voltage. However, presently AC voltage generation, transmission and distribution are commonly used in the world. To obtain a required DC voltage from the AC network to switch-mode power semiconductor-based converters. The following common trends in the design of modern switch-mode AC/DC power converters could be distinguished:

1) lower cost and simpler design,
2) better construction density, or in other words, smaller volume and weight,
3) high efficiency (lower losses),
4) reduced distortion of input current.

As it is known, a smaller and more compact power supply unit can be designed by the reduction of power loss in the converter and an increase in the operation frequency. Thus, the size and cost of magnetic components can be reduced. Moreover, minimization of switching losses contributes significantly to increased efficiency and reasonable thermal design of the whole power supply. In addition to higher-frequency operation and lower losses, the issue of input current distortion becomes more significant. A wide use of switch-mode converters has created a new situation where the use of converters with incorporated power factor correction is beneficial.

*Power switching devices*
Development of new, faster generations of switching devices stimulates the increase of switching frequencies in converters leading to a smaller volume of power supplies.
There are two main kinds of energy loss in a switch device: switching losses and conduction losses [H6]. Switching losses occur as the switching device, further mentioned as a switch, turns on and off, and the conduction losses occur, when the switch is in on-state and conducting current. Switching losses are dependent on the switching speed and conditions in the switch during the commutation interval and conduction losses are dependent on the switch resistance, or voltage drop. There are two main types of power switching

devices employed in modern switch-mode converters: metal-oxide semiconductor field effect transistor (MOSFET) and insulated-gate bipolar transistor (IGBT). It is accepted that losses in the power converter depend on the parameters of a switch and on the topology in which it is used. Some of the losses can also create stresses to the power semiconductors which in the long term may affect the reliability of the power supply. Thus, it is important to know where they arise and how to control them [H6].
Each switching device has different switching and on-state characteristics. The merits and selection criteria of these devices can be classified according to:

1) on-state conduction capability,
2) permissible reverse voltage,
3) switching characteristics,
4) cost.

IGBTs have smaller die areas than power MOSFETs of the same ratings, which typically means a lower cost, while power MOSFETs are used in the majority of applications due to their ease of use and their higher frequency capabilities [H6]. The development of MOSFET and IGBT devices is an unceased process, resulting in increased current, voltage and switching capabilities.

*Power quality and EMC*

Operation at an increased frequency leads to certain EMC problems and some topological issues like parasitic inductances and capacitances that often need special solutions. A good practice for EMI reduction is a ZVS implementation in switch-mode converters [H3].
In addition, increasingly more consumer electronics devices should comply to the IEC 61000-3-2 standard (limits for harmonic current emissions, equipment input current ≤16 A per phase). Thus, an input current correction must frequently be provided in modern power supplies.

*Combined solutions*

In view of these facts, many new solutions and topologies have been proposed, which appear to improve one or more parameters of AC/DC power supplies. To minimize switching losses some of them use soft-switching techniques, like in [RC1-RC13 or W9, PT3]. Others concentrate on power factor improvement [PF1-PF13]. Another approach is to minimize and hybridize discrete components in one planar structure [L1-L2]. However, an increasing number of present papers describe solutions where one or more approaches are combined [PF4, PF5, PF8, PF10, PF11, RC6, PT6 and PT7].
In this study, in addition to a new resonant topology described, a novel method for the power factor correction by a simple implementation of the mentioned topology is proposed. Thus, the topology belongs to the class of combined solutions. In particular, it would be applicable to low-impedance and sharply varying loads.

*Conventional hard-switched power converters*
The most conventional switch-mode power converters are known as "hard-switched". The output voltage of such converters is controlled by varying the gating pulse width or, in other words, by PWM. At the end of each switching cycle the switch turns off at a current peak value, thereby causing high switching loss in the device. Moreover, additional snubber or other protection circuits are also needed that increase overall complexity of the circuit. At present, the maximum frequency of the "hard-switched" operation is limited to around 40 kHz, depending on the converter power level.

## 1.2 Resonant switch-mode converters

The size and weight of magnetic components, like a power transformer or an inductor, could be significantly reduced by an increase in frequency to hundreds of kHz or above. Such a frequency of operation without over-dimensioned thermal design can be achieved by help of a conversion topology such as in a resonant switch-mode power converter.

### 1.2.1 Resonant networks

As different from "hard-switched" PWM converters, resonant switch-mode converters include additional resonant circuit(s). Thus, they combine properties of both switching and resonant circuits. Natural properties of a resonant circuit allow one to minimize switching losses. Therefore, resonant topologies are applied in high-density power supplies.
These converters comprise inductive and capacitive components to achieve a resonant condition. This leads to zero switching current at turn off instants, known as a ZCS. As a result, the switching losses in a switch are significantly decreased, thereby allowing a considerable increase in the switching frequency. The maximum switching frequency in this case is defined by the switching speed of the semiconductor and the parameters of control and gating circuits.
The most common types of resonant converters classified by conversion according to [H3] are:

1) DC to high frequency AC inverters,
2) resonant DC - DC converters,
3) resonant inverters or rectifiers producing the line frequency AC.

Also, resonant converters could be classified into: quasi-resonant, link-resonant and load-resonant [RC12]. The simplest resonant converter topology is the load-resonant converter in which the load forms a part of the resonant circuit [RC13]. The resonant converter proposed and discussed further in the thesis belongs to the class of load-resonant DC-DC converters.
The typical load-resonant converter contains a resonant *LC* circuit. The most common types of resonant circuits are shown in Figure 1.1.

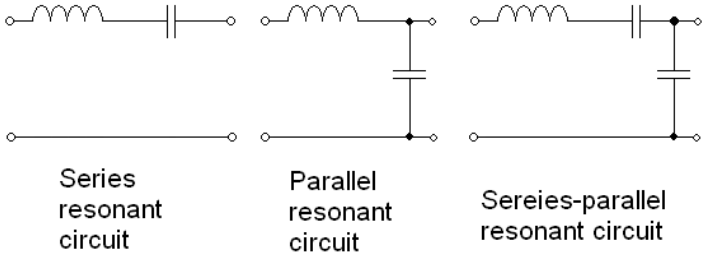


**Figure 1.1 Resonant *LC* circuits used in switch-mode converters**

As the use of resonant converter topologies could help to reduce the switching losses, it enables operation with high switching frequencies, even in the megahertz range that is the key point in the design of high-density power supplies. The technique of reduction of switching losses is also called a soft-switching. As "soft-switched" semiconductors are turned on or off at the zero crossing of their voltage or current waveforms, so it can mitigate some of the mechanisms of switching losses and possibly reduce the generation of EMI [H3].

There are several types of resonant converter topologies. The most popular according to [H4] is the configuration shown in Figure 1.2.

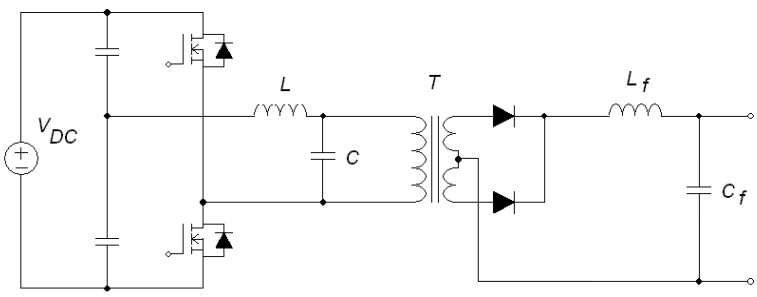


**Figure 1.2 Half-bridge parallel load-resonant DC/DC converter**

In the parallel resonant power converter (PRC) depicted in Figure 1.2, the DC voltage is converted into square-wave high-frequency alternating voltage using the half-bridge inverter. The voltage of the resonant capacitor C is transformer-coupled, rectified by fast diodes, and filtered to obtain the output DC voltage. The ripple in DC output is defined by the values of $L_f$ and $C_f$. The output voltage is regulated by the control of the inverter switching frequency. The parallel resonant converters appears as a voltage source, hence, could be used for multiple output voltage applications [H9].

Instead of parallel loading, the resonant circuit can be series-loaded, as shown in Figure 1.3. The transformer is placed here in series with the tuned *LC* circuit. The series resonant circuit provides also a DC voltage blocking feature in the transformer primary winding. Advantages and disadvantages of different resonant circuits are given in Table 1.1.

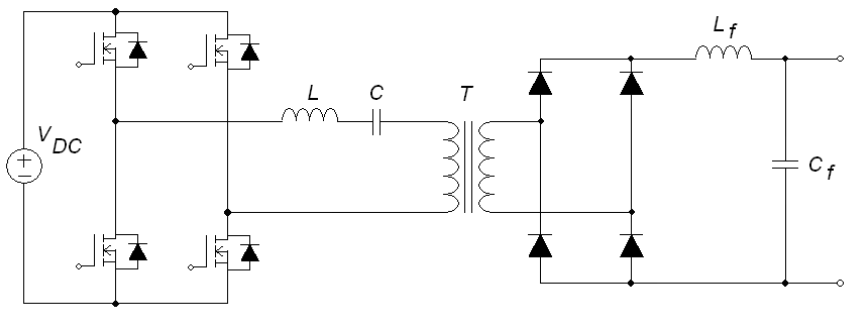


**Figure 1.3 Full-bridge series load-resonant DC/DC converter**

The series resonant converter (SRC) is considered more suitable for high output voltage and low output current applications.
A series-parallel resonant converter is the combination of the series resonant converter and the parallel resonant converter (Figure 1.4).

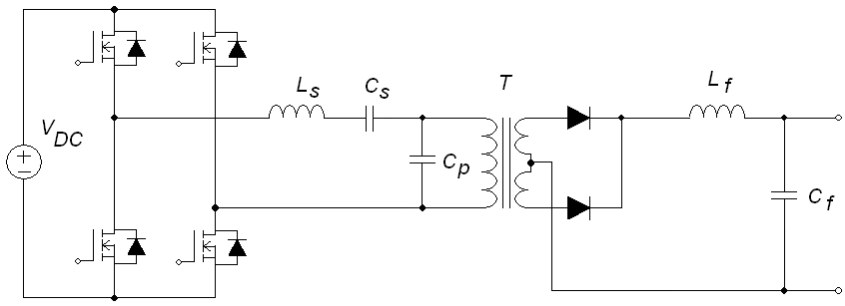


**Figure 1.4 Full-bridge series-parallel load-resonant DC/DC converter (SPRC)**

Figure 1.4 shows that the resonant circuit of the converter consists of a series branch composed by $L_S$ and $C_S$ and a parallel branch by $C_P$. The series-parallel converter has the advantages of both serial and parallel resonant converters. Thus, proper selection of resonant components eliminates the disadvantages inherent to a "simple" resonant converter. For example, a high-efficiency can be obtained in the range from full-load to small load current [RC7]. The series-parallel resonant converter is the best choice for applications with the requirement of low voltage and high current regulated DC output, such as in telecommunication systems, battery charging and welding.
If needed, output rectifier in these resonant converters could also be implemented in full-bridge passive (as in Figure 1.3) or active topology with a simple two-winding transformer.
To summarize, there are three well-known types of load-resonant converters that differ in their form of reactive components connection (Figure 1.5).

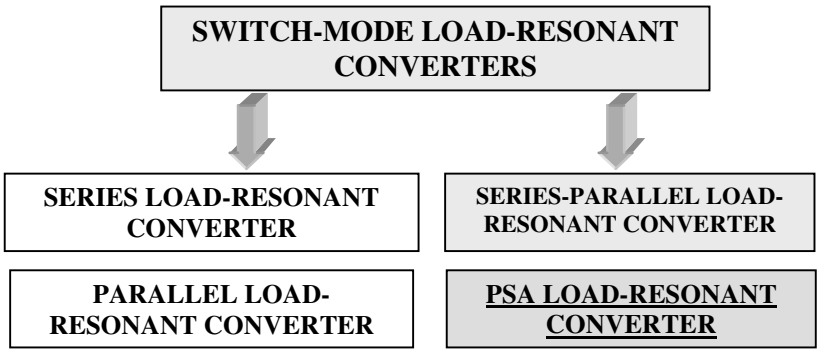


**Figure 1.5 Classification of load-resonant switch-mode converters**

In this study a new type of a resonant converter is proposed. It can be classified as a switch-mode load-resonant converter in the group of converters incorporating both types of resonance in one topology. It is a switch-mode PSA (parallel and series resonance alternating) load-resonant converter.
The main advantages and disadvantages of three well-known resonant topologies are given in Table 1.1. Quasi-resonant and other resonant topologies are beyond the interest of this work.

**Table 1.1 Load-resonant converters' main properties**

| *Topology* | *Advantages* | *Disadvantages* |
|---|---|---|
| **Series resonant converter** | 1) Capacitor on the primary side blocks possible DC voltage - full-bridge inverter topology can be easily implemented.<br>2) Switch current almost directly dependent on load current –low conduction losses at light-load<br>3) Short-circuit protection capability | 1) Poor voltage regulation under no-load or at light-load<br>2) High ripple current in output filter capacitor, not for low-voltage and high-current applications<br>3) Output voltage step-down characteristic |
| **Parallel resonant converter** | 1) Step-down and step-up characteristic<br>2) Low-voltage high-current applications<br>3) Short-circuit proof<br>4) Suitable for multiple outputs | 1) The current in switches and reactive components independent of load - decreased efficiency at light-load |
| **Series-parallel resonant converter** | 1) Advantages of both types, without their disadvantages<br>2) High efficiency can be obtained from full-load to very small load current (<10% of rated)<br>3) Inherent ability to control the current and limit the voltage under short-circuit and open-circuit conditions | 1) Some design issues: parallel capacitor should be carefully selected<br>a) Higher value – higher circulating current<br>b) Lower value – higher upper frequency at light loads |

### 1.2.2 Control techniques for load-resonant converters

Compared to usual PWM converters, control in resonant converters is much more complex [H8] due to the presence of resonant circuit with fast transient response. There are three commonly used methods [RC13] for output power control in load-resonant converters.

*Variable frequency control*

It is the simplest and most commonly used method. Output is regulated by controlling the switching frequency $f_{sw}$. The feedback controller determines the switching frequency according to the error between the reference and converter output [H8]. The transient response of this control is rather poor. It takes several cycles to attain a new steady state. As the main disadvantage, it is difficult to design suitable EMI filters as the switching frequency is varying. Also, this method of power control removes the benefit of zero switching [RC12].

*Fixed frequency pulse-width modulation*

The output voltage is regulated by varying the phase shift between voltages driving the two half-bridges. The control for this method is relatively complex. As the load current decreases, the control pulse width is decreased by the phase shifting of the gating signals [RC7, RC8].

*Dead-time control [RC12]*

This is a very complex method of power control. It needs a digital controller, many feedback and control circuits. However, this method maintains zero switching condition in a certain range.

Some other control methods are also possible, for instance, a capacitor voltage clamped converter [H8]. During one switching period there are short time intervals when the capacitor voltage is clamped at a certain value. By varying the duration of this clamping, the output voltage can be regulated and due to this less stress appears on circuit components. Drawbacks are complex analysis and control, higher number of switched devices needed. Usually it is used for series resonant converters.

None of these methods of power control in load-resonant converters allow a wide range in the modulation of the output power without incurring significant switching losses or introducing output current ripple [RC13].
In our work a very simple fixed frequency pulse-width modulation method (changing of the gating pulse width as in conventional hard-switched converters) will be employed and analyzed.

## 1.3 Power factor correction in single-phase AC/DC converters

Commonly, the problem of poor power factor could be solved in different ways. The most well-known one is the implementation of boost or buck-boost converters [PF10, PF11] placed between the mains and the switch-mode converter, as shown in Figure 1.6.

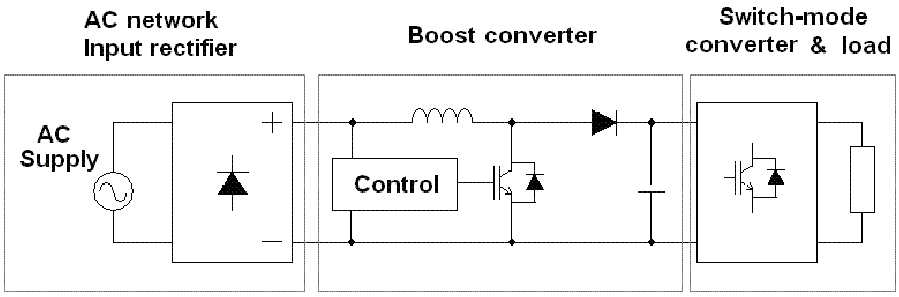


**Figure 1.6 Simplified circuit of AC/DC converter with power factor correction**

The main drawback of such a solution is an additional energy transformation stage (Boost converter) that will decrease converter efficiency and a special controller with feedbacks is needed. However, such single-stage solutions as the integrated boost-forward converter are available [H10]. Another solution, active rectifiers based on PWM converter topology [PF2, PF12], as shown in Figure 1.7, are used.

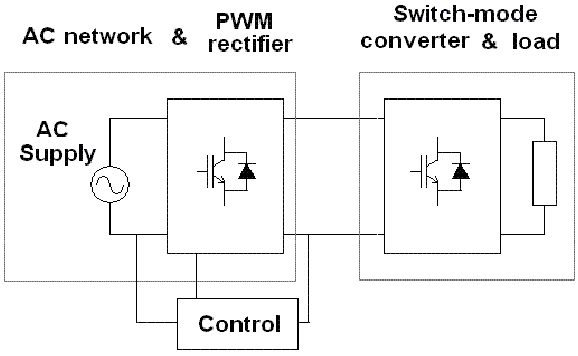


**Figure 1.7 Simplified circuit of AC/DC converter with PWM rectifier**

The drawbacks of such topologies increase the number of switches and complicate control.

However, these topologies make close to unity power factor possible. Different topologies are proposed characterized by the implementation of special additional circuits to achieve a power factor correction, like in [PF13].

Finally, switch-mode converters having an inherent resistive input characteristic that can be exploited for the power factor correction [PF5, RC6] exist. Their advantage is a simple topology without additional control circuits. They have

not perfect, but have a relatively high power factor. The PFC in SM-PSA converter could be related to the last ones.

## 1.4 PSA converter basics

*History, development, motivation*

The main conception of the mains frequency PSA converter, reported in a number of papers [PSA1-PSA10] was developed by Dr. Kuno Janson at the Department of Electrical Machines and Fundamentals of Electrical Engineering at Tallinn University of Technology.

As a specific feature, this converter consists two type of resonance, parallel and series, that could take place simultaneously or separately. The duration of each resonance type depends on load parameters. Thus, this converter could be related to load-resonant converters.

The most simple circuit topology of the proposed PSA converter is shown in Figure 1.8.

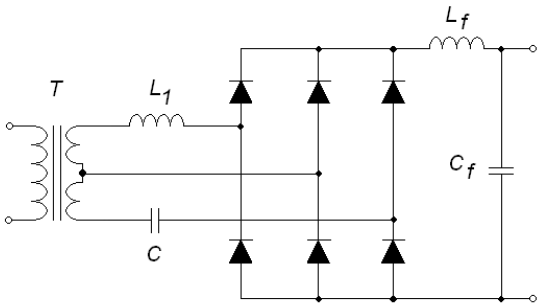


**Figure 1.8 Basic resonant circuit of the PSA converter**

As seen in Figure 1.8, the converter includes a transformer *T* with a tapped secondary winding, resonant components $L_1$ and *C*, which form parallel or series resonant circuits, and an output full three-phase rectifier bridge. Advantages inherent to this resonant converter topology are as follows:

1) simple topology,
2) whole operating range: from no-load to short-circuit
3) fast and parametrical output self-adjusting
4) parametrical limiting of load short-circuit current without overloads in converter elements,
5) operation "friendly" to supplying AC network because of its much better power factor compared to well-known diode bridge rectifiers.

The most significant disadvantage of this converter at mains frequency is a large capacitance of *C* and inductance of *L* needed for converter operation.

However, this PSA converter was initially developed to supply the MW range DC arc furnaces, so the weight and size of the converter were relatively insignificant. Presently, two arc furnaces (rated 1 and 8.5 MW) in Russia operate well with a PSA converter. More detailed information on the PSA converter will be presented in the next chapter.

The idea to adopt this converter for lower-power needs was proposed in 2000. As at higher frequency, the size of resonant capacitors and inductors decreases, the PSA converter becomes more competitive in the low-power range. In the same year, studies of switch-mode PSA (SM-PSA) converter started. The first results were published in 2002 [PSA7]. It was confirmed that the required capacitance and inductance of a resonant circuit in a PSA converter are significantly lower at high frequencies. Also, in [PSA7] the results regarding the basic characteristics of a SM-PSA converter were reported and the main properties of arc welding with the requirements for welding sources were described. The further development of this study proved worthwhile and more detailed research of the SM-PSA converter that was conducted during the author's doctoral research. The most significant results of this research are presented in this thesis.

## 1.5 Modeling and analysis

In this thesis the main method for the analysis of the converter is a time-domain analysis.

The present analysis of the converter by the time-domain method appears a simple due to different new versions of circuit modeling and simulating software and quite powerful computers. Also, the solving mechanisms of simulation programs have turned out more robust with less convergence problems. However, just about ten years ago it was a very inconvenient and slow process.

Using the time-domain analysis, a set of differential equations is obtained and solved in each time interval.

The frequency-domain analysis is also used in the thesis to represent an input impedance of the converter during the output short-circuit. It represents the input voltage and the input current as the sum of harmonics. A harmonic equivalent circuit excited by the voltage and current harmonics yields state variables that can be represented as the sum of the responses of each individual harmonic component.

*Simulation of the converter*

The PSA load-resonant converter mode was composed using the PSCAD v3.0.7 and PSIM v.7.0 simulation software packages. Two types of simulation were carried out during the study. The main type of simulation, the time-domain analysis, utilizes the full model of the converter with more or less "real" models of power switches. The calculation time step was selected 10 or 20 ns depending on the overall simulation time. The magnetizing current of the inverter transformer was neglected.

The second simulation method is a small signal ac analysis of the simplified SM-PSA circuit to calculate the frequency-response of the proposed converter. It was used only once as it can be implemented for certain load conditions like short-circuit in the case of SM-PSA converter.

*Load of the resonant converter*
A welding power supply was an attractive focus since a useful product could be designed. Thus, a single-phase power source for manual arc DC welding was mainly studied.

## 1.6 Purpose of the study

*Contents brief description*

The main purpose is twofold: first, to introduce a new switch-mode load-resonant converter having a very simple structure of power and control circuits, and second, to describe and analyze its ability of input current shaping without additional circuits, sensors and control.
In order to achieve these goals, the proposed switch-mode load-resonant PSA converter was analyzed. Converter operation was verified both by computer simulation and by experimental tests. The study focused on the following:

1) disclosure of operation peculiarities inherent to the switch-mode PSA converter,
2) selection of optimal topology and reactive components for the switch-mode PSA converter

For convenience, chapters of this thesis are briefly described below:

*Chapter 2: Mains frequency PSA converter*

The properties, parameters and calculation of the mains frequency PSA converter are described and some converter operation principles are explained. An overview of the peculiarities inherent to the mains frequency PSA converter is provided.

*Chapter 3: Switch-mode PSA converter*

Calculation methods and main aspects of the design procedure for the switch-mode PSA load-resonant converter are discussed. The operation of the high-frequency PSA converter having DC voltage supply both during steady-state and transient processes is analyzed. Influence of resonant component values on the output characteristic and switching losses is also described. In particular, zero-current switching maintaining is discussed. Along with computer simulation results, some experimental results are presented.

*Chapter 4: PFC in switch-mode PSA converter*

In addition to the previous chapter, the phenomenon of indirect power factor correction (IPFC) in the proposed switch-mode PSA load-resonant converter is described. It is shown that the proposed SM-PSA topology can operate as a power factor correcting device without additional components or special control techniques. That correction method and the corresponding topology have a patent pending [PT2].

*Chapter 5: Comparison, analysis and conclusions*

In the final chapter the results of the study are presented. The switch-mode PSA converter and other conventional load-resonant switch-mode converters are compared. Conclusions and recommendations for future developments finalize the thesis.

# 2. Mains frequency resonant converter with parametric parallel and series resonance alternation

*This chapter is mainly based on the thorough research conducted by Kuno Janson at the Department of Fundamentals of Electrical Engineering and Electrical Machines, Tallinn University of Technology (TUT), described and published in [PSA1 – PSA6, PSA9, PSA10]. This chapter was included because the topic has been attached relatively little attention to. The information presented in this chapter was selected regarding its significance in relation to the analysis that follows.*

## 2.1 Development of a single-phase PSA converter

*Mains-frequency AC/DC resonant converters*

Three main types of mains-frequency resonant converters are distinguished: a series resonance converter, a parallel resonance converter and, a converter with alternation of parallel and series resonances (PSA), developed at the Department of Electrical Machines and Fundamentals of Electrical Engineering at TUT. In these network-frequency resonant converters, load current passes through resonant capacitors and inductors and usually these converters tolerate output short-circuit and could be used to supply loads like the electric arc.

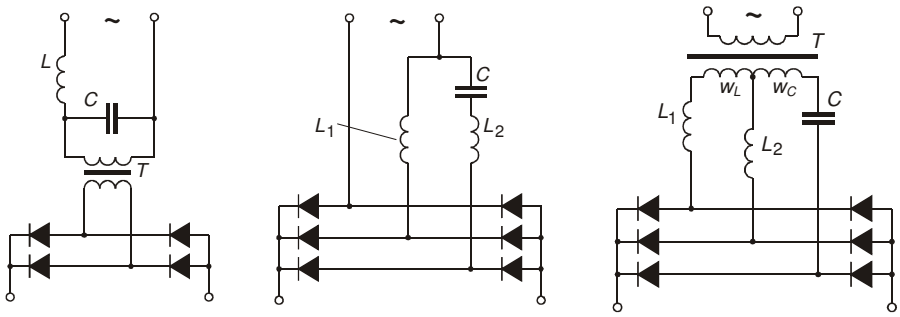


a) b) c)

**Figure 2.1 Series (a), parallel (b) and PSA (c) resonant converters**

The series-resonance network frequency converters are known as Boucherot circuits [H5] (it has to be mentioned that in switch-mode resonant converters, this topology is classified as parallel resonant). In these circuits the load is connected in parallel either to the capacitor or inductor of the series resonant circuit, as in Figure 2.1 a. The currents through the inductor and capacitor increase when load resistance is increasing. Maximum currents and maximum capacity of the capacitor and inductor are determined by the transformer

parameters. Also, with load resistance increasing the voltage could increase up to the saturation of the transformer.
The converter with parallel resonance represented in Figure 2.1 b operates fully in the parallel resonant mode when the load circuit is short-circuited. In addition to the main inductor $L_1$ an additional inductor $L_2$ is introduced here to reduce higher harmonics in the network current [PT4, PT5]. This converter has the highest currents through the resonant capacitor and inductor during the load short-circuit, as shown in Figure 2.2.

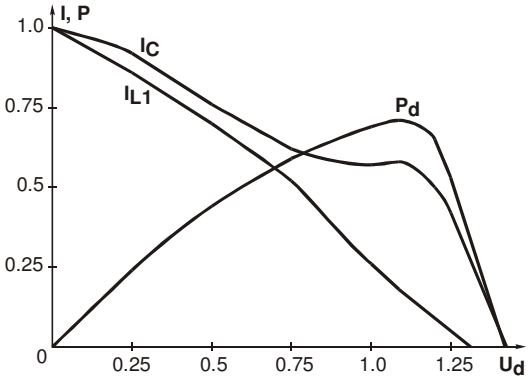


**Figure 2.2 The current of main inductor ($I_{L1}$), capacitor ($I_C$) and output power of the mains frequency parallel resonant converter ($P_d$)**

The output power is the highest at the output voltage $U_d$ approximately equal to the supply voltage. The currents in the inductor and capacitor are significantly lower at the maximum output power compared to the short-circuit. Rated power of reactive components has to be selected from the short-circuit mode in this case. Additional inductor $L_2$ increases the voltage and power of capacitor C.
As it is seen in Figure 2.1, the PSA converter differs from the parallel resonant converter, depending on how the converter supply voltage is arranged. There is a transformer with tapped secondary winding in the PSA converter and the main inductor $L_1$ separated now from the capacitor C by transformer secondary windings. The transformation of the parallel resonant converter into the PSA converter is illustrated in Figure 2.3.
This modification of the supply voltage arrangement leads to a significant difference in parameters and characteristics of the resonant converter. As compared to the parallel and series resonant converters, the PSA converter can form both types of resonant circuits: parallel or series, resulting in the corresponding resonant circuit running parametrically according to the load condition. Resonant circuit formation in the PSA converter will be discussed later in this chapter.

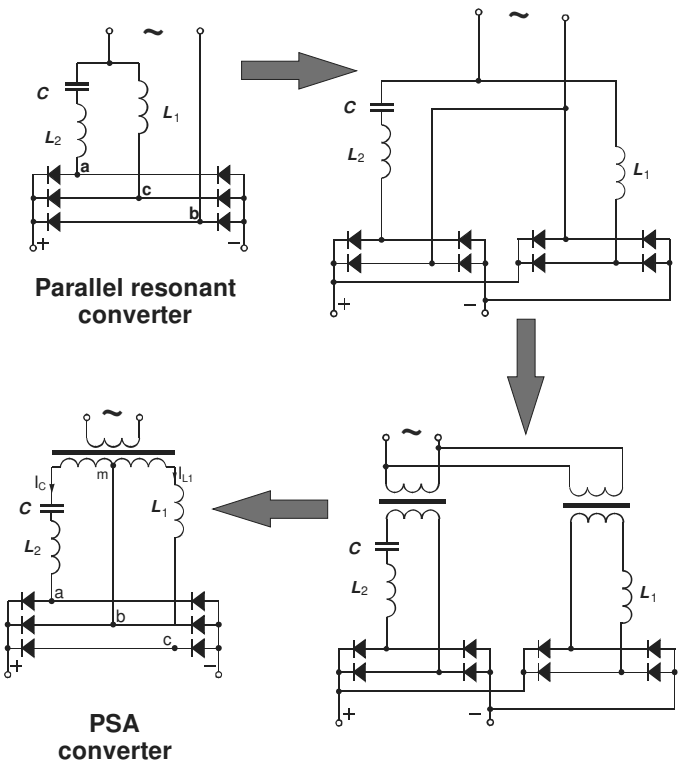


**Figure 2.3 Transformation from a parallel resonant converter to PSA converter**

This modification changes the characteristics of the converter, as shown in Figure 2.4. In the PSA converter currents through the capacitor $C$ and the main inductor $L_1$ are approximately the same from no-load to nominal mode. In the nominal mode ($U_d$=1), the converter output power $P_d$ is the highest.
A comparison of the three converter types depicted in Figure 2.1 states that the PSA converter has the lowest unit power [PSA2].

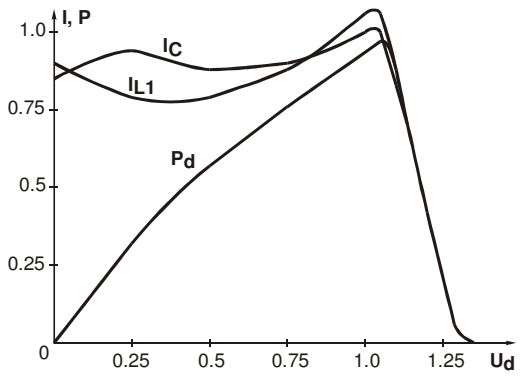


**Figure 2.4 The current of inductor $I_{L1}$, capacitor $I_C$ and the output power $P_d$ of the PSA converter**

## 2.2 Role of additional resonant inductor

*Placement of additional inductor*

The modifications of a single-phase PSA converter differing in the placement of the additional inductor $L_2$ are shown in Figure 2.5. Common topology of these circuits includes a transformer having two secondary windings ($W_2$=$W_L$ and $W_3$=$W_C$), which are connected in series. The winding $W_L$ and the inductor $L_1$ form a phase-shifting circuit where the current $I_{L1}$ lags the voltage. The winding $W_C$ and capacitor $C$ form another phase-shifting circuit where the current $I_C$ leads the voltage. The common connection point $m$ of windings $W_L$ and $W_C$ is connected to the rectifier bridge directly or through the additional reactor $L_2$, as shown in Figure 2.5 c.

As it was mentioned, the additional inductor is useful for reducing harmonics in the line side current.

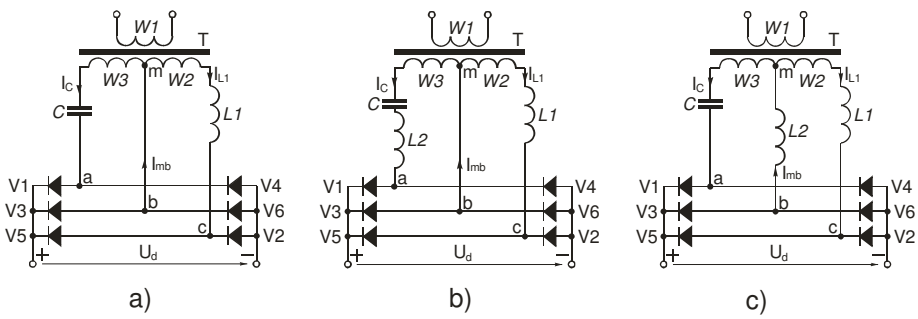


**Figure 2.5 Single-phase PSA-converters: (a) - without additional inductor**
**(b) - additional inductor is in series with the capacitor**
**(c) - additional inductor is connected to transformer tap**

If the additional inductor $L_2$ is absent (Figure 2.5 a), the current in the circuit: *a – capacitor C – winding* $W_3$ *– b*, can vary very rapidly. Such fast current variations cause distortions of the input current waveform. By adding an inductor $L_2$, higher harmonics will decrease in correspondence with the decrease of the resonant frequency of resonant circuit $L_2C$.

When calculating the resonant frequency it should be kept in mind that the leakage inductance of the transformer windings has to be added to the inductances of inductors $L_1$ and $L_2$.

The additional inductor $L_2$ may also be connected in between the point $m$ and point $b$ (Figure 2.5 c). Usually, a circuit that has smaller current suits better for inductor $L_2$ placement. To define a better place for $L_2$, let us take a look at Figure 2.6 that show load dependent current curves for the capacitor branch $I_c$ and the middle branch $I_{mb}$.

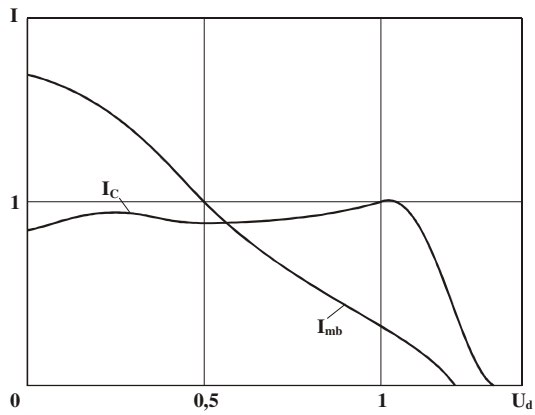


**Figure 2.6 Currents through the capacitive branch $I_C$ and through middle branch $I_{mb}$**

The current $I_{mb}<I_c$ at higher output voltage $U_d>0.5U_{dn}$ and $I_{mb}>I_c$ at smaller output voltage $U_d<0.5U_d$. In case the PSA converter is operating most of the time at a lower output voltage, it is reasonable to connect the additional inductor $L_2$ in series with the capacitor $C$. Otherwise, it is reasonable to use the circuit depicted in Figure 2.5 c. Thus, the additional inductor can be dimensioned for lower current.

## 2.3 PSA converter with resonant components on the primary side

*Increasing the capacitor operating voltage*

The circuits shown in Figure 2.5 are not the best solution if the converter has to provide high current at low voltage. These circuits will be featured with too high capacitance, having large weight and dimensions. At low output voltages it is reasonable to use the circuit shown in Figure 2.7. This circuit includes two transformers $T_1$ and $T_2$ and the reactive components connected to the primary side. The capacitor $C$ is connected to the primary side of the transformer $T_1$, where it operates with smaller current and higher voltage. Therefore, the required capacitance is reduced as compared to the capacitance needed to install on the secondary side.

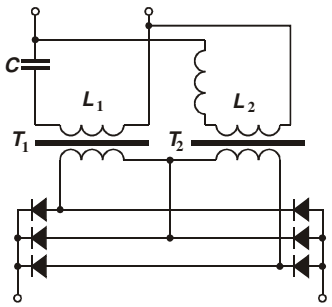


**Figure 2.7 Capacitor voltage increasing**

One shortage of the circuit in Figure 2.7 is a possible saturation of the transformer that should be considered during converter design.
Another way to increase the operating voltage capacitor of the (up to 2 times), regardless of whether the capacitor is placed on the primary or secondary side, is to employ circuit with the additional inductor $L_2$ connected in series with the capacitor, as in Figure 2.5 b.

## 2.4 Basics of PSA converter parameter calculation

### 2.4.1 Distribution factors

Still, it is not that all the PSA converters with the same circuit have the same parameters. Inductances, capacitances and voltages of transformer windings could be varied within some range. For example, converter transformer includes two secondary windings. Voltages of these windings can be chosen equal or different. This choice is characterized by the ratio of their no-load voltages

$$K_E = \frac{U_{WC0}}{U_{WL0}}, \tag{2.1}$$

where $U_{WC0}$ is the no-load voltage of the winding in the capacitive branch; $U_{WL0}$ is no-load voltage of the winding in the inductive branch. Factor $K_E$ could also be named as the converter voltage distribution factor.
For the converter with two inductors $L_1$ and $L_2$, the ratio between the reactances of the additional inductor $L_2$ and the main inductor $L_1$ is

$$K_L = \frac{x_{L2}}{x_{L1}} \tag{2.2}$$

that could also be named the inductance distribution factor, where $x_{L2}$ is the inductive reactance of the additional inductor; $x_{L1}$ is the inductive reactance of the main inductor.
The reactive load in the transformer secondary windings can be mutually compensated in the short-circuit mode either totally or partly. This is characterized by the ratio between the reactive powers of the transformer secondary windings:

$$K_Q = \frac{Q_{LK}}{Q_{CK}}, \tag{2.3}$$

where $K_Q$ is the reactive power distribution factor for the short-circuit mode; $Q_{LK}$ is the reactive power of the inductive branch in the case of short-circuit; $Q_{CK}$ is the reactive power of the capacitive branch in the case of output short-circuit.
Values of distribution factors $K_E$, $K_L$ and $K_Q$ are subject to the power supply designer choice. Converters with the same circuit and distribution factors can have different nominal voltages and currents, but they will have the same power factor, the shape of the output characteristic, the same amount of current higher harmonics etc.

For different loads a suitable modification of the PSA converter should be selected and then proper values of the components and distribution factors should be defined.

### 2.4.2 Defining of reactive component values

Commonly, the desired output parameters of the converter are specified by load parameters, where typically, load voltage $U_{dn}$ and current $I_{dn}$ are indicated. In our initial design procedure we used a special system of related units, where index $_B$ means a base value, the more detailed information on the calculation and design of converter could be found in [PSA1, PSA2].The expressions defining the relative parameters for the circuit depicted in Figure 2.5 c are as follows:

summed secondary voltage of the transformer at no-load

$$U_{dn} \approx U_B = U_{WC0} + U_{WL0} \tag{2.4}$$

total power of the converter

$$S_{BP} = U_{WC0} I_{WCK} + U_{WLO} I_{WLK} \tag{2.5}$$

base value of current

$$I_{BP} = \frac{S_{BP}}{U_B} \tag{2.6}$$

relative reactance of the main inductor $L_1$

$$x_{L1}^* = \frac{K_E(K_Q+1) - x_{SL}^* \cdot K_E \cdot K_Q (K_E+1)^2}{(K_E+1)^2 \left[K_E \cdot K_Q (1+K_L) + K_L\right]} \tag{2.7}$$

relative reactance of the capacitor $C$

$$x_C^* = x_{SC}^* + x_{L1}^* \cdot K_L (1 + K_E \cdot K_Q) + \frac{K_E^2 (K_Q+1)}{(K_E+1)^2} \tag{2.8}$$

relative reactance of additional inductor $L_2$

$$x_{L2}^* = K_L \cdot x_{L1}^*, \tag{2.9}$$

where $x_{sC}$ , $x_{sL}$ are the equivalent leakage inductances of the corresponding windings.

After that, knowing the required nominal load voltage $U_{dn}$ and current $I_{dn}$ the initial, a rough value of the reactance of the converter $Z_{BP1}$ can be found according to the next expression:

$$Z_{BP1} = \frac{U_{dn}}{I_{dnp}} \ , \tag{2.10}$$

$$\text{where} \quad I_{dnp} = \frac{I_{dn}}{3} \tag{2.11}$$

Then, initial values of reactive components could be calculated using the relative and base values defined above.

$$X_L = x_{L1}^* \cdot Z_{BP1} \tag{2.12}$$

$$X_C = x_C^* \cdot Z_{BP1} \tag{2.13}$$

Then, it is best to verify calculated results by the computer simulation. If the deviation between the desired and simulated results is significant, it should be corrected by refining the calculated above parameters. Finally, on the basis of computer simulation we obtain more precise values of reactive components.

## 2.5 Characteristics and peculiarities of single-phase PSA converter

This section reviews the properties inherent to the PSA converter and explains the process of parallel and series resonance alternation in the converter. To introduce the currents of the PSA converter (having topology as in Figure 2.5 c as a function of the load voltage $U_d$, the corresponding diagram is represented in Figure 2.8, where the converter has $K_E$=0.63; $K_L$=0.46; $K_Q$=1.19. Figure 2.8 shows currents through different components of the converter and its output and input currents.

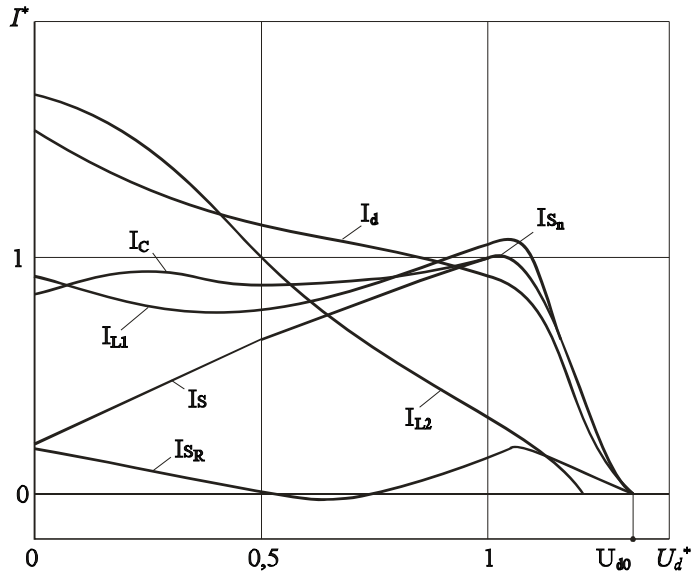


**Figure 2.8 Output current ($I_d$), line current ($I_S$), resonant capacitor current ($I_C$), current through the main resonant inductor ($I_L$) as a function of the load voltage $U_d$**

As different from an ordinary diode rectifier, a single-phase PSA converter has the following specific features.

- The maximum value of the line current is in general the same as the nominal value $I_{Sn}$ in the Figure 2.8. Moving from the nominal point to short-circuit, instead of increasing, the line current decreases. Thus, the primary winding of the transformer cannot be overloaded.
- The current of the capacitor $I_C$ and the main inductor $I_L$ does not change much in the movement from the nominal operation to short-circuit (usually

changes up to 10–20 %). In general, it means that it is not possible to overload the capacitor, main inductor and the secondary windings of the transformer.

- When moving from the nominal operation to short-circuit, the rectified output current $I_d$ will increase, but not drastically, up to 2 times. Maximum increase depends on the parameters of the selected reactive components. Such behavior is almost in correspondence with the operating mode of a current source.
- When moving from nominal current to no-load the voltage $U_d$ changes from 1.3 to 1.7 times (depending on the parameters of the selected reactive components). This corresponds to some extent to the operation mode of a voltage source.
- The current through the additional inductor $I_{L2}$ is strongly dependent on the load voltage. By moving from the nominal operation mode to the no-load, current $I_{L2}$ turns to zero before the load current $I_d$, i.e. the current through the middle branch (between points *m* and *b* in Figure 2.5 c) is absent and two secondary windings are connected in series and operate with exactly the same currents as one winding.
- At short-circuit, the current $I_{L2}$ increase about 3–5 times compared to its nominal current and becomes almost equal to the output current $I_d$. At that, the current $I_{L2}$ is roughly equal to the sum of the currents $I_{L1}$ and $I_C$. Hence, we can suggest the parallel connection of the secondary windings.
- The reactive component of the line current is small in all operation modes ($I_{SR}$ in Figure 2.8). In the range of nominal current the reactive component is usually inductive and could be in the range 10–40 % of the nominal current.

## 2.6 Commutations in output diode bridge rectifier

As it is obvious from the previous part the PSA converter operates well in a very broad load range from no-load to short-circuit. To clarify its operational peculiarities it is necessary to describe how the changing of currents $I_L$, $I_{mb}$ and $I_C$ is accompanied by changes in the currents of diodes and also in the intervals during which these diodes are turned on. A descriptive drawing for nominal operation is shown in Figure 2.9.

According to Figure 2.9, in the nominal mode diodes are turning on and off 6 (six) times in each half-cycle. The half-cycle is divided into 6 intervals ($\upsilon_C$, $\gamma_L$, $\upsilon_{LC}$, $\gamma_C$, $\upsilon_L$, $\gamma_p$), where each time interval has its own circuit.

In the range close to the nominal $U_d$=1, the current circuits of the diode bridge and their variation order is the same as for a conventional three-phase rectifier.

Similarly to a three-phase rectifier, we can also name the intervals as commutation intervals, when two valves from the anode group or cathode group are turned on simultaneously. In the nominal mode, there are three different commutation intervals in each half cycle, which are marked as $\gamma_p$, $\gamma_C$, and $\gamma_L$. Between the commutation intervals in the nominal mode, there are three intervals, in which only two diodes are turned on. These intervals are denoted as $\upsilon_C$, $\upsilon_{LC}$, and $\upsilon_L$.

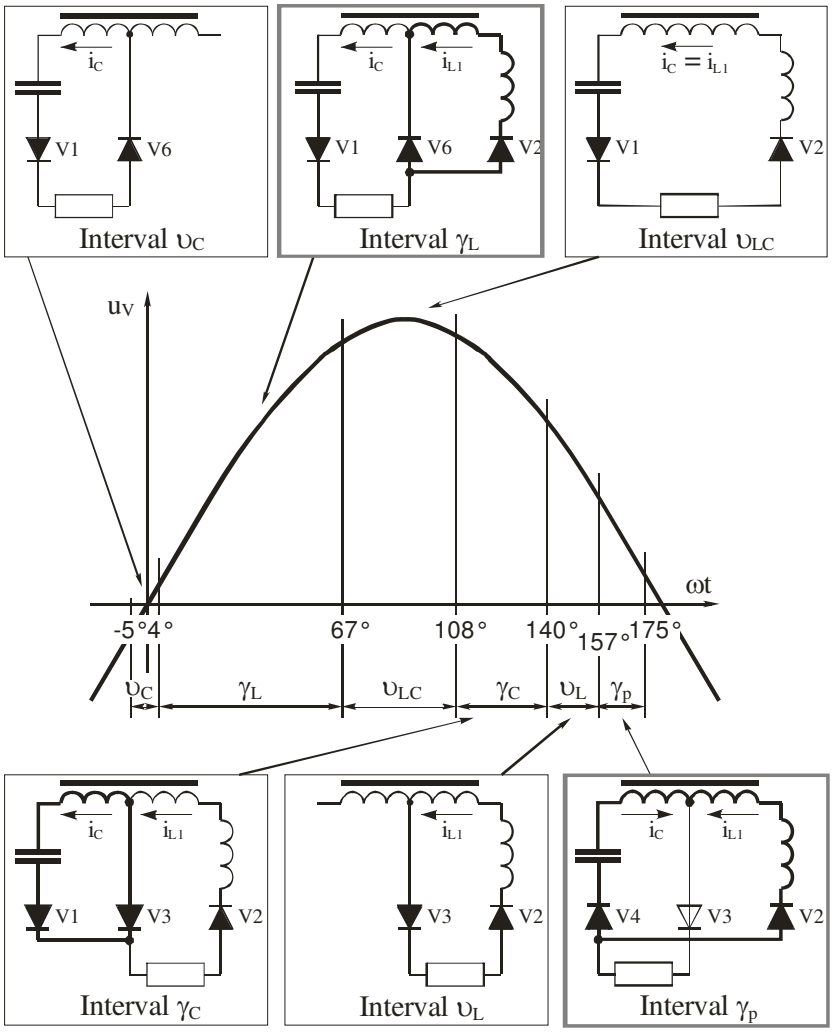


**Figure 2.9 Current conducting circuits of PSA converter and their duration in nominal mode**

In conventional rectifiers the transformer windings involved in the commutation process are short-circuited during the commutation periods. During short-circuit the rate of current changing is determined by the transformer leakage inductance. In the case of large leakage inductance the rate of current change is low and therefore, higher harmonics in the line current are reduced, but very high leakage inductances still cannot be used due to the low power factor.
The PSA converter is an exception in this sense. The capacitor is compensating the effect of inductances. This enables one to use higher inductances to slow down commutations. In the PSA converter the commutation is slowed down by the transformer leakage inductance as well as by the reactors $L_1$ and $L_2$.

The commutation circuits are, in fact, *LC* resonant circuits. The natural frequency of the oscillating circuit $L_1C$ in $\gamma_p$ is approximately equal to the line voltage frequency. Due to the low natural frequency the speed of current variations in this commutation circuit is low.
The natural frequency of the oscillating circuit $L_2C$ in $\gamma_C$ is higher than the network voltage frequency. This natural frequency $f_0$ can be determined in relation to the network frequency $f_m$ by the next expression:

$$\frac{f_0}{f_m} = \sqrt{\frac{x_C}{x_{sC} + x_{L2}}}, \tag{2.14}$$

where $x_c$ is the reactance of capacitors at line frequency, $x_{sC}$ is the equivalent leakage inductance of the capacitive branch in the winding $W_3$, and $x_{L2}$ is the inductive reactance of the additional inductor $L_2$ at network frequency.
In case an additional inductor is absent and the transformer is of traditional construction, the natural frequency is approximately equal to the 5$^{th}$ harmonic frequency. To decrease the line current distortion the natural frequency of the circuit should be decreased. This could be done by adding an inductor $L_2$, increasing the leakage inductance of the transformer or adding an inductor in series with the capacitor C. To summarize: higher harmonics in the line current of the PSA converter are mainly dependent on the parameters of the commutation LC circuits.
In addition, if the converter output is no-loaded or has some light load, the duration of the interval $\upsilon_{LC}$ grows up to 180° and, thus, converter will operate in a series resonance mode. If the converter output is short-circuited the duration of the interval $\gamma_p$ grows up to 180° and, thus, the converter will operate in the parallel resonance mode.

## 2.7 Self-adjusting to load

*Parametrical variation of transformer average turns ratio*
"Transition" from series to parallel resonance could take place at each half-cycle and it depends on the load condition. When the load voltage is low the interval of parallel operation increases, then, the average transformation ratio for one half-cycle also increases. Such phenomenon of smooth variation of the transformer turns ratio is unusual. In a conventional diode rectifier with a matching transformer, the line current is proportional to the rectified current $I_d$ in the case of a resistive load.
The relation of the output current $I_d$ and the current $I_1''$ (normalized to the secondary side line without magnetizing current) could be named as the converter current transformation ratio $K_{TI}$.

$$K_{TI} = \frac{I_d}{I_1''} \tag{2.15}$$

Figure 2.10 shows the current transformation ratio $K_{TI}$ as a function of output voltage per unit $U_d^*$ in the parametrically compensated PSA converter (curve 2).

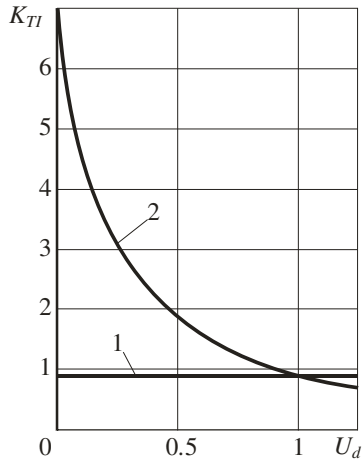


**Figure 2.10 Current transformation ratio $K_{TI}$ for a simple single-phase diode rectifier (curve 1) and for PSA converter (curve 2)**

As compared to the conventional diode bridge rectifier (curve 1), in which the relation between the supplied current and the rectified current is constant, a marked difference is obvious. As it is seen, moving from open-circuit to short-circuit will lead to about a 10-fold change of the current transformation ratio. The change of the current transformation ratio $K_{TI}$ is caused by the reactive power compensation in the converter and due to the parallel operation of secondary windings.

Because of the changing ratio $K_{TI}$ the PSA converter could be named as "soft" and self-adjusting to the load. Such a parametrically compensated converter reacts smoothly to load changes.

## 2.8 Input current distortion

*Steady-state*

There are oscillograms of the single-phase PSA converter currents on AC and DC sides shown for three different load voltages in Figure 2.11 (computer simulation). The input current phase regarding the input voltage $U_S$ changes very little as the load voltage changes. Thus, the displacement power factor remains high. The waveforms of the input current at different loads are of “good” shape and their $THD_i$ is in the range 5–10%. Ripple of the rectified current (as no output smoothing filters are installed) is the lowest in the nominal mode.

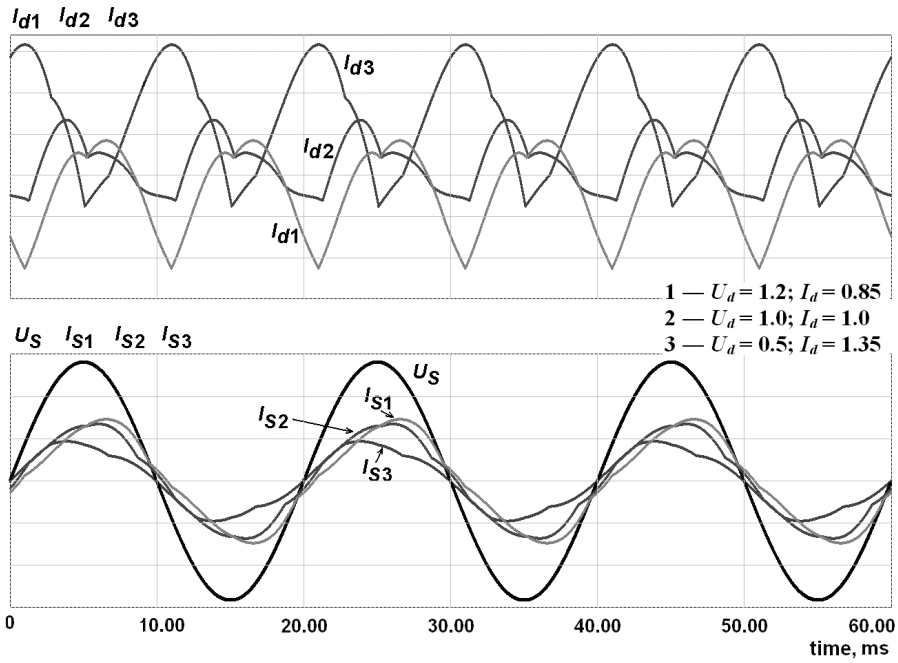


**Figure 2.11 Oscillograms of output and input currents at three output voltages**

Ripple of the rectified current increases if the load changes regarding to the nominal operation point. At load voltages above $1.2U_d$ the load current becomes fragmentary. More information about the converter behavior and the waveforms could be found in [PSA 1, PSA2]

## 2.9 Conclusions

The distinctive property of PSA converters is the presence of one or more inductive and one capacitive branch which can form parallel or series resonant circuits by the natural commutation of diodes in the output rectifier bridge.

Many combinations of PSA-converter current conducting circuits that have different characteristics exist. The peculiar characteristics of the PSA are based on the electromagnetic processes in these circuits, where reactive components are switched from parallel into series connection and vice versa. Thus, the alternation of the parallel and series resonant circuits, which are tuned to the network frequency, takes place and the converter could be characterized as a converter with parametric alternation of parallel and series resonances.

Due to series and parallel reactive power compensation the power factor of the converter is high from no-load to short-circuit (in the nominal mode up to 0.99).

During the no-load condition the converter operates in the series resonance mode. When it is approaching to the output short-circuit, the PSA converter begins operating in the parallel resonance mode without any auxiliary regulation. At average load, at every half-cycle of the network voltage, the transition from series to parallel resonance and vice-versa is taking place.

Converter operation could also be characterized as a transformer with the variable turns ratio.
When the secondary windings operate in the parallel mode the average transformation ratio is increasing. Because of this, during the transition from the nominal operation to short-circuit the transformation ratio becomes twice higher. This phenomenon could be named as self-adjustment to the load. This feature could be used when supplying consumers that need more or less constant power at a variable load.
The converter fits perfectly for supplying DC electric arc and solves the problems with reactive power compensation, flicker and higher harmonics.

The PSA converter has the following features:

- High power factor. This solves not only the problem of reactive power compensation, but also mitigates disturbances in line in the case of deeply varying load
- Parametric limitation of short-circuit currents that makes it possible to supply an electric arc even with the uncontrollable converter
- Small overloads during the transients and fast transient times (less then one half-period of supply voltage)
- High efficiency
- Self-adjusting to load

The main disadvantage of the mains-frequency PSA converter is a significant capacitance and bulky dimensions of the capacitor *C*. The PSA converter and conventional SM converters are compared in table 2.1 below.

**Table 2.1 Comparison of the PSA converter with switch-mode converters [PSA1]**

| *Advantages* | *Disadvantages* |
|---|---|
| 1. Cost for average/high powers is 2–3 times less<br>2. PSA converter has 3–4% higher efficiency<br>3. Self-adjusting to load, short-circuit current limitation<br>4. Lower EMI and noise | 1. Larger weight and size<br>2. Slightly lower power factor (0.99–0.995)<br>3. Output current regulation in the whole range is problematic |

# 3. Switch-mode PSA converter

This chapter describes different resonant network topologies, steady-state and transient behavior of the SM-PSA converter having a DC voltage power supply shown in Figure 3.1.

A welding power source is an attractive purpose for the switch-mode PSA (SM-PSA), as a useful product can be created. Hence, a welding arc will be considered mainly as a load of the SM-PSA converter. To be more exact, in this study a load is a MMA DC welding arc with the welding current up to 150 A. In the computer model the welding arc was substituted with the circuit according to the expression $U_{arc}=U_{back\text{-}emf} + R_a \cdot I_{arc}$, [W2, W3 and AD2], where $U_{back\text{-}emf}$ is a voltage-source (back-emf) at voltage equal to 20 V and $R_a$ is a small series resistance equal to 0.04 Ohm. Thus, for the welding current of 150 A the resulting voltage drop will be 26 V.

## 3.1. Basics of a generalized switch-mode PSA converter

### 3.1.1 Power circuit of SM-PSA and control

Switch-mode PSA converter development was started in 2000 and some preliminary results are described in [PSA7, PSA8]. The main advantage of the SM-PSA over the mains-frequency PSA converter is the reduced volume and size of reactive components, such as the inductor, transformer and capacitor. Also, if transformer windings are designed properly, their leakage inductances could be used instead of resonant inductors in a SM-PSA converter. Moreover, at high frequency above 100 kHz, an inductance of wires or busbars in the resonant circuit could be sufficiently high to substitute for the resonant inductors as well.

According to previous chapter (Figure 2.5), for loads like manual DC welding arc characterized by relatively low operating voltages and frequent output short-circuits, it is preferable the circuit with an additional inductor in the capacitive branch. Also, this topology reduces significantly the harmonics in the capacitor voltage.

In this research we take into consideration the converter having inductances in all three branches of the resonant network: in capacitive – $L_3$, in middle – $L_2$, in inductive – $L_1$. As it will be discussed later, the correct selection of inductor $L_2$ helps to reduce switching losses in the inverter.

Generally, the SM-PSA converter could also be named as a *LLLC* resonant converter.

The most common power circuit of the SM-PSA converter having full-bridge inverter topology is shown in Figure 3.1. As it is seen, the studied *uncontrolled* SM-PSA converter has a simple power circuit.

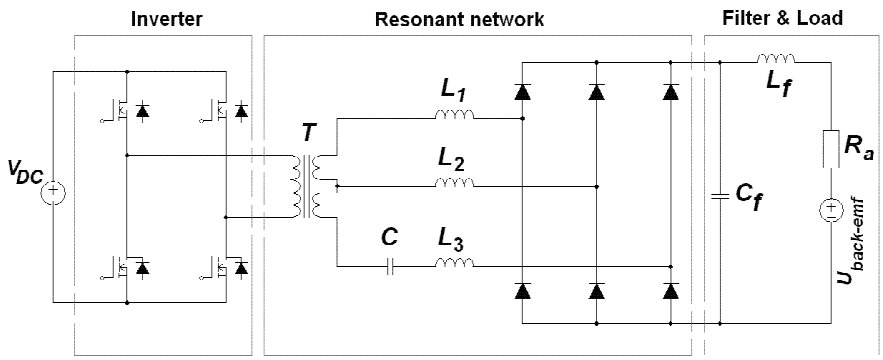


**Figure 3.1 High-frequency PSA converter with full-bridge inverter topology**

The gating circuit, not represented in this figure has a very simple structure, as it contains only a simple PWM block with transistor drivers and without any feedback or control circuits. It is possible due to the properties inherent to the PSA converter, i.e. self-adjusting to load and short-circuit current parametrical limiting.

In this study, output current regulation is implemented by simple changing of the width of gating pulses, not by changing the frequency, as in most high-frequency resonant converters [H3]. Thus, the design of input and output filters is simplified, as the converter has one base switching frequency. However, output current can also be regulated by changing the frequency that will be described briefly at the end of this chapter. Also, a fixed-frequency phase-shifted control method could be implemented, but this variant remains beyond the scope of this work.

As compared to some resonant topologies proposed specially for the power supply of the welding arc, like [PT1, PT3], it is obvious that the SM-PSA converter has an advantage of very simple control circuit.

### 3.1.2 Inverter circuit topology

In principle, the inverter circuit for different power levels could be implemented using different topologies, like single-forward, fly-back, half-bridge, asymmetrical bridge [PT2, AD1]. In the case of single-switch topology like fly-back, transformer flux is improved, as it becomes bidirectional due to the peculiarities of PSA resonant circuits commutations [PT2].

As full-bridge topology delivers twice as much power as half-bridge circuit with the same switch ratings [H7] and has relatively lower losses [H2] it was selected for further analysis and discussions. However, the final selection of topology most appropriate for specific production demands will remain a tradeoff between the unit cost and the parameters of the designed converter.

### 3.1.3 Switching frequency of the inverter

*The key variable – the one inverters address – is frequency. Increasing the frequency of the primary power enables reducing size and mass of the transformer* [W8].

### 3.1.3.1 Discrete reactive components

In the beginning, the acceptable range of switching frequency is to be defined. Generally, with switching frequency high as possible, the values of reactive components in the resonant network become smaller, but on the other hand, there are some practical limitations that should be kept in mind during power supply design. Firstly, with the higher switching frequency, the switching losses are higher. Secondly, with the switching frequency increasing, the influence of the skin and proximity effects in the transformer windings is increased. Thus, non-uniform current distribution in the conductor cross-section may result in increased heating of wires and magnetic components in the case of poor design [HT1, HT3, HT4, HT12].

Thirdly, at some specific frequencies undesirable resonant effects in the transformer windings could arise due to parasitic capacitance in the transformer windings [HT4, HT6].

Fourthly, the permissible operating voltage of real capacitors decreases with the frequency increasing [HT10, HT11]. A polypropylene capacitor was selected for the analysis due to its constant value of capacitance over a wide frequency range. Thus, the example (Figure 3.2) shows that the acceptable RMS voltage for 1 μF capacitor at frequency 40 kHz is only 20% of its rated AC voltage.

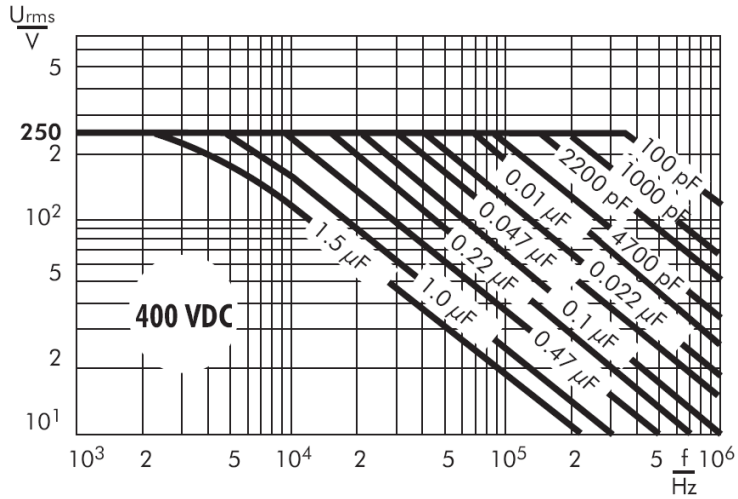


**Figure 3.2 Permissible AC voltages in relation to frequency at 10°C internal temperature rise (polypropylene capacitor FKP4 [HT11])**

Thus, the resonant capacitor operating at high frequency should be carefully selected, in particular for capacitors having relatively large capacitance. In this case, some parallel capacitors could provide a better solution as they have a higher operating voltage and the current sharing between capacitors could reduce losses as well. Another solution is to use a double-transformer topology, as in Figure 2.7, with the resonant capacitor placed on the primary side.

Finally, a high-frequency voltage and its harmonics can lead to possible electromagnetic interference (EMI) with surrounding electronic devices [H3].
The lower level of switching frequency is much easier to define. It is usually desirable to have frequency above the maximum of human audible band, which is about 20 kHz.

### 3.1.3.2 Planar transformer and combined planar *LCT* components

As a result of the efforts to miniaturize electronic devices, planar topologies become more and more popular in modern electronic equipment. Application of specifically designed LCT components is very attractive as they include a required transformer *T*, inductor *L* and capacitor *C* in one body. To reach the lower size and weight of planar components, the switching frequency is usually above 200 kHz [HT2, L1, L3].
Although it is desirable to design and implement the all-in-one *LCT* planar component specific for our SM-PSA converter, it is beyond the intention of the given effort. Only some initial information is introduced here for the proper planar component to be developed. More information on the design and calculation of planar structures could be found, for example, in [HT2, HT8].
The planar transformers have one unique characteristic in their construction [HT8]. Namely, their construction supposes a very precise location of windings and due to this leakage inductances could be predicted and controlled with high accuracy from unit to unit. That is a benefit in SM-PSA converter production. The construction of one *LLCT* planar structure [HT2] is given in Figure 3.3. It also shows has parallel and series resonant circuits are formed in a planar structure.

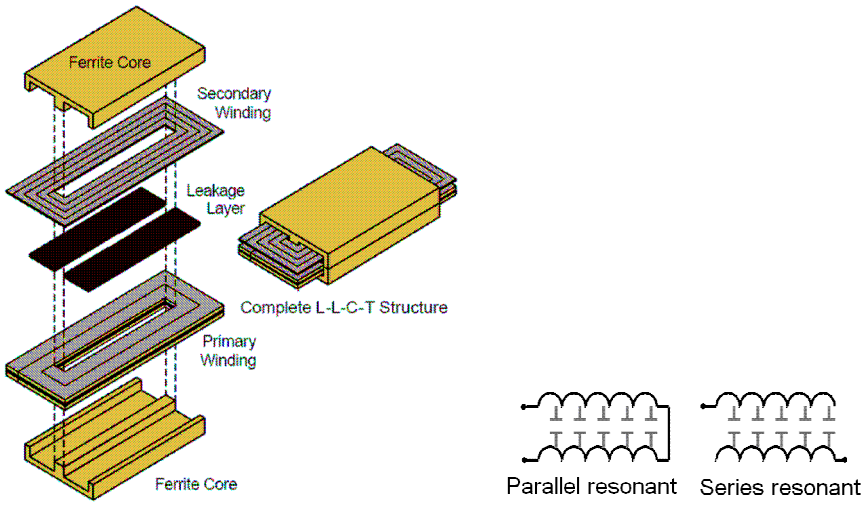


**Figure 3.3 Principles of combined planar structure construction [HT2]**

During the SM-PSA topology design the required capacitance for the resonant capacitor installed on the secondary side may turn out too high for a compact planar structure. In this case, the approach mentioned in the previous chapter is applicable, namely, the capacitor can be moved to the primary side as in

Figure 3.4, and at that, the required capacitance decreases proportionally to the transformer turns ratio squared.

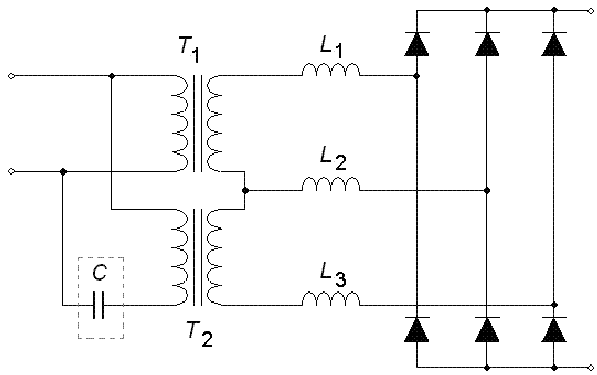


**Figure 3.4 SM-PSA converter with the capacitor on the primary side**

However, two transformers are needed in this case. The other way for the decrease in the capacitance value is to increase the $L_3$ inductance.
As a planar transformer has a relatively small number of turns, often there is only one-turn secondary winding, it has to be supplied with the voltage of sufficiently high frequency to operate with acceptable flux density and magnetizing current. Faraday's law is applicable to planar transformers too and could be used to define the number of turns.

$$N = \frac{U_{peak} \cdot \left(10^4\right)}{K_f \cdot f \cdot A_C \cdot B_{ac}}, \tag{3.1}$$

where
$U_{peak}$ – supply voltage peak value, V,
$K_f$ – waveform coefficient (1 for square wave voltage, 1.11 for sine wave),
$A_c$ – core cross section area, cm$^2$,
$B_{ac}$ – alternating current flux density in the core, T.

### 3.1.4 Conclusion

This study focuses on a resonant network built from discrete components. Considering all the abovementioned facts and a necessity to simulate converter operation during relatively long intervals, switching frequency $f_s$=80 kHz (40 kHz inverter output) was selected both for the computer model analysis and for prototype design and testing. Though higher frequencies are also possible, it is not essential for the study of the SM-PSA converter operation.

## 3.2 Basic calculation procedure for resonant network of a SM-PSA converter

As discussed in the previous chapter, operation of the SM-PSA with an additional inductor in the capacitive branch is more practical when the operating voltage is much lower than the no-load voltage that is to some extent true in the case of arc welding. On the other hand, the inductance connected in series with the resonant capacitor increases voltage on this capacitor that has adverse effect on large capacitances, particularly at high frequencies (Figure 3.2).

The values of reactive components are defined briefly in Chapter 2 and in detail in [PSA1, PSA2]. However, those calculations were developed for a resonant converter having only one additional resonant inductor. As in this work, different topologies of switch-mode PSA converter were studied, the corresponding equations were changed accordingly (leakage inductances are not taken into consideration as they can be added to the inductances of the corresponding series inductors).

The main difference between the SM-PSA converter and the mains frequency PSA converter is in the supply voltage waveform. The mains frequency PSA converter has an ideal or nearly ideal sinusoidal input voltage. The studied SM-PSA converter in its turn is supplied with a quasi-rectangular bidirectional voltage. Thus, the harmonic contents in the supply voltage could be a reason for some deviations between the simulation and calculation results for the converter calculated on the basis of the sine input voltage approach.

However, the first evaluation of reactive component values with assumption that input voltage is of sinusoidal shape usually is a good practice.

First of all, for analysis, the generalized resonant network of the SM-PSA (Figure 3.5 a) could the substituted with the circuit represented in Figure 3.5 b. As it is seen, the output is short-circuited, and, hence, the PSA converter operates entirely in the parallel resonance mode. In this case current conducting circuits remain the same (not changing) during the whole half-cycle of supply voltage. This fact simplifies the calculation procedure for reactive components.

Voltage distribution factor $K_E$=1 and the initial relation of the reactive powers at load short-circuit (with the assumption of sinusoidal supply voltage) is $K_Q$=1.

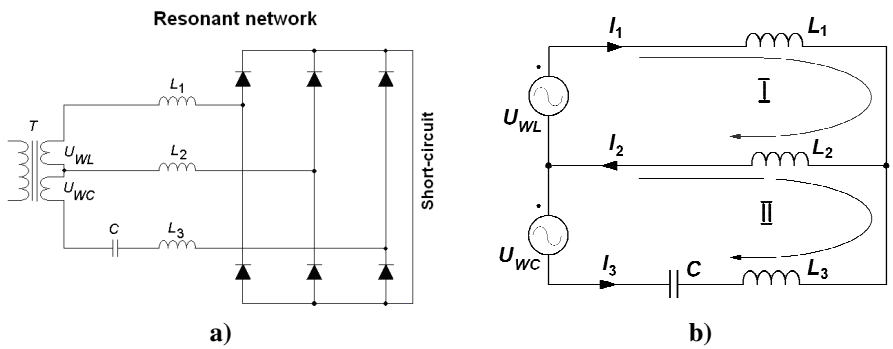


**Figure 3.5 Substitution of short-circuited PSA resonant network (a) by equivalent circuit (b) with the assumption of sine supply voltage and ideal diodes**

The other extreme is an open-circuit shown in Figure 3.6 a and light-load conditions (Figure 3.6 b) are also taken into account during the evaluation.

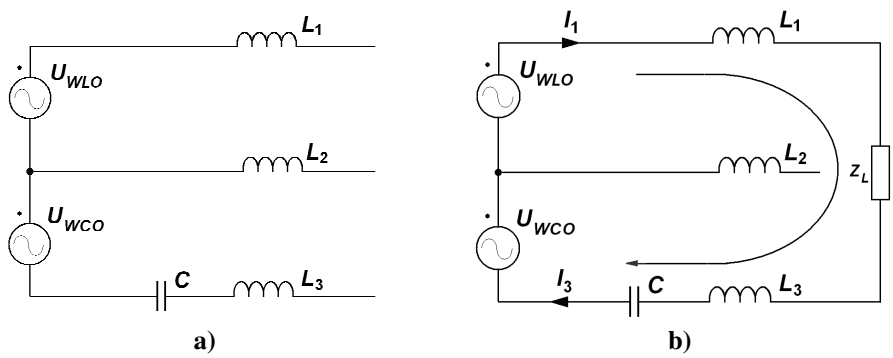


**Figure 3.6 Equivalent PSA circuit for no-load (a) and light-load conditions (b)**

The output voltage of the converter at no-load or light-load is a sum of two secondary winding voltages (voltage sources $U_{WC}$ and $U_{WL}$ in the equivalent circuit). Here, at light-load the converter is operating in entirely series resonance mode.

First, updating expressions 2.7–2.9 in accordance with the new resonant topology that incorporates resonant inductors in each branch, the following equations are derived:

$$x_{L1}^{*} = \frac{K_E \cdot (K_Q + 1)}{(K_E + 1)^2 \cdot (K_E K_Q (1 + K_{L2}) + K_{L2})}, \tag{3.2}$$

$$x_{L2}^{*} = K_{L2} \cdot x_{L1}^{*}, \tag{3.3}$$

$$x_{L3}^{*} = K_{L3} \cdot x_{L1}^{*}, \tag{3.4}$$

$$x_{C}^{*} = K_{L3} \cdot x_{L1}^{*} + K_E^2 \cdot \left[ \frac{K_Q + 1}{(K_E + 1)^2} \right] + K_{L2} \cdot x_{L1}^{*} \cdot (1 + K_E \cdot K_Q). \tag{3.5}$$

Then, considering that that operation during the output short-circuit (Figure 3.5) is of more interest to welding, the relative short-circuit impedance can be calculated according to the expression

$$x_{SC}^{*} = x_{L1}^{*} + x_{L2}^{*} \tag{3.6}$$

Next, the equation defining the base impedance $Z_B$ of the resonant converter follows

$$Z_B = \frac{(U_{WLO} + U_{WCO})/2}{I_{sc}/2\sqrt{2}} = \frac{\sqrt{2}(U_{WLO} + U_{WCO})}{I_{SC}}, \tag{3.7}$$

where $I_{SC}$ is a desirable output short-circuit current.

Finally, multiplying the corresponding relative value by the relation of the base impedance to the relative short-circuit impedance we can find absolute values for the resonant components in the first estimation

$$x_{L,C} = x^*_{L,C} \cdot \frac{Z_B}{x^*_{SC}} \tag{3.8}$$

The most complicated task here is the selection of appropriate parameters $K_{L2}$ and $K_{L3}$. In any case, the values of resonant components should be checked and refined with the help of computer simulation. In a simplified approach $L_2$ could be neglected, but, as it will be discussed further, the presence of $L_2$ is desirable to improve the switching performance of the inverter. Along with that, changing of $K_Q$ could be useful during the search for an optimal operation, of the converter, output characteristics and to define the relation of the short-circuit current to the rated load current.

Solving the equations given above with the set of parameters $K_{L2}$ and $K_{L3}$ varying from 0 up to 1 (0 to 100%) and setting $K_E$=1, $K_Q$=1, the 3D plots represented in Figures 3.7 – 3.8 were constructed.

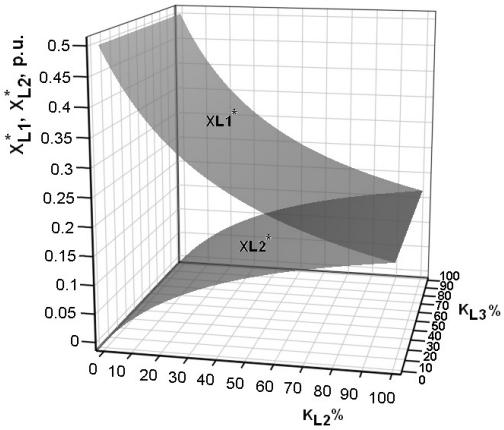


**Figure 3.7 Reactance of inductors $L_1$ and $L_2$ as a function of inductance distribution factors $K_{L2}$ and $K_{L3}$**

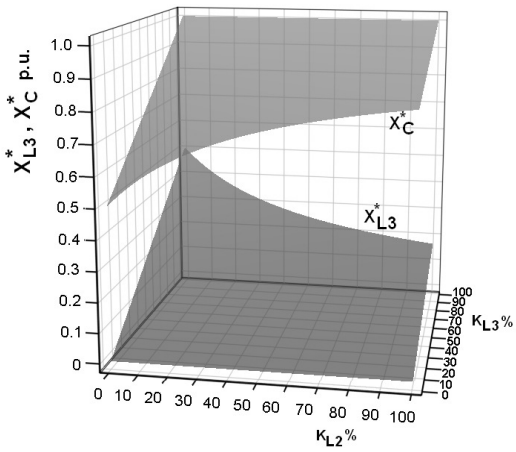


**Figure 3.8 Reactance of inductor $L_3$ and capacitor $C$ as a function of inductance distribution factors $K_{L2}$ and $K_{L3}$**

As a result of the analysis of Eqs. 3.2–3.3 and the corresponding plots in Figure 3.7, it is suggested that the relative reactance of main inductor $L_1$ depends on the factor $K_{L2}$ value, thus, with $K_{L2}$ increasing the inductance of $L_1$ decreases exponentially, while the relative reactance of $L_2$ increases exponentially. The value of $K_{L3}$ is not important here, but it must be taken into account during the calculation of the light-load operation (Figure 3.6) or defining the voltage on the resonant capacitor.

The nature of the relative reactance $x^*_{L3}$ in Figure 3.8 is more complicated as it depends on both factors $K_{L2}$ and $K_{L3}$. Relative reactance $x^*_{L3}$ has the highest value when $K_{L3}$ is at its maximum while $K_{L2}$ is minimal. The minimal value of $x^*_{L3}$ occurs when $K_{L3}$ is equal to zero regardless of the $K_{L2}$ value.

The relative reactance of the capacitor $C$ shown also in Figure 3.5 is also the function of both factors $K_{L2}$ and $K_{L3}$. The reactance of the capacitor is the largest and consequently capacitance the smallest, if $K_{L3}$ is of maximal value.

These plots in Figures 3.7–3.8 and expressions (3.2–3.5) allow a rough selection of the reactive components. To define the values of $C$, $L_1$, $L_2$ and $L_3$ more accurately, computer simulation is needed. After simulation, if necessary, the base impedance $Z_B$ can be correspondingly changed to achieve the desired output characteristics. As mentioned above, $K_Q$ variation can also be used to obtain better or more optimal characteristics for the specific converter loads.

However, at present, practical selection of the reactive components is a tradeoff between the acceptable operating voltage on the resonant capacitor and the values of resonant inductances.

The values of reactive components in the resonant circuit, as in Figure 3.1, could be very simply calculated, provided the secondary windings of the transformer have the same voltages. The example of such calculation for different topologies of resonant circuit is given in Table 3.1.

**Table 3.1 Calculation procedures for different topologies of the SM-PSA converter**
Parameters: $f_{sw}$=40 kHz, $U_{WLO}$=$U_{WCO}$=40 V, goal: $I_d$=150 A (±2%), $I_{sc}$=(180–225 A)

| *Topology* | *Simplest topology* $L_1C$ | *Series additional inductor in capacitive branch.* $L_1L_3C$ | *Full topology* $L_1L_2L_3C$ |
|---|---|---|---|
| Schematic | 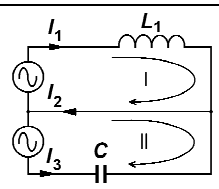 | 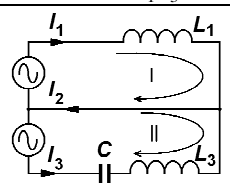 | 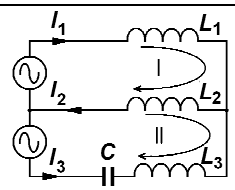 |
| Equation system | $\begin{cases} I_1 + I_3 = I_2 \\ U_{WL} = I_1 \cdot X_{L1} \\ U_{WC} = -I_3 \cdot (-X_C) \end{cases}$ | $\begin{cases} I_1 + I_3 = I_2 \\ U_{WL} = I_1 \cdot X_{L1} \\ U_{WC} = -I_3 \cdot (X_{L3} - X_C) \end{cases}$ | $\begin{cases} I_1 + I_3 = I_2 \\ U_{WL} = I_1 \cdot X_{L1} + I_2 \cdot X_{L2} \\ U_{WC} = -I_3 \cdot (X_{L3} - X_C) - \\ - I_2 \cdot X_{L2} \end{cases}$ |

| | | | |
|---|---|---|---|
| Initial values of reactive elements for $Z_B = \frac{U_{WCO}}{I_{sc}/2\sqrt{2}}$ $K_E$=1, $K_Q$=1 | $x^*_{SC} = x^*_{L1} = x^*_C$<br><br>$X_C$=0.629 Ohm<br>$X_{L1}$=0.629 Ohm | $x^*_{SC} = x^*_{L1} = \lvert x^*_C - x^*_{L3} \rvert$<br><br>$X_{L1}$=0.629 Ohm<br>$X_C$ =0.629+$X_{L3}$<br>$X_{L3}$=0.251 Ohm<br>$X_C$=0.88 Ohm | $x_{L1} + 2 \cdot x_{L2} + (x_{L3} - x_C) = 0$<br><br>set $K_{L2}$=0.5 &<br>$K_{L3}$=0.12<br>$X_{L1}$=0.419 Ohm<br>$X_{L2}$=0.21 Ohm<br>$X_{L3}$=0.05 Ohm<br>$X_C$=1.3 Ohm |
| *Simulation no 1* | $I_{weld}$=135 A<br>$I_{sc}$=180 A | $I_{weld}$=146 A<br>$I_{sc}$=194 A | $I_{weld}$=92 A<br>$I_{sc}$=135 A |
| Correction 1 | new $Z_B$=0.556<br><br>$X_C$=0.556 Ohm<br>$X_{L1}$=0.556 Ohm | new $K_Q$=0.95<br><br>$X_{L1}$=0.629 Ohm<br>$X_{L3}$=0.251 Ohm<br>$X_C$=0.849 Ohm | $Z_B = \frac{U_{WCO}}{I_{sc}/2}$<br>$X_{L1}$=0.296 Ohm<br>$X_{L2}$=0.148 Ohm<br>$X_{L3}$=0.036 Ohm<br>$X_C$=0.92 Ohm |
| *Simulation no 2* | $I_{weld}$=152 A<br>$I_{sc}$=202 A | $I_{weld}$=152 A<br>$I_{sc}$=201 A | $I_{weld}$=130 A<br>$I_{sc}$=192 A |
| Correction 2 | - | - | new $K_Q$=0.63<br>$X_{L1}$=0.296 Ohm<br>$X_{L2}$=0.148 Ohm<br>$X_{L3}$=0.05 Ohm<br>$X_C$=0.72 Ohm |
| *Simulation no 3* | - | - | $I_{weld}$=153 A<br>$I_{sc}$=215 A |

According to this table, at least one correction step is required to achieve the desired output characteristics. Both the base reactance $Z_B$ and the factor $K_Q$ can be varied to achieve this goal. The diagrams given below are to help define the value of the capacitor and the inductor for $L_1L_3C$ and $L_1L_2L_3C$ topologies.

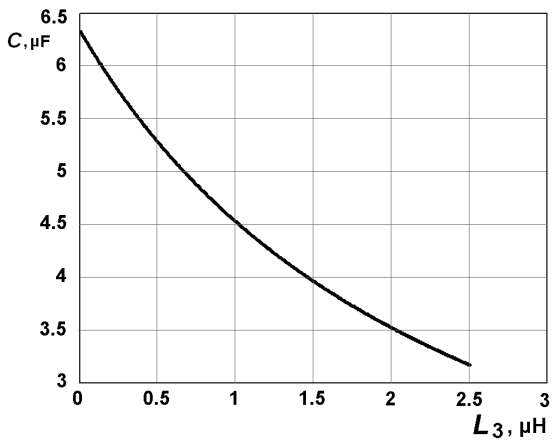


**Figure 3.9 Value of resonant capacitor *C* in relation to the inductance of the inductor $L_3$ for $L_1L_3C$ topology**

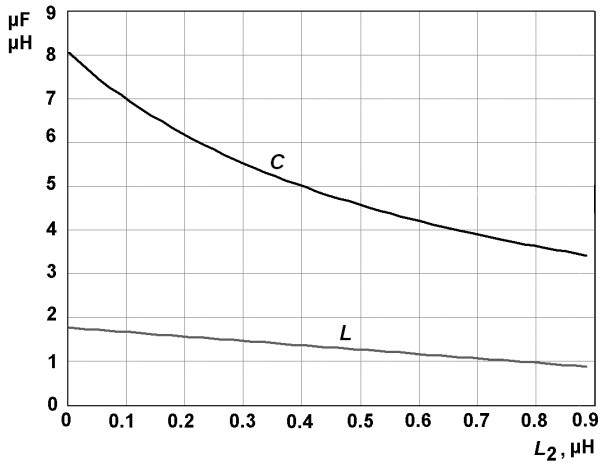


**Figure 3.10 Value of resonant capacitor *C* and resonant inductor $L_1$ in relation to the inductance of inductor $L_2$ for $L_1L_2L_3C$ topology**

Figure 3.10 shows that with the inductance of the additional inductor increasing the values of the required resonant capacitance *C* and the main inductance $L_1$ decrease.

The following diagrams (Figures 3.11.-3.14) show the simulated characteristics of the converters having the parameters calculated in Table 3.1.

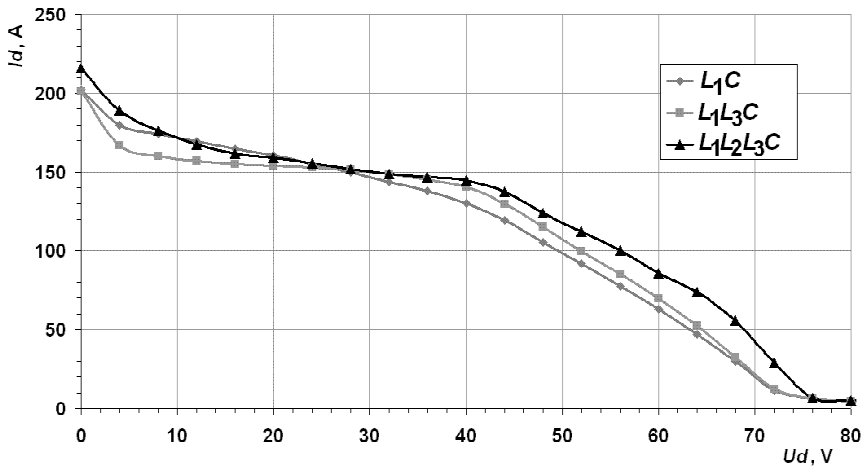


**Figure 3.11 Output characteristics for different resonant network topologies**

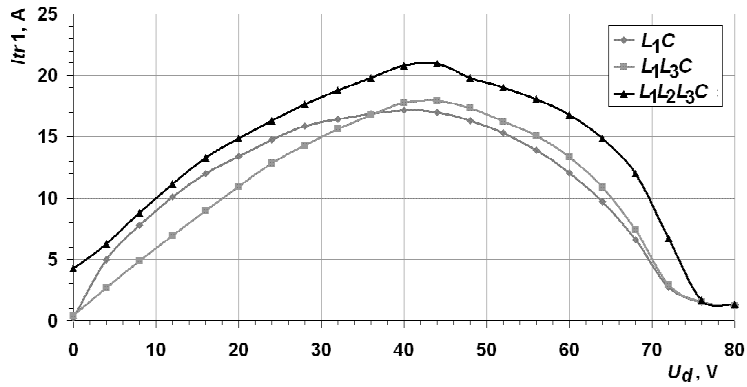


**Figure 3.12 Current through transformer primary winding for different resonant network topologies**

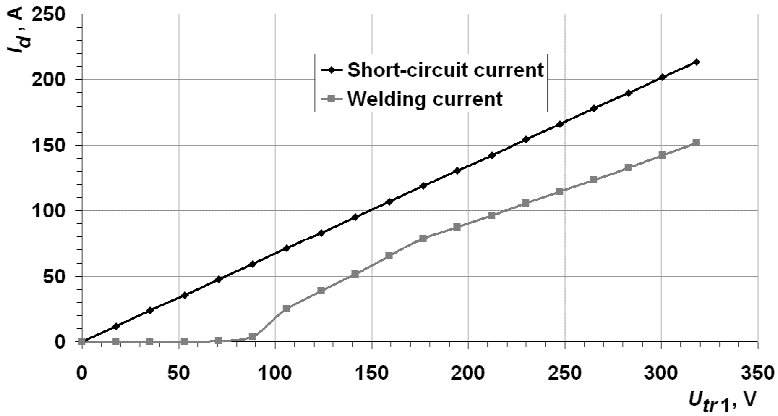


**Figure 3.13 Regulation characteristic for $L_1L_2L_3C$ topology**

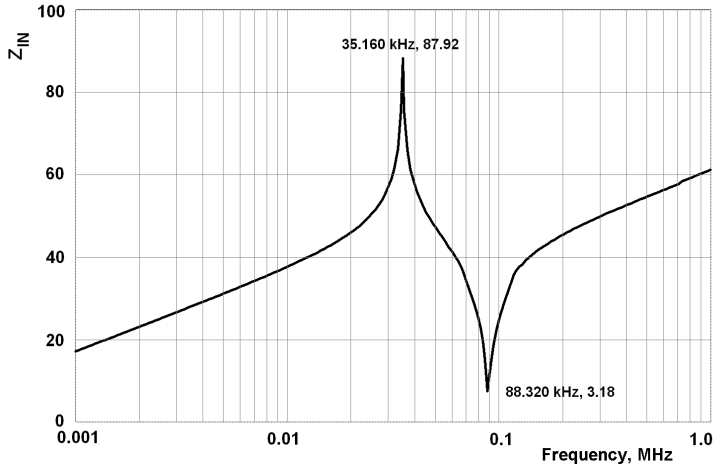


**Figure 3.14 Frequency response of $L_1L_2L_3C$ topology in a short-circuit mode ($Z_{IN}$ – input impedance)**

Simulation results in Figures 3.11 and 3.12 show that no significant difference between various *LC* topologies in the case of sinusoidal supply voltage occurs.
The study described in this part was conducted with the assumption of the sinusoidal voltage power source, instead of the quasi-square wave voltage inherent to the inverter power source. However, this assumption simplifies significantly the estimation and calculation of resonant component values as only the fundamental component is taken into account. Further refining of the values of inductors and capacitor is possible by the simulation of corresponding computer model with the full-bridge inverter power source that will be described in the next part.
The resonant network of SM-PSA converter can have different topologies in terms of placement and values of additional inductors. At that, the values of resonant components could vary in a wide range in different topologies, while the output characteristics remain almost the same (Figure 3.11). Transformer primary current $I_{tr1}$(Figure 3.12) is slightly higher for $L_1L_2L_3C$ topology because of its substantially different factor $K_Q$ equal to 0.63. Regulation curve introduced in Figure 3.13 was obtained by changing the input sine voltage $U_{tr1}$ amplitude value. It has almost a linear nature and as is shown, the same correlation between the short-circuit current and welding current is kept until the voltage on the secondary windings of transformer decreases below minimal operating voltage.
The frequency response of short-circuited SM-PSA converter with the $L_1L_2L_3C$ topology is given in Figure 3.14, where one local maximum at 35.160 kHz and one local minimum at 88.320 kHz are clearly visible. This information could be useful during the design of the switch-mode PSA converter, in particular in case of output regulation by frequency control.

## 3.3 Some features in the design of the inverter transformer

### 3.3.1 Selection of transformer no-load voltage

As stated at the beginning of this chapter, the suggested load is a DC welding arc, thus the defining of the required output voltage is based on the properties of welding arc. As it is known [W2, W3], the voltage of the MMA welding process could vary from zero at short-circuit and up to no-load voltage, which is defined by converter parameters. There are some guidelines for output voltage selection:

- the value of no-load voltage must be sufficiently high to keep welding at lower currents [PSA7, W2];
- during manual arc welding arc length fluctuations occur, and consequently, to obtain a stable welding arc it is beneficial to have a sufficiently high no-load voltage;
- however, maximal no-load voltage must be limited to meet safety standards, so for example according to the *British Safety Standard 638, Part 10, from 1990* or to *ГОСТ Р МЭК 60974-1-2004* (equivalent to *EN60974-1*), no-load DC voltage cannot exceed the value of 113 V.

No-load voltages of modern MMA inverter power supplies [W4-W7] range from 50 to 90 VDC. It should be noticed that for safety reasons some of the power supplies have automatic voltage reduction at no-load or if output circuit resistance exceeds 200 Ohm.
Based on the abovementioned, value of summed output no-load voltage selected for the transformer secondary windings equals 80 V.

### 3.3.2 Distribution factor $K_E$

In most switching power supplies having transformers with tapped secondary windings, the secondary turns are equal, thus, usually the voltage distribution factor $K_E$ is 1. In general, there is no reason to change this parameter and in this study $K_E$ is equal to 1.

### 3.3.3 Leakage inductance

In contrast to the common trend to reduce leakage inductance in power electronic transformers some leakage inductance is useful for resonant converters as it could be used to replace fully or partly additional inductors, as $L_1$ and $L_3$ in a SM-PSA converter (Figure 3.1). Here we describe some basic techniques for leakage induction estimation in the case of typical transformer construction with E or U cores.

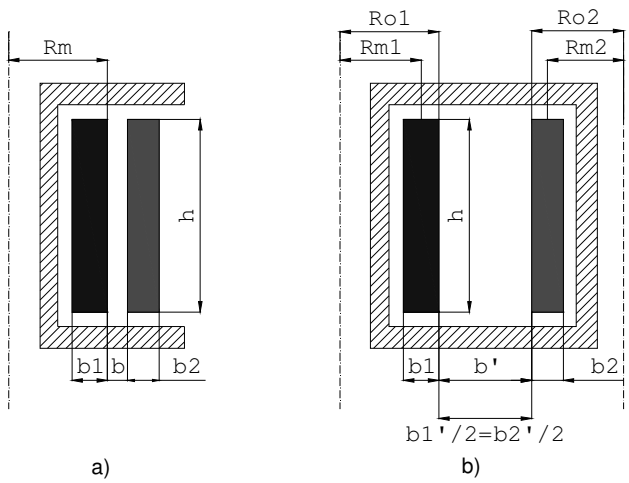


**Figure 3.15 Coaxial windings (a) and windings placed on different limbs of the transformer (b)**

In the first approximation leakage inductance for coaxial windings placed on the round core (coaxial placement), as in Figure 3.15 a, could be calculated according to [HT6]

$$L_s = \frac{\mu_0}{2\pi h} N^2 p \left( b + \frac{b_1 + b_2}{3} \right), \tag{3.9}$$

where $p=2\pi R_m$.
If the leakage inductance of coaxial windings is not sufficient to substitute the resonant inductor, it could be increased by placing windings on different limbs

of one core. The approximate calculation of leakage inductances for similar windings placed on different limbs of one magnetic core, as in Figure 3.15 b, could be made with the following equation [HT6]:

$$L_s = \frac{\mu_0}{h} N^2 \left( R_m \frac{b_1 + b_2}{3} + b' \left( R_o + \frac{b'}{2} \right) \right), \tag{3.10}$$

Also, leakage inductance of the transformer winding can be increased by using a core with an air gap [HT13]. For rectangular cores (Figure 3.16), which are common for power electronic transformers, the another equation (3.11)

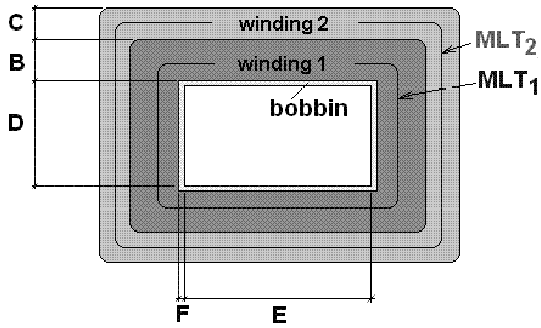


**Figure 3.16 Cross-section of rectangular coaxial windings**

$$L_s = \frac{\mu_0}{h} N^2 MLT \left( b + \frac{b_1 + b_2}{3} \right), \tag{3.11}$$

can be used, where according to [HT8] the mean length turn (MLT) could be found by the expressions

$$MLT_1 = 2(D+2F) + 2(E+2F) + \pi B, \tag{3.12}$$

$$MLT_2 = 2(D+2F) + 2(E+2F) + \pi(2B+C) \tag{3.13}$$

However, these expressions are only a rough estimation of leakage inductance values. To obtain more accurate results, a corresponding 3D computer model of the transformer must be created and solved by one of the FEM programs, as shown, e.g. in Figure 3.17.

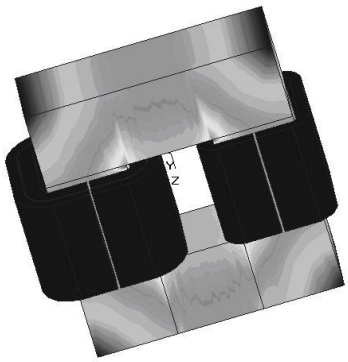

**Figure 3.17 A 3D model of a high-frequency transformer solved by *MagNet* software *(Infolytica Ltd)***

Certainly, the most accurate and reliable results can be obtained after appropriate testing of a ready-built transformer; the test procedures could be found, e.g. in [HT6, HT7, HT9]. Moreover, in order to meet the design goal such as high power density, special attention must be paid to core and winding loss mechanisms and thermal issues [HT14].

### 3.3.4 Inductance of wires or busbars in the resonant network

In addition to transformer leakage, the inductance of connecting conductors in the resonant network must be taken into account, especially at higher switching frequencies (>100 kHz). Usually, for high currents, rectangular busbars such as in Figure 3.18 are used.

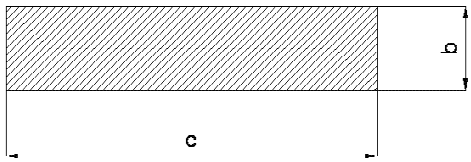


**Figure 3.18 Cross-sectional area of a rectangular busbar**

The Litz wire is also sometimes used for skin and proximity effects mitigation, but it is not typical because of its high cost. Calculation of flat busbar inductance suggested in [HT5] is presented below. The equation for the inductance of a rectangular non-magnetic conductor at high frequencies is

$$L = \frac{\mu_0 l}{2\pi}\left(\ln\frac{2l}{\breve{g}} - 1\right), \tag{3.14}$$

where
$l$ – busbar length,
$\breve{g}$ – geometrical coefficient defined from the chart in Figure 3.19.

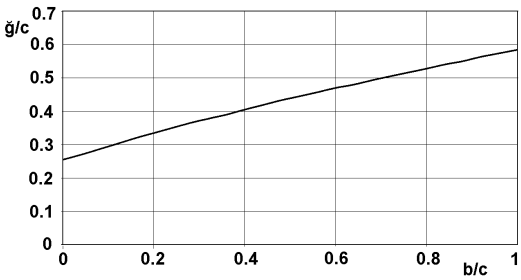


**Figure 3.19 Coefficient for busbar inductance calculation**

For instance, an inductance of busbar having the length of $l$=10 cm, width $b$=15 mm and height $h$=2 mm is calculated. The result obtained is $\breve{g} = 0.31 \cdot c$ and according to equation 3.14 the inductance of this busbar yields 55 nH.

To summarize, it is important to take into account both leakage inductance of transformer and inductances of connecting conductors in the resonant network of SM-PSA converter. Their values could be sufficient to constitute the required resonant components or, in the worst case, spoil the normal operation of the converter, especially at higher frequencies.

## 3.4 Comparison of different resonant topologies of a SM-PSA converter

As compared to the SM-PSA converter analyzed in section 3.2, the inverter circuit in a real SM-PSA converter produces a voltage of quasi-rectangular waveform instead of the sine voltage.

In this part different topologies of the resonant part in a switch-mode PSA converter will be compared because of the following reasons:

1) their output characteristics and regulation characteristics,
2) minimization of switching losses in the inverter switches,
3) special attention will be paid to the resonant capacitor voltage.

Along with the steady-state analysis, a transient behavior of the switch-mode PSA is also described in this part. As the load of the SM-PSA converter is a welding process, so it could be conditionally represented by three main states, namely

1) short-circuit ($I_d$=150–200 A, $U_d$=0 V),
2) welding (maximal $I_d$=150 A, $U_d$=26 V),
3) no-load or open-circuit ($I_d$=0 A, $U_d$=80 V),

Thus, these states will be under consideration during the simulation and analysis of the converter operation.

### 3.4.1 $L_1L_3C$ resonant network

#### 3.4.1.1 Output and regulation properties

The resonant network of SM-PSA converter studied first contains two resonant inductors $L_1$ and $L_3$, as shown in Figure 3.20. The inductance value of $L_3$ will be varied to explore its influence on the converter properties.

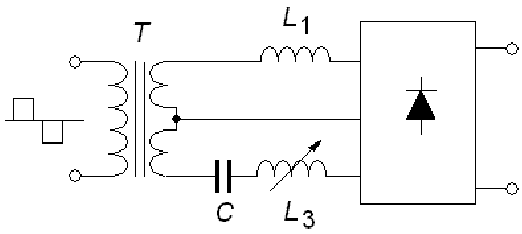


**Figure 3.20 $L_1L_3C$ resonant network of SM-PSA**

However, in the middle branch there is always some small inductance present that is not absolutely neglected and taken into account during the simulation of the computer model. It consists 3% of $L_1$ inductance.

Here, with the $L_3$ varying values of the resonant capacitance $C$ and inductance $L_1$ remain the same that means changing of $K_Q$.

A computer model with the following parameters was created:

$U_{dc}$=320 V – rectified and smoothed mains (AC 230 V) voltage supplied to the inverter input,

$t_d$=2 μs – pause between gating pulses in the inverter diagonals or “dead time”,

$K_E$=1 – voltage distribution factor, $K_Q$=variable – reactive power distribution factor,
$K_T$=8:1:1 – transformer turns ratio,
$Z_b$=0.41 – base impedance of the resonant converter,
$K_{L2}$=0.03,
$K_{L3}$ varies from 0 up to 1 p.u. of $L_1$.
Simply changing the value of $K_{L3}$ leads to the changing of other resonant components values. To avoid this, factor $K_Q$ must change with $K_{L3}$ changing according to the following table:

| $K_{L3}$ | 0.03 | 0.1 | 0.2 | 0.3 | 0.4 | 0.5 | 0.6 | 0.7 | 0.8 | 0.9 | 1 |
|---|---|---|---|---|---|---|---|---|---|---|---|
| $K_Q$ | 1.23 | 1.16 | 1.07 | 0.98 | 0.88 | 0.79 | 0.69 | 0.6 | 0.5 | 0.41 | 0.32 |

The table shows that in the given case a linear dependence $K_Q$=1.26 – 0.94·$K_{L3}$ between $K_Q$ and $K_{L3}$ exists. The diagram in Figure 3.21 shows the effect of the value of $K_{L3}$ ($K_Q$) on the load current both during welding and during short-circuit.

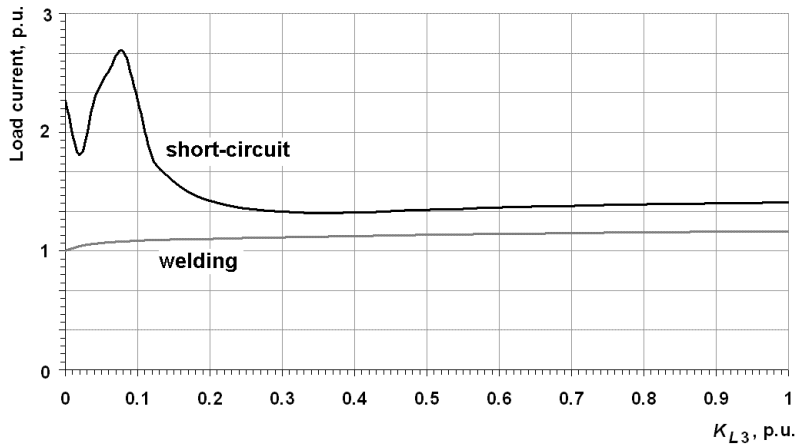


**Figure 3.21 Output current in relation to $K_{L3}$ in $L_1L_3C$ resonant circuit (simulation)**

Figure 3.21 shows that the short-circuit current is "unstable" in the range of low $K_{L3}$ (from 0 to 0.2) or the same at $K_Q>1$. In this range, the peak value of short-circuit current could even exceed the welding current more than 2.5 times. Thus, the range of reasonable $K_{L3}$ starts from 0.2 p.u. Further selection of optimal $K_{L3}$ is a tradeoff between the installed capacitance and the maximal acceptable voltage on this resonant capacitor $C$. As it is suggested to have voltage on the resonant capacitor $C$ acceptable for the real capacitor, the $K_{L3}$ value was selected equal to 0.28.
To achieve the welding current of 150 A indicated at the beginning of the chapter, parameter $Z_B$ was increased by 7%, reaching 0.44. Other parameters remained the same. Calculating equations 3.2–3.5 with the suggested coefficients, we obtain relative values of resonant components and using equations 3.6–3.7, the absolute values given in Table 3.2.

**Table 3.2 Values of resonant components in the $L_1L_3C$ resonant network for $K_{L3}$=0.28, $K_Q$=1.**

| *Relative values* | *Base impedance $Z_B$* | *Absolute values* |
|---|---|---|
| $X_{L1}^* = 0.472$ | 0.44 (modified) | $L_1$=1.7 μH |
| $X_{L2}^* = 0.014$ | | $L_2$=0.05 μH |
| $X_{L3}^* = 0.132$ | | $L_3$=0.48 μH |
| $X_C^* = 0.66$ | | $C$=6.6 μF |

The output characteristic for the $L_1L_3C$ SM-PSA converter having these parameters is represented in Figure 3.22.

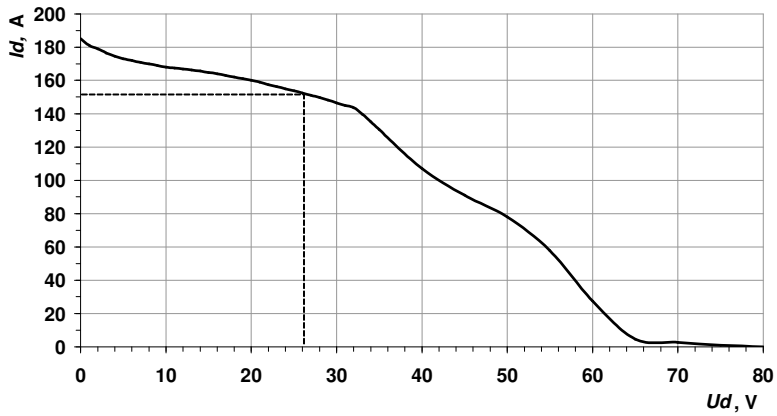


**Figure 3.22 Output characteristic of the $L_1L_3C$ SM-PSA converter**

It is seen that the short-circuit current is only 20–25% higher than the welding current. It corresponds to the general requirements for the welding source [PSA7, W2, W3].

The regulation characteristic introduced in Figure 3.23 for the given converter was obtained by changing the width of the gating pulses of the switches. The curves show that the short-circuit current is not changing significantly with the pulse width changing and only at the relative pulse width lower than 0.25 ($t_d$>9.5 μs) it starts decreasing. Thus, even at small welding currents the short-circuit current could be comparatively large, this fact should be taken into account during real prototype design. The welding current decreases more or less linearly with the pulse width decreasing.

The "unregulated" segment in short-circuit current curve ($a$ = 0.44…0.76 in Figure 3.23) could probably be explained by the injection of higher harmonics inherent to the quasi-square voltage waveform produced by the inverter.

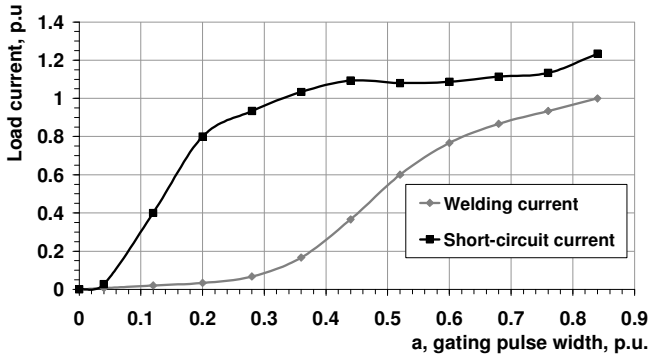


**Figure 3.23 Regulation characteristic for the $L_1L_3C$ SM-PSA converter**

To select the optimal inductance $L_3$ for the topology $L_1L_3C$ the following diagram was constructed by computer simulation.

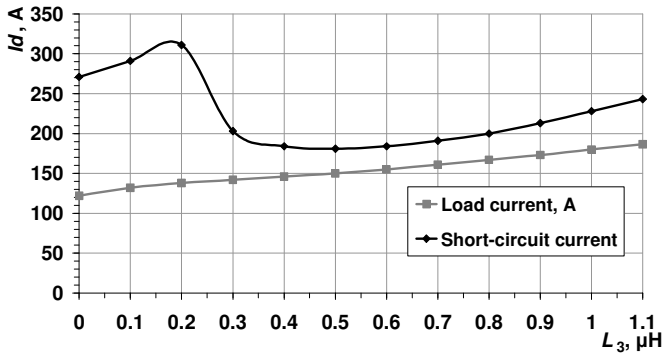


**Figure 3.24 Dependence of welding and short-circuit currents on $L_3$ value**
**$L_1$=1.7 μH, $L_2$=0.05 μH, $L_3$=varying, $C$=6.6 μF, $Z_B$=0.44**

As it is seen, Figure 3.24 corresponds to Figure 3.21. It confirms that the reasonable range for inductance $L_3$ starts from 0.4–0.5 μH since the short-circuit current becomes too high at lower values of $L_3$. The optimal $L_3$value is 0.5 μH.

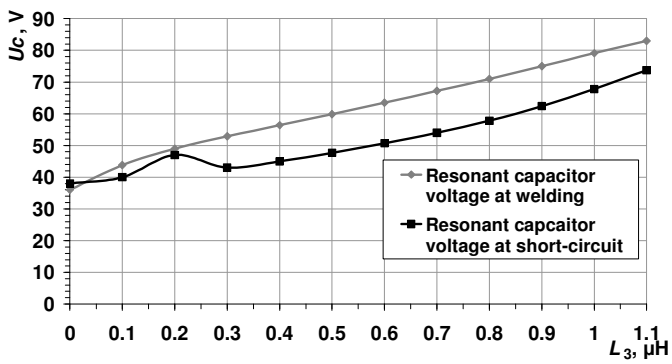


**Figure 3.25 Resonant capacitor voltage at different $L_3$ values**

Figure 3.25 shows that the voltage on the resonant capacitor is higher during welding and increases linearly with $L_3$ increasing. Thus, for resonant topology $L_1L_3C$, the reasonable range for inductance $L_3$ is between 0.2 and 0.3 of $L_1$ inductance (0.3 μH–0.5 μH in Figure 3.24).

### 3.4.1.2 Operation in the switching cycle

To receive a more complete picture of the processes taking place in the inverter of the SM-PSA converter it is useful to know the waveforms of currents and voltages in the inverter switches. To explore the possible shapes of inverter current waveforms, the converter model was simulated with the abovementioned parameters and $L_3$ – varying from 0 up to 65% at full load ($a$=0.84 or $t_d$=2 μs). The results of the simulation are given in Figure 3.26.

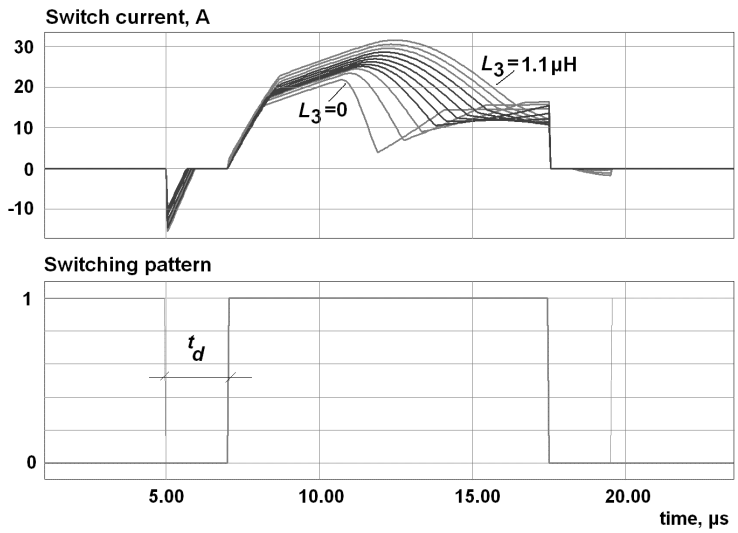


**Figure 3.26 Inverter switch current waveform (including reverse diode) during welding at different values of $L_3$**

In the analysis of waveforms in Figure 3.26 it becomes obvious that despite the resonant nature of the converter circuit, currents in switches do not naturally cross zero and at the turn-off instant they are about at half of their peak value.

During short-circuit, as depicted in Figure 3.27, the RMS value of the switch current for most $L_3$ values will be even lower than during welding, that corresponds to the PSA converter behavior. However, its value at the turn-off instant could be very high especially at small values of $L_3$ (here, maximum turn-off current is at $L_3$=0.2 μH). Thus, the optimal value of $L_3$ in view of turn-off current minimization is between 0.5 μH and 0.9 μH.

As it is seen, during short-circuit a current through the switch has a higher frequency than the switching frequency due to higher oscillating frequency of the circuits forming the resonant network at short-circuit.

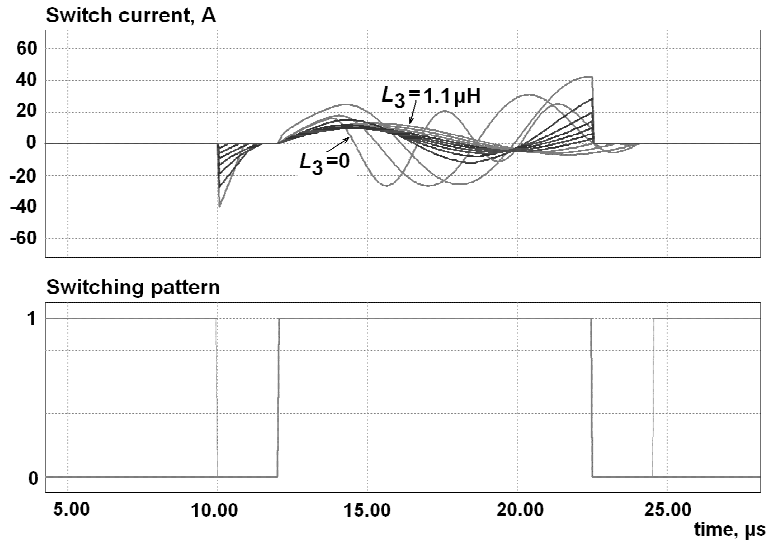


**Figure 3.27 Inverter switch current waveform (including reverse diode) during short-circuit at different values of $L_3$**

### 3.4.1.3 Conclusion

In view of ZCS implementation, the $L_1L_3C$ topology with simple PWM control is not appropriate and it could be conditionally named as a "half-hard switching". Also, the value of $L_3$ must be carefully selected, on the one hand, to avoid excessive short-circuit currents and on the other hand, to limit voltage on the resonant capacitor, or in other words, $K_Q$ must be equal to 1 or less ($K_Q \leq 1$). In addition, to have more "soft" switching characteristic at the short-circuit, the value of $L_3$ must be higher than 0.3 μH ($K_Q < 1$).

### 3.4.2 $L_1L_2C$ resonant circuit

#### 3.4.2.1 Output and regulation properties

The next topology presented differs from the previous one as it includes the additional resonant inductor $L_2$ in the middle branch while no additional resonant inductor in the capacitive branch is present. The corresponding resonant circuit shown in Figure 3.28 will be discussed in this part. The inductor $L_2$ is shown variable as its value selection effect on converter parameters will be studied.

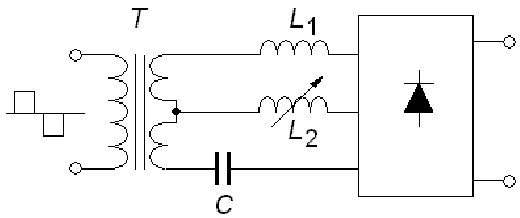


**Figure 3.28 $L_1L_2C$ resonant network of SM-PSA**

A small inductance consisting 3% of $L_1$ inductance and representing leakage and/or inductance of connectors in the capacitive branch is taken into account during simulation.

The following parameters were used for simulation:

$U_{dc}$=320 V – rectified and smoothed mains (AC 230 V) voltage supplied to the inverter input,

$t_d$=2 μs – pause between gating pulses in the inverter diagonals or "dead time",

$K_E$=1 – voltage distribution factor, $K_Q$=variable – reactive power distribution factor,

$K_T$=8:1:1 – transformer turns ratio,

$Z_B$=0.4 – base impedance of the resonant converter,

$K_{L3}$=0.03,

and $K_{L2}$ varying from 0 up to 1, the diagram shown in Figure 3.29 was created.

Similarly to the previous topology, in the range of low values of the additional inductance $L_2$ (from 0 up to 0.4 of $L_1$), the short-circuit current could be excessively high as compared to the welding current.

Thus, the acceptable range for MMA welding would start from $L_2$ equal to 0.5 μH. In Table 3.3, relative and absolute values of resonant components are optimized on the basis of the information depicted in Figure 3.29.

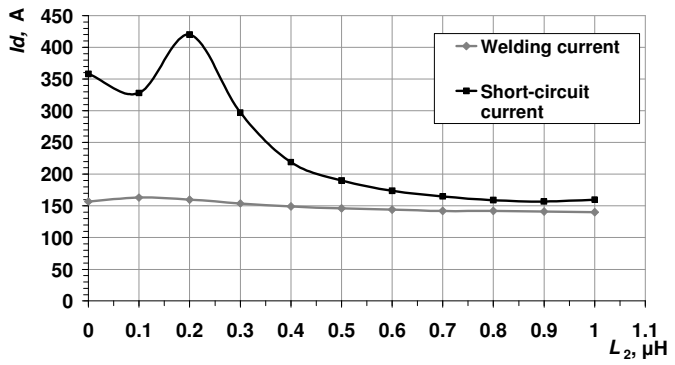


**Figure 3.29 Dependence of welding and short-circuit currents on $L_2$ value $L_1$=1 µH, $L_2$=0.05 µH, $L_3$=varying, $C$=6.6 µF**

**Table 3.3 Values of resonant components for $K_{L2}$=0.5, $K_O$=0.61**

| *Relative values* | *Base impedance $Z_B$* | *Absolute values* |
|---|---|---|
| $X_{L1}^* = 0.284$ | 0.4 | $L_1$=1 µH |
| $X_{L2}^* = 0.142$ | 0.4 | $L_2$=0.5 µH |
| $X_{L3}^* = 0.008$ | 0.4 | $L_3$=0.05 µH |
| $X_C^* = 0.64$ | 0.4 | $C$=6.6 µF |

The output characteristic for the $L_1L_2C$ SM-PSA converter with these parameters is shown in Figure 3.24.

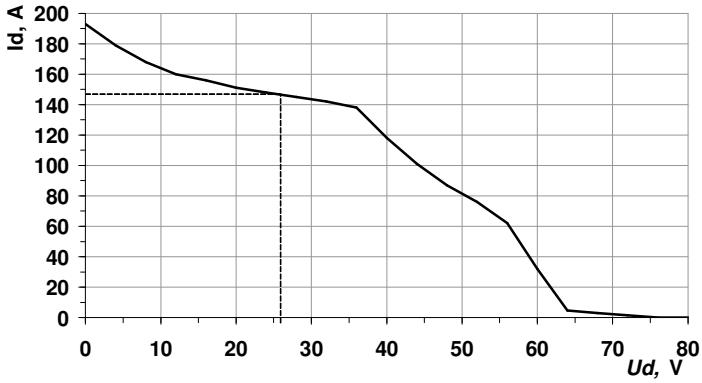


**Figure 3.30 Output characteristic of the $L_1L_2C$ SM-PSA converter**

It is seen that the output characteristic is similar to the characteristic of the $L_1L_3C$ circuit in Figure 3.22. But in the load voltage range 20–30 V inherent to the welding process, the load current with the $L_1L_2C$ circuit changes less (about 2 times) as compared to the $L_1L_3C$ circuit.

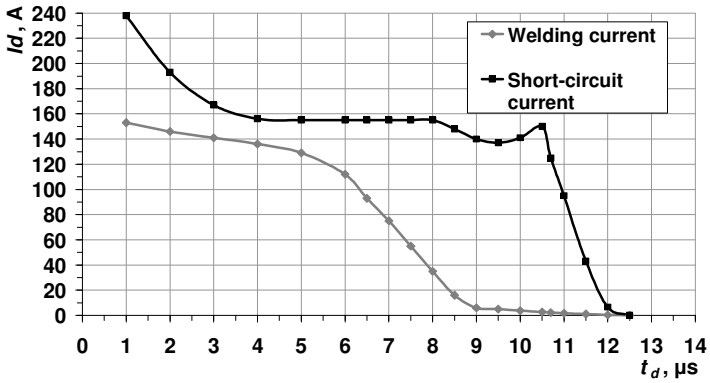


**Figure 3.31 Regulation characteristic for $L_1L_2C$ SM-PSA converter**

The regulation characteristic introduced for the given topology (Figure 3.31) differs from the previous one as it is less linear. It is also represented as a function of "dead time" between gating pulses. It could be conventionally divided into three linear parts, the first before $t_d$=5.5 µs, the second between 5.5 and 9 µs and the last one from 9 to 12.5 µs. It is also shown that at lower than 2 µs "dead time" short-circuit current grows much faster as compared to the welding current. Short-circuit current curve, in its turn, could be divided into three conditionally linear parts. Thus, the second part, between 4 µs and 10.5 µs, shows that current is not responding to changing in the gating pulse width. In general, the process of changes in short-circuit current does not correspond to changes in the welding current.

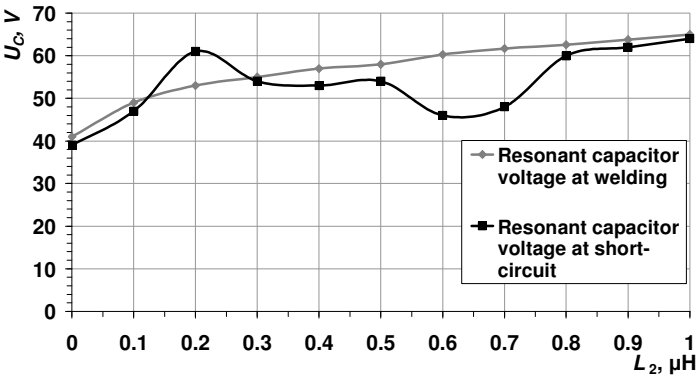


**Figure 3.32 Resonant capacitor *C* voltage during welding and short-circuit as a function of $L_2$ value**

The diagram depicted in Figure 3.32 shows that resonant capacitor voltage increases with $L_2$ increasing. Or it could be concluded that with $K_Q$ decreasing voltage on the capacitor increases. Thus, based on the output characteristics and resonant capacitor voltage in the resonant $L_1L_2C$ topology, the reasonable range for the inductance $L_3$ is between 0.5 and 0.8 of $L_1$.

### 3.4.2.2 Operation in the switching cycle

Current waveforms through inverter switches for the $L_1L_2C$ topology were studied. A converter model was simulated with the parameters given above and $L_2$ – varying from 0 up to 100% at full load ($a$=0.84 *or* $t_d$=2 μs). The results of the simulation are given in Figures 3.33 and 3.34.

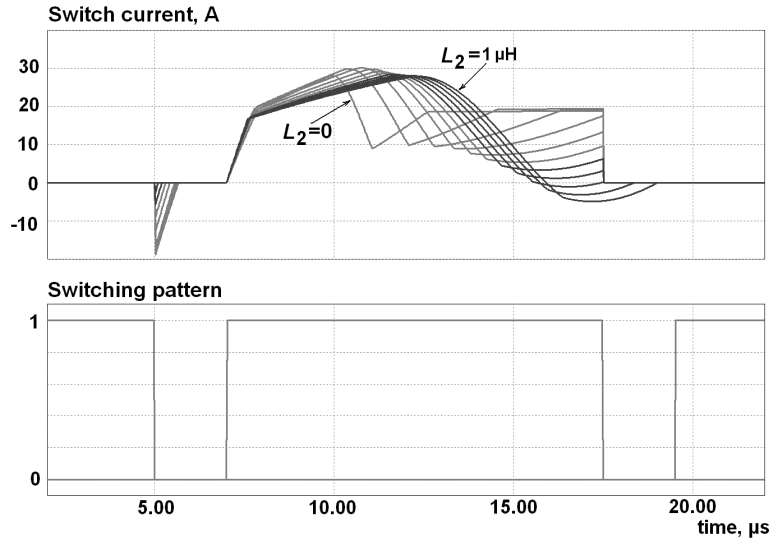


**Figure 3.33 Inverter switch current waveform (including reverse diode) during welding at different values of $L_2$**

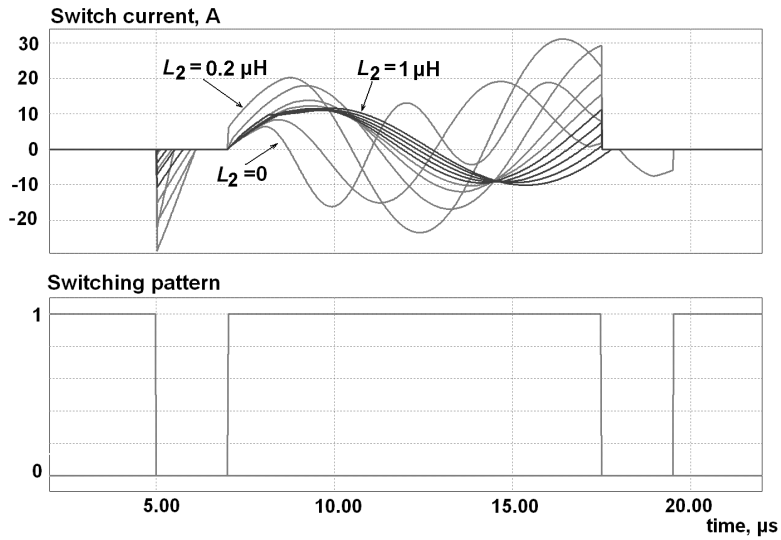


**Figure 3.34 Inverter switch current waveform (including reverse diode) during short-circuit at different values of $L_2$**

From the analysis of the waveforms in Figure 3.33 it is obvious that the switch current naturally crosses zero when $L_2$ value is higher than 0.8 μH. Hence, it is possible to implement a ZCS technique for this $L_1L_2C$ topology having an additional inductor $L_2$ with sufficient inductance.

Analogously to the $L_1L_3C$ topology, during the short-circuit process the current in the switch has oscillations with a frequency higher than the switching frequency, as shown in Figure 3.34. The smaller $L_2$ is the higher the frequency of oscillation. The most favorable shape of the current and current value at the turn-off instants here is also at $L_2$ values equal or higher than 0.8 μH. Also, seen that during short-circuit at $L_2$=0.2 μH the switch current has the "worst" shape that corresponds to the maximal value of short-circuit current, as represented in Figure 3.29. Regarding turn-off losses minimization the best value of $L_2$ in the case of short-circuit is 0.9 μH (0.9 of $L_1$)

#### 3.4.2.3 Conclusion

A conclusion can be drawn that the $L_1L_2C$ topology is appropriate for ZCS implementation, provided the value of $L_2$ is correctly defined. Here, the optimal value of $L_2$ consists almost 80% of the main inductance value. One of the drawbacks is the significant increase of the relation of the short-circuit current to the welding current during regulation at higher $t_d$.

### 3.4.3 $L_1 L_2 L_3 C$ resonant circuit

#### 3.4.3.1 Output and regulation properties

The last topology we review is the $L_1L_2L_3$C resonant circuit. In this topology additional inductors are placed in each branch of the resonant network, as shown in Figure 3.35.

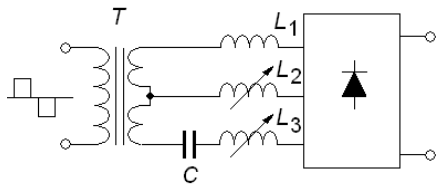


**Figure 3.35 $L_1L_2L_3C$ resonant SM-PSA network**

First of all let us define an acceptable value for the resonant inductor in the capacitive branch $L_3$. Figures 3.25 and 3.32 show that an increases in the resonant capacitor voltage is more pronounced for the $L_1L_3C$ circuit with the additional inductance growing. Thus, it would be reasonable to keep $L_3$ as small as possible. Based on this consideration, the factor $K_{L3}$ we select is equal to 0.2 for the $L_1L_2L_3C$ topology.

The parameters of the simulated circuit are: $U_{dc}$=320 V, $t_d$=2 μs, $K_E$=1, $K_T$=8:1:1, $Z_B$=0.4. Varying $K_{L2}$ from 0 up to 1, the diagram shown in Figure 3.36 was created.

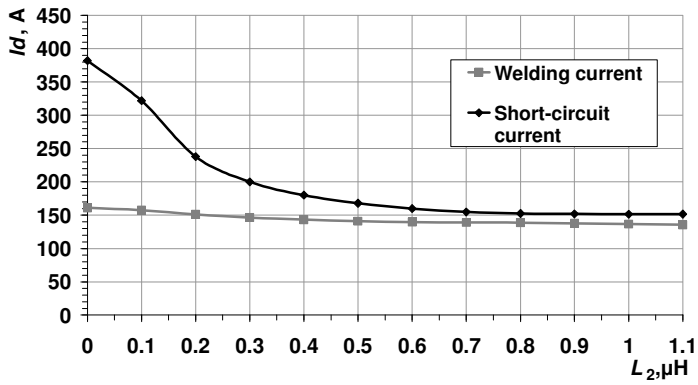


**Figure 3.36 Dependence of the welding and short-circuit currents on the $L_2$ value for $L_1L_2L_3C$ topology $L_1$=1.1 μH, $L_2$ varying from 0 to 100% of $L_1$, $L_3$=0.2 μH, $C$=6.6 μF**

Curves presented in Figure 3.36 show that even at low $L_3$ (selected below the optimal range for the $L_1L_3C$ topology) and $L_2$ starting from 0.3 μH (0.27 of $L_1$), the welding and short-circuit currents are in good correlation.

The next step is to define resonant capacitor voltages for different $L_2$ values. The corresponding simulation results are presented in Figure 3.37.

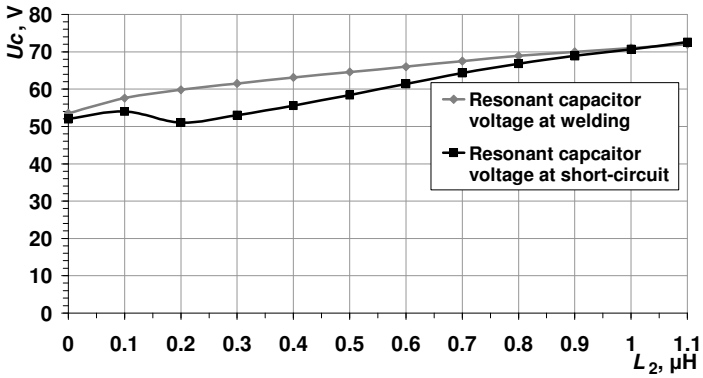


**Figure 3.37 Dependences of resonant capacitor voltage on the $L_2$ value**

Taking into account the results both in Figures 3.36 and 3.37 we can conclude that the reasonable range of the inductance $L_2$ starts from 0.3 μH ($K_{L2}$=0.27), as at lower $L_2$, short-circuit current becomes too high. Regarding to the acceptable capacitor voltage, the maximal advisable value of $L_2$ is about 0.7 μH ($K_{L2}$=0.63).

**Table 3.4 Optimal values of resonant components in $L_1L_2L_3C$, $K_O$=0.92**

| *Relative values* | *Base impedance Z* | *Absolute values* |
|---|---|---|
| $X_{L1}^* = 1$ | 0.4 | $L_1$=1.1 μH |
| $X_{L2}^* = 0.63$ | 0.4 | $L_2$=0.7 μH |
| $X_{L3}^* = 0.18$ | 0.4 | $L_3$=0.2 μH |
| $X_C^* = 2.2$ | 0.4 | $C$=6.6 μF |

The output characteristic for the $L_1L_2L_3C$ SM-PSA converter with the parameters given in Table 3.4 is shown in the Figure 3.38.

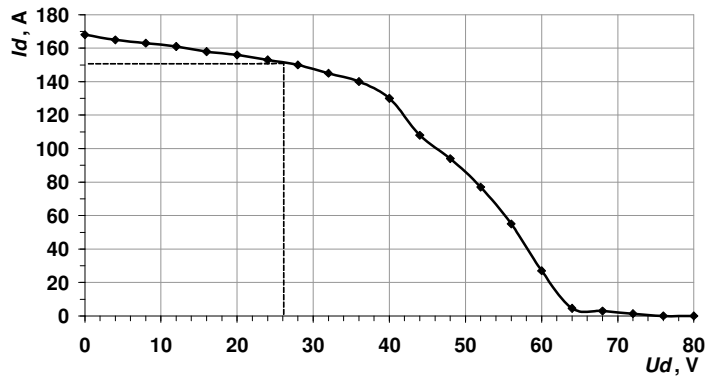


**Figure 3.38 Output characteristic of the $L_1L_2L_3C$ SM-PSA converter**

The represented characteristic fits well for manual arc welding. It is characterized by inherent short-circuit current limitation as the two previous

(Figures 3.30 and 3.22) ones and has a relatively slightly changing current in the welding range (load voltage 20–30 V).
The next diagram in Figure 3.39 shows the effect of the regulation of the welding (short-circuit) current on the changes in the gating pulse width.

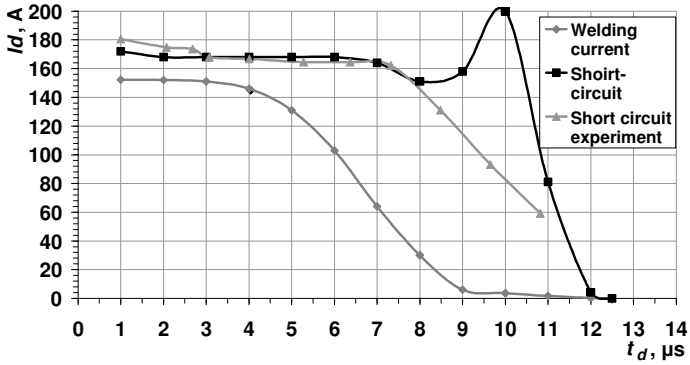


**Figure 3.39 Regulation characteristic for the $L_1L_2L_3C$ SM-PSA converter (simulated and measured)**

The regulation characteristic for the welding current of converter with the $L_1L_2L_3C$ topology could be conventionally divided into three more or less linear parts, the first below $t_d$=4 µs, the second between 4 and 9 µs and the last one from 9 to 12.5 µs. The short-circuit current curve simulated is of interesting nature, as it has a sudden current peak near $t_d$=10 µs or, in other words, at very "narrow" quasi-square supply voltage. Probably, it could be explained by some specific errors in the created model or in simulation software, as it is seen that the experimentally defined short-circuit current curve has no such a peak. Short-circuit current, in its turn, can be divided into two linear parts, one from 1 to 7 µs and the other from 7 to 11 µs. In addition, there is an output power of the converter with the $L_1L_2L_3C$ topology shown in Figure 3.40.

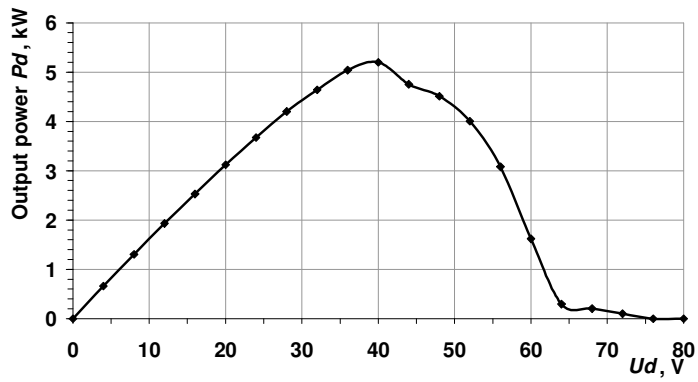


**Figure 3.40 Output power of the $L_1L_2L_3C$ SM-PSA converter in relation to the load voltage ($t_d$=2 µs)**

It is obvious that the converter has an ample reserve of power that is an advantage in view of obtaining a stable welding arc.

### 3.4.3.2 Operation in the switching cycle

As in the previous parts, the current through the switch will be discussed for the $L_1L_2L_3C$ topology too. Simulated switch currents are shown in Figures 3.41 to 3.43.

The converter model was simulated with the parameters given above in Table 3.4 and $L_2$ – varying from 0 up to 100% at full load ($a$=0.84 or $t_d$=2 μs).

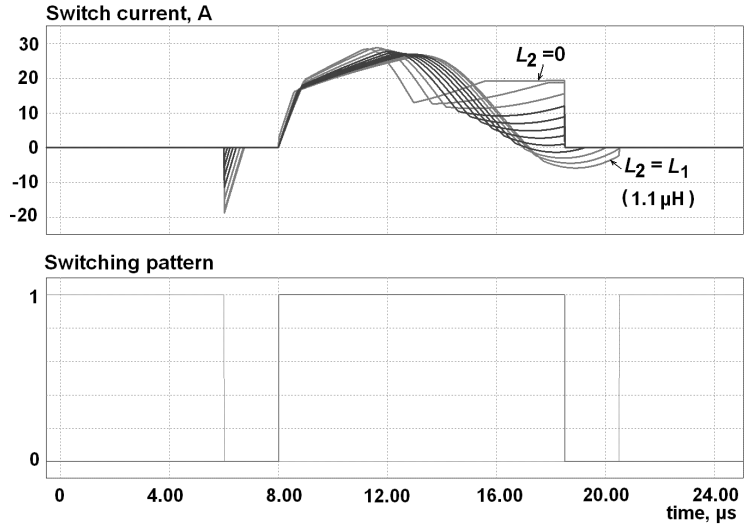


**Figure 3.41 Inverter switch current (including reverse diode) during welding at different values of $L_2$**

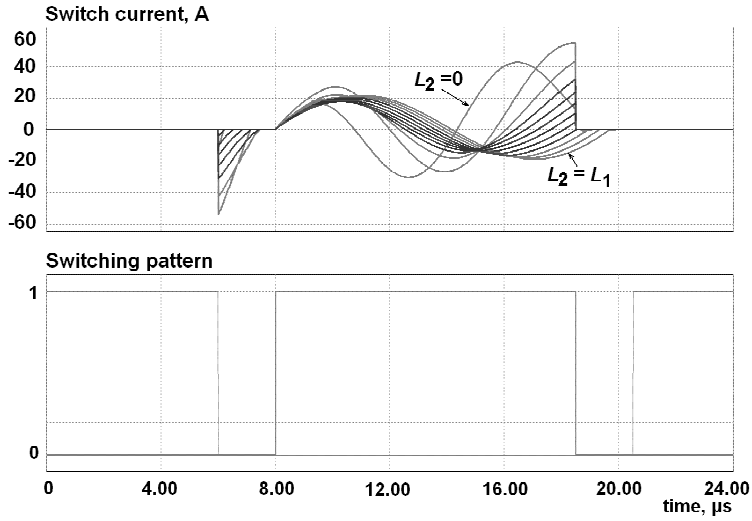


**Figure 3.42 Inverter switch current (including reverse diode) during short-circuit at different values of $L_2$**

As the load voltage during the welding process is in permanent change due to the fluctuations in the electric arc length, an additional oscillogram of the switch current versus the load voltage for the converter with the $L_1L_2L_3C$ topology is used, shown in Figure 3.43.

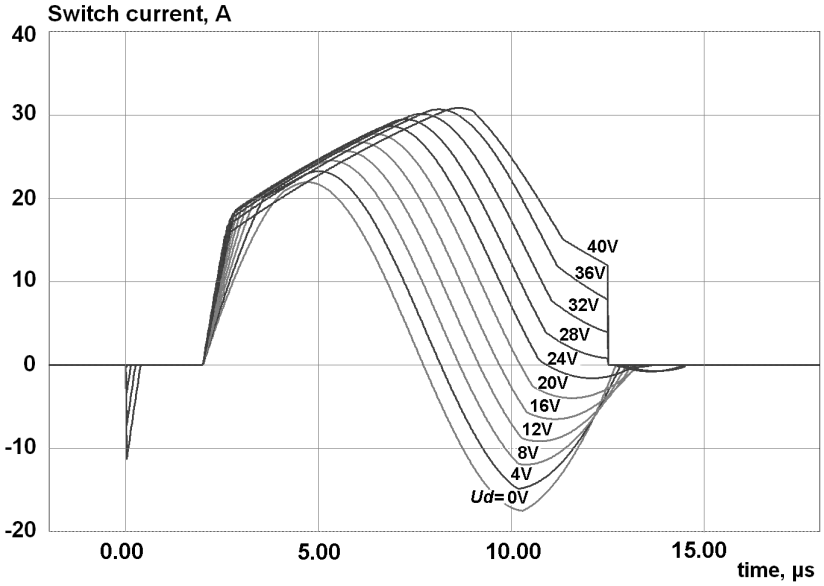


**Figure 3.43 Switch current waveforms (including reverse diode) for different values of load voltage $U_d$ ($L_1L_2L_3C$ parameters as in Table 3.4)**

The value of $L_2$ in Figure 3.41 corresponding to the ZCS condition is near 0.7 µH. Also this value is appropriate for the short-circuit operation (Figure 3.42). A lower value of the $L_2$ inductance will lead to the switching losses increment. A higher value of $L_2$ is basically acceptable if the resonant capacitor tolerates a higher voltage (Figure 3.37).

The switch current waveforms at different load voltages for optimally selected resonant components in the $L_1L_2L_3C$ circuit are given in Figure 3.43. Thus we obtain a ZSC condition during the welding process when the arc voltage could vary in a relatively wide rage (usually from 0 to 35 V for 150 A welding arc). The ZCS if the inverter switch is possible up to the arc voltage 28 V, which is higher than the nominal voltage for 150 A arc equal to 26 V. Thus, during the welding process ZCS is achievable in the whole voltage range and only at higher voltages inherent to cutting process ZCS is no longer running. However, the value of the switch current at the turn-off instant is less than half of its peak value.

In conclusion, the $L_1L_2L_3C$ topology is also appropriate for ZCS implementation if the corresponding value of additional resonant inductor is correctly defined. At that, the distribution factor of the reactive power for the short-circuit mode remains less than one or $K_Q$<1.

### 3.4.4 Summary of different SM-PSA converter *LC* topologies

In this part, three different resonant topologies of the SM-PSA were introduced. The topology with an additional resonant inductor in the middle branch is preferable regarding switching losses minimization, as it facilitates ZCS implementation. With an appropriate selection of the additional resonant inductor $L_2$ current through switch crosses zero naturally before the turn-off instant. However, this condition is valid for a relatively narrow range during the regulation of the output power by the changing in the width of gating pulses. Extension of the ZCS range during the output regulation could be the next step in the converter development. Another artifact of such output an regulation, as compared to regulation with the sine supply voltage as in Figure 3.13, during short-circuit is a zone of output current "non-responding" to changes in the width of gating pulses, as in Figures 3.23, 3.31, 3.39. Most probably it could be explained by higher harmonic contents in the inverter voltage that is changing together with the width of the gating pulse. The variations of higher harmonics in the quasi-rectangular waveform can be represented according to the diagram below.

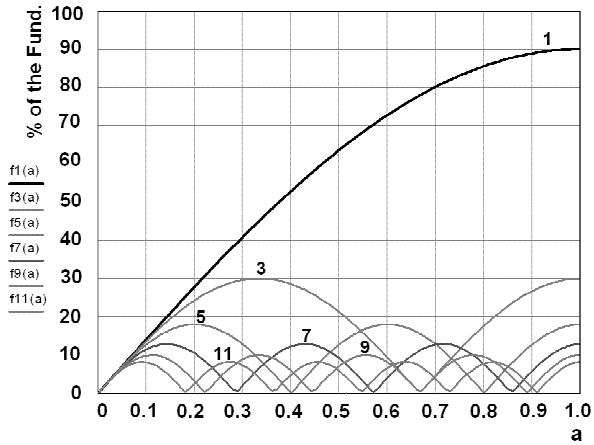


**Figure 3.44 Harmonics of "quasi"– rectangular waveform versus pulse width (*a*=1 for rectangular waveform)**

This diagram along with a frequency characteristic given in Figure 3.14 (page 44) allows one to conclude that the $3^d$, $5^{th}$ and $7^{th}$ harmonics of the inverter voltage are in the range of low input impedance of the PSA resonant circuit and, thus, even at the inverter voltage RMS value decreasing, the output current during short-circuit will receive an extra higher-frequency current injection causing the output current "non-responding" to the regulation.

Capacitor voltage depends mainly on the additional inductance value, the larger the value of the additional inductor ($L_2$ or $L_3$) the higher the voltage on the

resonant capacitor. At that, the $L_1L_3C$ topology has a higher voltage on the resonant capacitor as compared to the other two topologies.
If a constant current is advantageous for a specific welding process, the $L_1L_2L_3C$ topology has a better output characteristic because output current changes slightly in the range from short-circuit to welding (Figure 3.38).

It can also be concluded that for the $L_1L_2C$ and $L_1L_2L_3C$ topologies, the values of resonant inductors must be selected in accordance with the equation

$$\frac{L_1}{L_2 + L_3} \leq 1.2\,, \tag{3.15}$$

to achieve a ZCS in the range of the load voltage from 0 up to 0.35 p.u. of the no-load voltage.

Finally, it is to be remind that all of these output characteristics and other parameters were obtained by the converter having no feedbacks or special control circuits, but just due to the characteristics of the PSA converter operation, as described in Chapter 2.

## 3.5 Transients during the welding process

### 3.5.1 Inverter circuit

The next step in describing the properties of the proposed SM-PSA converter is to study its operation under load variations. As we develop the source for manual arc welding, consequently the load is an electric arc, which is characterized by a wide range of output voltage variations and relatively fast changes between the three main states (short-circuit, welding and no-load). In order to verify converter operation during welding, the corresponding computer model was created and simulated. The simulation results are presented in the next figures.

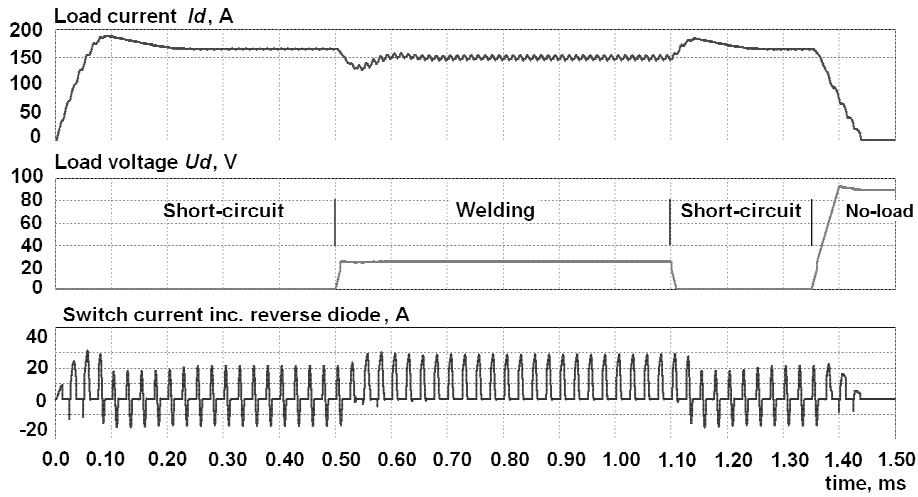


**Figure 3.45 Effect of short-circuit, welding and no-load transients to the current in the switch for the $L_1L_2L_3C$ topology with ZCS ($C$=6.6 μF, $L_1$=1.1 μH, $L_2$=0.7 μH, $L_3$=0.2 μH, $t_d$=2 μs)**

This figure does not show the voltage on the inverter switch as it is not changing significantly and has no stresses during transients. The current through the switch does not exceed its nominal value regardless the load condition or transient process. This confirms that switches in the inverter cannot be overloaded. At this, no current control is needed and current limitation occurs parametrically due to the PSA resonant network peculiarities.

### 3.5.2 Resonant network

It is also interesting to investigate processes in the resonant components during the transients in order to check if the current surges or overvoltages are present. A process analogous to that in Figure 3.45 was simulated. Currents through the resonant network elements, and also, the capacitor voltage are shown in the following pictures.

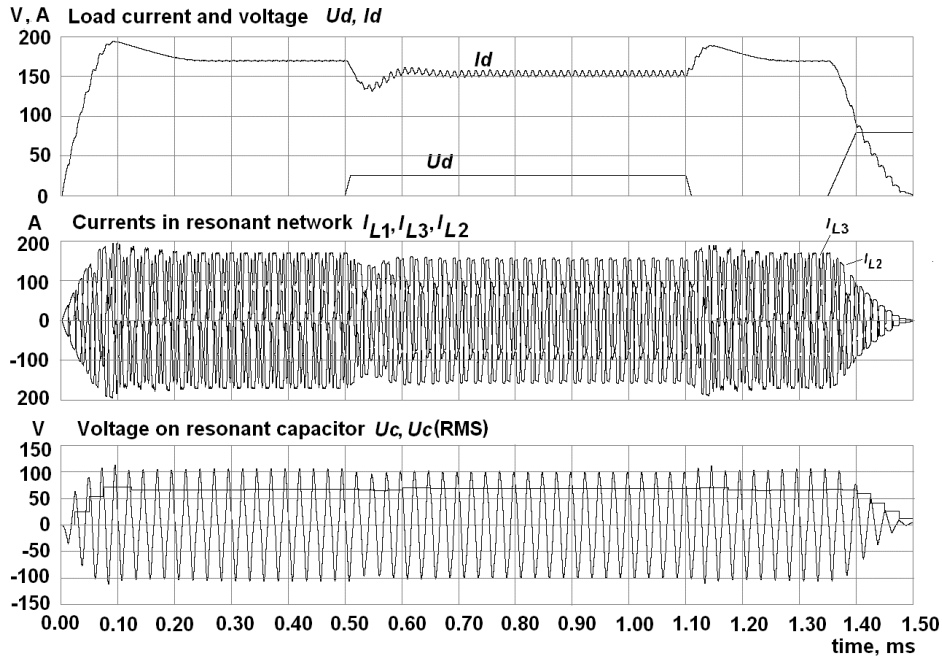


**Figure 3.46 Effect of short-circuit, welding and no-load transients on currents in the resonant part of the SM-PSA converter with ZCS ($C$=6.6 μF, $L_1$=1.1 μH, $L_2$=0.7 μH, $L_3$=0.2 μH, $t_d$=2 μs)**

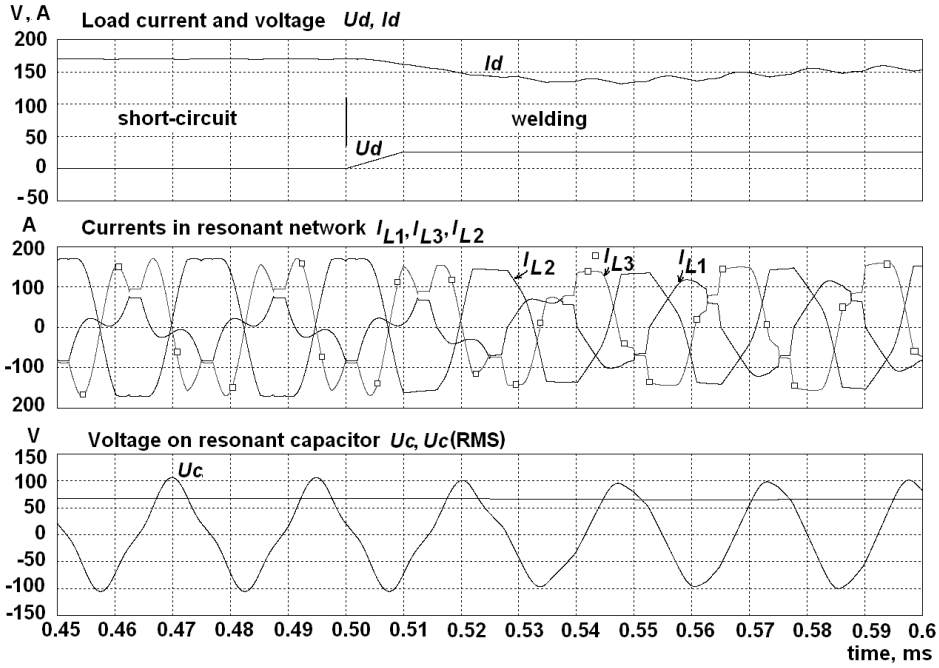


**Figure 3.47 Instant of transition from short-circuit to welding for the SM-PSA converter with ZCS ($C$=6.6 μF, $L_1$=1.1 μH, $L_2$=0.7 μH, $L_3$=0.2 μH, $t_d$=2 μs)**

Figures 3.46 and 3.47 show waveforms of currents and voltages in the resonant part of the SM-PSA converter during the welding process. As it is seen, currents and voltages of the resonant elements have their maximal values during short-circuit. However, these values do not exceed more than 20% values at welding. Thus, the resonant circuit elements must be calculated and selected for the short-circuit mode and, therefore, they will not be overloaded.
It is also obvious (Figure 3.47) that transient processes are relatively fast. Thus, if the voltage changes sharply (during 10 μs) from zero to some welding voltage, only 2 cycles of supply voltage will be needed to reach the new steady state for currents and voltages of the resonant network. At that, changing between states goes smoothly, without voltage spikes or current surges.

## 3.6 Alternative way of output regulation – frequency control

This part discusses briefly a possibility of output regulation by changing inverter voltage frequency. The $L_1L_2C$ topology with the parameters given in Table 3.5 was selected for this analysis.

**Table 3.5 Values of resonant components for the frequency regulation technique**

| *Absolute values* |
|---|
| $L_1$=2 μH |
| $L_2$=1.6 μH |
| $L_3$=0.05 μH |
| $C$=3.3 μF |

Output currents for two main states in the converter operation are presented: short–circuit and welding current in relation to the inverter output voltage frequency.

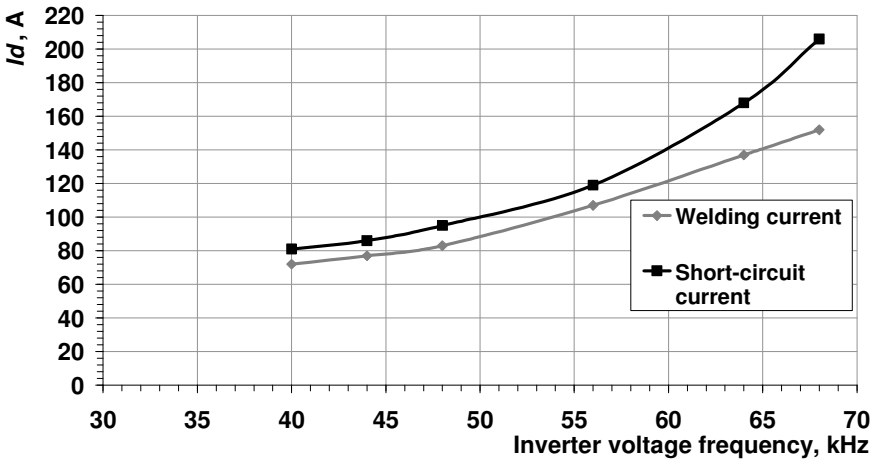


**Figure 3.48 Regulation characteristic (at constant $t_d$=2 μs)**

This diagram shows that with the switching frequency increasing the output currents increase too. Hence, the output regulation by the frequency control could also be implemented. At that, as the simulation shows, a ZCS could be obtained for the frequency range represented in Figure 3.48 (40–68 kHz). However, due to practical limitations of the resonant capacitor operation at higher frequencies, this type of output regulation remains beyond the scope of this research.

## 3.7 Output filter design

As we design a welding source, the output filter is an important part, in particular, the value of its filter inductance. This inductance is present to reduce the current ripple of the supply current to the welding arc [W11]. Major concerns faced during the filter design are

1) current stability of welding arc,
2) rate of current increase,
3) reduction of radiated noise,
4) decrease of current pulsation.

Parameters of the output filter are mainly depend on the selected switching frequency of the inverter and load requirements. Significant changes in the welding energy $U_{load} \cdot I_{load}$ during welding lead to an increase in spatter quantity [W3, PF12]. Characteristics of the welding arc dependent on the selected value of output filter inductance are given in Table 3.6.

**Table 3.6 Welding arc properties regarding the output filter inductance [W1, W3]**

| *Inductance is very small* | *Inductance is very high* |
|---|---|
| Very small droplets<br>High number of short-circuits/second | Very large droplets<br>Low number of short-circuits/second |
| Welding of very thin sheet metal | Welding of thick sheet metal |
| Weld may become cold and poor if the number of short-circuits is too high for the thickness of metal being welded. | With very large filter inductance the current increase rate at short-circuit is too low and metal drop can congeal on electrode tip. |

The minimal value of the output filter inductance $L_{f\min}$ can be defined [W10] according to the following expression:

$$L_{f\,\min} = U \frac{\Delta t_{\min}}{\Delta I_{\max}}, \tag{3.16}$$

where $U$ – is a nominal welding voltage, $\Delta t_{min}$ – time interval approximately equal to one cycle of the switching frequency, $\Delta I_{max}$ – acceptable welding current ripple at maximal load.

In our case for 150 A welding arc at and acceptable ripple of 20 A, the minimal filter inductance value is 13 μH.

Usually, there is a reversed $LC$ – filter circuit used in the output filter. Further calculation of the output filter is performed according to [H2]. First of all, the smoothing factor $q$ of the output filter is defined as follows:

$$q = 4\pi^2 f_{sw}{}^2 L_f C_f \,, \tag{3.17}$$

where $f_{sw}$ is an inverter switching frequency.
Usually, the recommended smoothing factor is between 3 and 30. In our study $q$ is 5. Hence, taking into account $L_{f\min}$ calculated above, the $C_f$ value will be 1.5 μF. Based on these calculations the output filter parameters were selected. Output filter inductance is $L_f$=16 μH and filter capacitor has the capacitance $C_f$=1.5 μF.
The role of the correct selection of output filter parameters is very important. Thus, if the capacitance value of the filter capacitor exceeds some certain value the output current will be only 100 A instead of 150 A. On the other hand, very low capacitance of the output filter together with minimal filter inductance increases current pulsation especially at low output currents.

## 3.8 Experimental results

To check the proposed SM-PSA converter $L_1L_2L_3C$ resonant topology a corresponding prototype was created. The resonant part of the converter is shown in Figure 3.49. It contains a center-tapped high-frequency transformer with increased leakage inductances:

1) leakage inductance of the secondary winding connected to the resonant capacitors was measured and found equal to 0.2 μH,
2) leakage inductance of the secondary winding connected to the resonant inductor (lower one in Figure 3.49) measured and found equal to 0.4 μH.

The measured turns ratio of the transformer is 8.5:1:1.

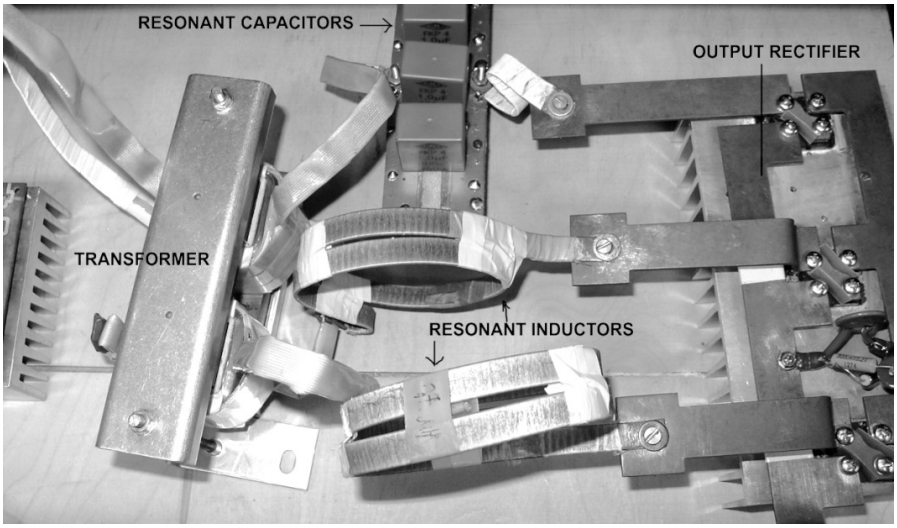


**Figure 3.49 Resonant part of SM-PSA converter prototype**

The values of the additional resonant elements are as follows:
Resonant capacitor: $C$=6x1μF, FKP1 400 VDC;
Resonant inductor in the middle branch 0.5 μH; total $L_2$=0.5 μH
Resonant inductor in the inductive branch 0.7 μH, total $L_1$=0.7+0.4=1.1 μH
Output rectifier was composed by three ultrafast power diode modules BYT200PIV-400 ($I_{F(RMS)}$=150 A, $I_{F(AV)}$=100 A, $V_{RRM}$=400 V, $t_{rr(max)}$=100 ns, $V_{Fmax}$=1.4 V).
Inverter circuit was implemented by the full-bridge topology with MOSFET IRFP460 switches.
A Closed Loop Current Sensor CSNR161 was used to monitor the current in the primary winding of the high frequency transformer.
In Figure 3.50 the picture of the initial prototype is shown with some short descriptions.

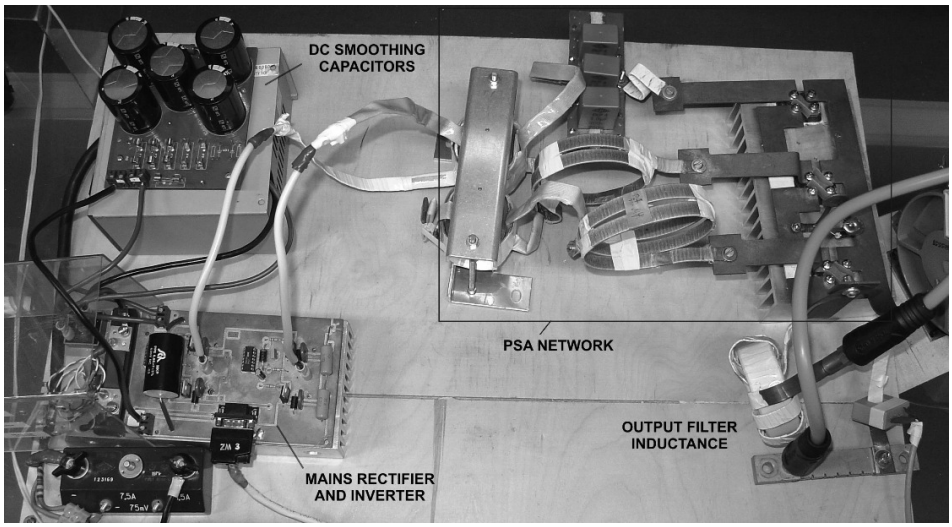


**Figure 3.50 Pioneer prototype of SM-PSA converter**

Output filter inductance was implemented on the iron powder toroidal core *T-400A-26* with 7 turns coil made of copper strap. The result of the filter inductance measurement was 11 μH plus 5 μH added by long connection wires, totally 16 μH. The filter capacitor is absent in the prototype.

### 3.8.1 Resistive load

Firstly, the converter operation was verified with the resistive load. Testing was conducted with DC-supply voltage 100 V. In the first test, the output was short-circuited and the transformer voltage and current of the primary winding were measured, depicted in Figure 3.51.

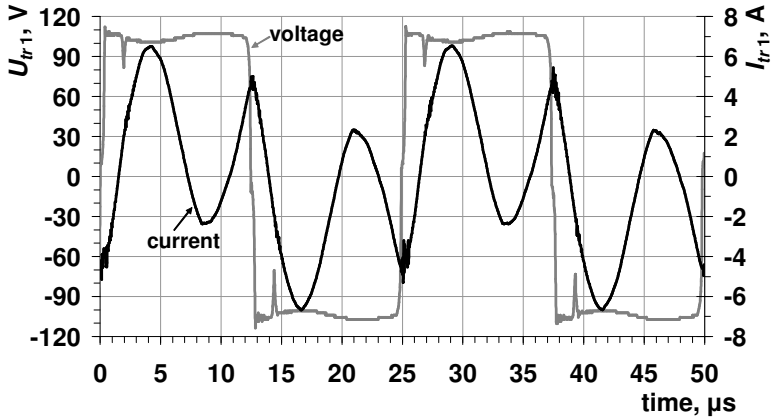


**Figure 3.51 Measured voltage and current of transformer primary winding at short-circuited output when $U_{dc}$=100 V and $t_d$=2.7 µs (output current 43 A)**

As it is seen, the current the in the primary winding has on oscillating nature that corresponds to the behavior of SM-PSA converter previously studied. However, as the prototype parameters are slightly different from the simulation parameters, and due to the transformer magnetizing current, the measured current waveform is not the best at the turn-off instant. At that, it is seen that short-circuit does not cause any overloads on the transformer primary winding. In addition, it is very likely that at the turn-on instant there is a ZVS condition. In Figure 3.52 the same short-circuit occurs, but only a gating pulse width has decreased. However, the output current has slightly increased that corresponds to the properties of SM-PSA converter studied in the previous section.

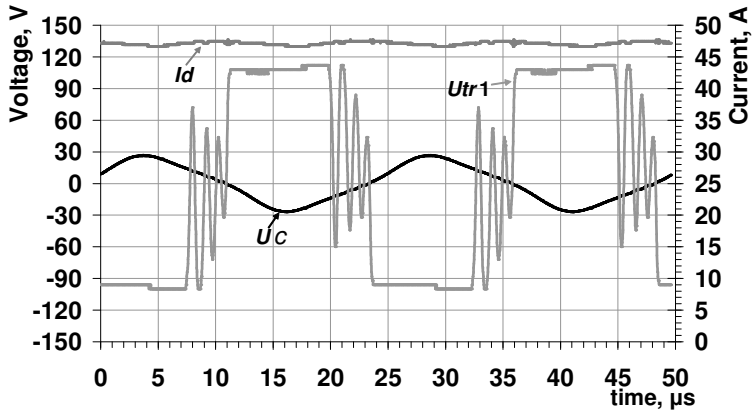


**Figure 3.52 Measured transformer primary voltage, output current and resonant capacitor voltage at short-circuited output ($U_{dc}$=100 V, $t_d$=6.6 µs, $I_d$= 47 A)**

It is also seen that as different from the previous picture (Figure 3.51), the primary voltage has an oscillating nature during "dead-time" intervals; that basically must be avoided by ZVS implementation. The measured resonant capacitor voltage RMS value is 17.1 V.

The following oscillogram shows the waveforms of the transformer primary voltage and current for the same circuit having some resistive load.

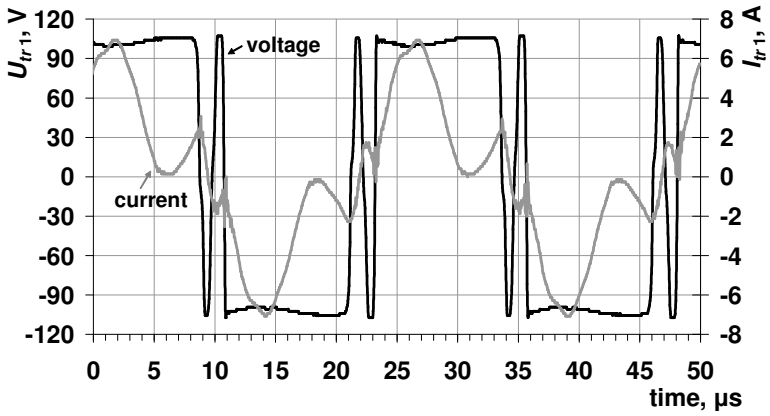


**Figure 3.53 Measured voltage and current of the transformer primary winding when $U_{dc}$=100 V and $t_d$=2.7 µs (resistive load $R_{LOAD}$= 0.1 Ohm, $I_d$= 43 A)**

As compared to the short-circuit state (Figure 3.51), the primary winding currents are similar, but with the load resistance increasing, current value at the turn-off instant is decreased. Thus, the switch is less stressed at the turn-off moment. The value of the output current remains unchanged.

### 3.8.2 Welding

Secondly, the prototype was tested during welding and at DC-supply voltage of 325 V that corresponds to the rectified and smoothed 230 V AC mains voltage.
Gating pulse width was selected equal to 5.9 µs ($t_d$=6.6 µs). The following diagram (Figure 3.54) shows measurement results of the manual welding process, including all three mains states: no-load, short-circuit and welding. This diagram also depicts transient processes during welding. The measured no-load voltage is 72 V. Short-circuit current is about 160 A. The measured welding current during manual arc welding is characterized by a significant current ripple having frequency 100 Hz that could be explained by insufficient smoothing capacitance after mains rectifier. Another reason is inadequate parameters or design of the output filter, particularly the effect of the filter capacitor must be controlled. These possible reasons of the welding current ripple must be carefully checked and eliminated as much as possible.

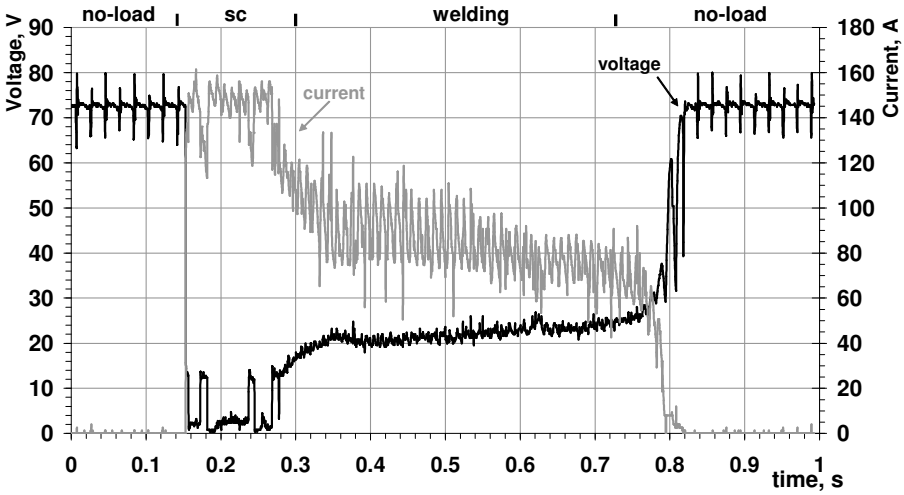


**Figure 3.54 Measured output voltage and current during welding while $U_{dc}$=325 V and $t_d$=6.6 µs (sc – short-circuit)**

Welding current is 80 A on average (at the time interval: 0.5–0.6 s) and voltage during welding is about 22–23 V that corresponds to the values presented in Figure 3.39. Thus, the rate of current increase is high enough for easy arc initiation. This verifies that the value of the selected filter inductance is not too high.

### 3.8.3 Battery charging

Another interesting option is to load the studied converter with a battery being charged. The 12 V, 60 Ah car lead-acid battery has been tested as a load. The DC-supply voltage of the inverter circuit was 120 V in this case. Gating pulse width was selected equal to $a$=6.6 µs ($t_d$=5.9 µs). The oscillogram of the output voltage and current along with the transformer primary voltage are presented in Figure 3.55.

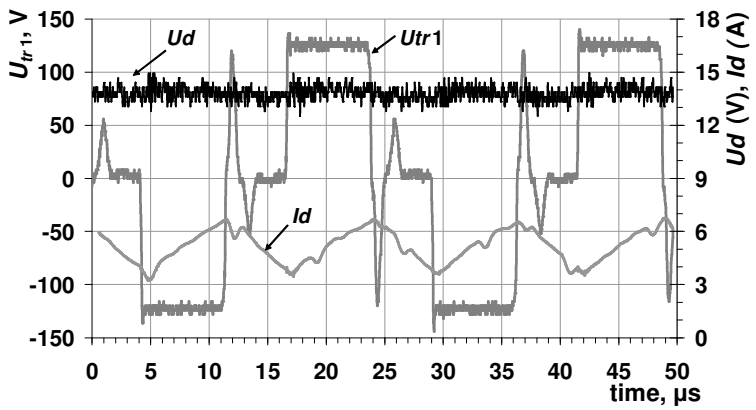


**Figure 3.55 Measured waveforms of the transformer primary voltage, load voltage $U_d$, and load current $I_d$ during 12 V battery charging**

The current ripple caused by the non-adequate parameters of filter circuit is also significant in this case. The measured charging current is 5 A on average while the load voltage is 13.8 V. However, this example verifies that the SM-PSA is also capable of battery charging.
If the filter inductance increases twice the load current value will increase up to 9 A and the ripple will decrease twice. Thus, output filter parameters must be defined separately for different load types depending on the load conditions and requirements.

## 3.9 Conclusions

In this chapter several aspects of SM-PSA converter design and operation were discussed. Firstly, the assumed load for the SM-PSA converter was specified. It is a manual welding arc with current up to 150 A. Secondly, the switching frequency range was defined regarding practical limitations concerning implementation of the resonant part. The inverter output voltage frequency was selected equal to 40 kHz in this research. Then, a simplified approach for the calculation of resonant components of the SM-PSA converter with different resonant topologies was presented. The simplification implies an assumption of the sinusoidal waveform of high-frequency voltage supplying the transformer primary winding, instead of a rectangular or quasi-rectangular one. After that some recommendations for the inverter transformer design were introduced. It was shown that transformer leakage inductance and inductance of connecting wires in the resonant network can partly or fully substitute the required resonant inductors.

A substantial part of the chapter was dedicated to the analysis of different SM-PSA resonant topologies having a typical full-bridge inverter power supply with regulation by the pulse width changing. It was shown that the condition close to ZCS is achievable for the $L_1L_2C$ and $L_1L_2L_3C$ topologies in the range close to the maximal output current (150 A) during the welding process. Moving from this point to lower output currents incurs increases in switching losses.
Output characteristics of different resonant topologies are presented and the corresponding voltage values on the resonant capacitor are shown. It is the $L_1L_2L_3C$ topology that has the output characteristic closest to the current source mode in the welding range.
In view of these consideration, $L_1L_2C$ and $L_1L_2L_3C$ topologies having $K_Q<1$ and $L_1/(L_2+L_3)<1.2$ are the most promising topologies for MMA welding that permit ZCS.
However, the approach of output regulation suggested is far from being perfect, as the output current has some intervals where it is not responding to changes in the gating pulse width. That is why an alternative way of output regulation is suggested and discussed briefly in the section 3.6. Namely, a switching frequency control method is suggested to achieve more linear output regulation.

The transient processes studied in section 3.5 verify that the transition from one state to another is fast and it takes about 2 half-cycles of the operating voltage to reach a new steady-state. At that, no stresses appear in waveforms of the converter components. As it was emphasized before, a short-circuit current is naturally limited without control. It can also be concluded that acceptable currents through resonant network components must be calculated for operation during output short-circuit, while currents in inverter switches for the rated load operation.

Experimental results given in the final part generally verify theoretical studies and confirm that the output filter design is essential for the "correct" operation of the converter. As it is seen, with the filter capacitor absent, the output current ripple is considerable. However, the converter is still capable of operating with the suggested loads maintaining the property of short-circuit current limiting.

# 4. PFC in the SM-PSA converter

## 4.1 Background - reasons of poor power factor and state of art

Reduction of electric power losses and reasonable consumption of energy is a challenge for modern electronic equipment. To determine optimal criteria for power consumption by converters, there are usually two aspects that lead to the unnecessary waste of power:

- line voltage and/or current waveform difference from the sine (distortion, THD),
- phase shift between line voltage and current (displacement power factor, DPF).

Such unnecessary power consumption could be minimized, if the power factor is kept equal to one.

$$PF = \frac{1}{\sqrt{1+THD_i^2}} \cdot DPF = 1, \tag{4.1}$$

$$DPF = \cos\varphi_1, \tag{4.2}$$

where $\varphi_1$ - phase shift between the first harmonics of voltage and current ($I_1$ and $U_1$), and

$$THD_i = \sqrt{\left(\frac{I_2}{I_1}\right)^2 + \left(\frac{I_3}{I_1}\right)^2 + \ldots + \left(\frac{I_n}{I_1}\right)^2}, \tag{4.3}$$

where $I_1 - I_n$ mains current harmonics.

Thus, the criteria for an ideal power consumption are DPF=1 and THD=0, i.e. input current is in phase with the mains voltage and does not contain higher harmonics.

For linear inductive loads compensation capacitor batteries are mainly used to increase the power factor.

For conventional modern power converters, which are mostly characterized by non-linear and variable input impedance, compensation capacitors are not acceptable due to the harmonic distortion of the consumed current. Such higher harmonic currents just overload the capacitors.

To improve the power factor in this case, passive methods are used for power factor correction. These use a network frequency *LC* circuits operating as higher frequency harmonic filters. In addition, a mains frequency PSA converter is implemented where the resonant components *L* and *C* form parametrically parallel or series resonant circuits. Both topologies reduce higher harmonics in the mains current and their advantage is simplicity. However, large weight, size and cost are drawbacks for the compact modern power supplies.

Another method is an active power factor correction, which uses a switch-mode converter to shape the line current. These converters are operating at

frequencies higher than the network voltage frequency and they contain controlled electronic switches [H1].
In most cases, circuits with high switching frequency are used to compose a sine-shape current with a zero phase shift. For example the sinusoidal input current is composed by a diode rectifier with a boost converter like in Figure 4.1.

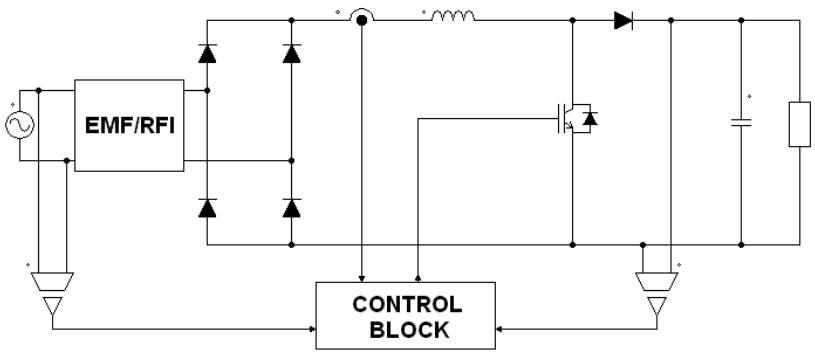


**Figure 4.1 Basic circuit of PFC with boost converter**

The advantage of this method is the reduced weight and size of coils and capacitors because of higher switching frequency. The disadvantage of purely boost topology is in an additional converter, which cannot be simultaneously applied to regulate the rectified voltage. Another disadvantage is a relatively complicated control circuit. However, single-stage solutions like an integrated boost-forward converter [H10] or modified boost converter [PF13] are available. The regulation of the rectified voltage can also be achieved by the buck-boost topology, like in [RC13]. Another solution is the use of active rectifiers based on the PWM converter topology [PF2, PF12].
In addition, so called “indirect” power factor correction methods are known where waveform of the input current is shaped by keeping the converter input impedance constant regardless of the load conditions [PF5, RC6]. Thus, if the converter has constant input impedance, the waveform of the line current becomes automatically similar to the line voltage waveform and, hence, no distortion appears in the current waveform. Such converters could be also named as converters with inherent resistive impedance.

In the following part, the ability of the SM-PSA converter to operate as a converter with partly stabilized input impedance will be discussed. No additional circuits or control methods were used.

## 4.2 Properties of PSA appropriate for PFC

In this study, we will discuss the ability of the proposed uncontrolled SM-PSA converter to operate as a converter with partly stabilized input impedance, which helps to improve the power factor.

The topology of one possible embodiment for the PFC switch-mode PSA converter is shown in Figure 4.2, and its main distinctive property is that the DC smoothing capacitor is absent after the input rectifier. Thus, the supply voltage for the inverter circuit has a shape of the rectified, but unsmoothed mains voltage pulsating from some small value up to the amplitude of the mains voltage.

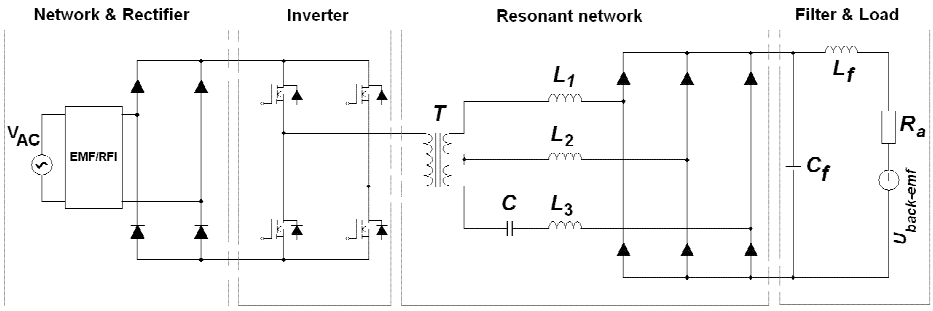


**Figure 4.2 Proposed topology of the AC/DC PFC SM-PSA converter**

The inverter circuit can have different topologies, like half-bridge or asymmetrical bridge or even to be represented by a single switch chopper. The output voltage of such an inverter is a quasi square-wave with modulated amplitude ($u_{s3}$ in Figure 4.3).

The resonant network of the SM-PSA converter is connected between the inverter and the smoothing filter. As the PSA converter has the property of self-adjusting to a load, so with the input voltage changing the PSA converter will evidently tend to change the average transformation ratio (Figure 2.10, page 30) to meet the load condition. Such a change of the transformation ratio will very likely bring to some improvements in the shape of the input current.

In this topology, the SM-PSA converter will not function as a higher harmonics filter as it was at the mains-frequency PSA reviewed in Chapter 2. The practical effect achieved here is the result of using to some degree inversely proportional dependence between the output voltage and current in the SM-PSA converter as depicted in Figures 3.11, 3.22 and 3.30 (less correspondence in Figure 3.38) from the previous chapter.

## 4.3 Principles of operation

Shaping of the input current with the help of SM-PSA is presented in the diagram, in Figure 4.3 (losses are not taken into consideration).

The alternating mains voltage is rectified into unsmoothed unidirectional voltage half-waves, which are transformed into high-frequency voltage by means of inverter switches. Then, this amplitude-modulated high-frequency voltage is delivered to the power factor correcting circuit, having stabilized input impedance. The role of this circuit plays a resonant part of the SM-PSA circuit. The stabilized input impedance is represented by admittance $g_s$ in the diagram.

In an ideal case, the input admittance $g_s$ is always constant and the converter consumes power $p$ from the mains, the instantaneous value of which could be defined by the multiplication of the input admittance $g_s$ and voltage $u_{s3}$ squared

$$p = g_s \cdot u_{s3}^2 . \tag{4.4}$$

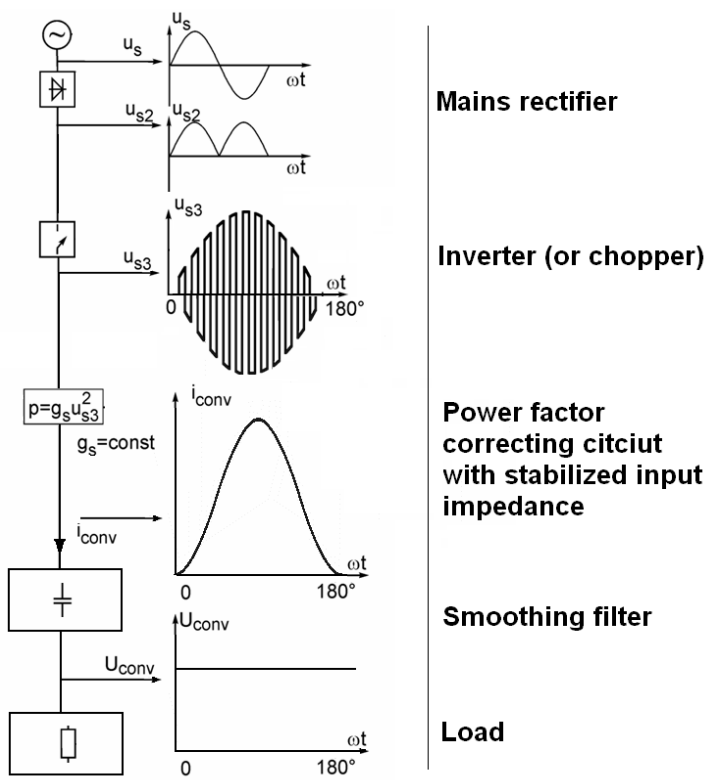


**Figure 4.3 Diagram of the proposed method for power factor correction in AC/DC converters**

Then the rectified and smoothed voltage is delivered from the smoothing filter to the load. In an ideal case the circuit connected between the mains and the smoothing filter has to correspond to the following two requirements:

1) the input impedance of the converter circuit is constant and consequently, the instantaneous power consumed from the mains is proportional to mains voltage squared,
2) the instantaneous values of the current and voltage supplied from the converter circuit to the smoothing filter are inversely proportional and, thus, the instantaneous power delivered to the smoothing filter does not depend on the voltage in the case of the filter with capacitor or on the current in the case of the filter with a choke (operates like a constant power source).

This makes it possible to consume power from the mains proportionally to the instantaneous value of the mains voltage squared that means stabilization of input impedance or, in other words, a better power factor.
Implementation of the proposed SM-PSA converter allows the abovementioned requirements to be followed with reasonable accuracy, as will be shown further. Along with that, an increase in the frequency of the resonant network supply voltage will reduce the size of the converter.

The value of the output current $i_{conv}$ is defined by dividing the instantaneous mains power $p$ by the voltage on the filter output $u_{conv}$.
If the input voltage $u_{s3}$ is not changing the converter maintains constant power, which could be defined as $p=u_{conv}\cdot i_{conv}$=const and it is independent of the output voltage. In the case of the varying input voltage $u_{s3}$, the instantaneous power $p$ depends only on instantaneous value of the input voltage $u_{s3}$ (losses are not taken into consideration).

The advantage of this PFC method is that no current or voltage control is needed. It is only necessary to provide the required relation between the mains voltage and instantaneous power as well as between the instantaneous values of voltage and current in the output filter.
Thus, during no-load operation, output voltage should become theoretically infinitely large, and, during short-circuit operation, the output current becomes theoretically infinitely large. However, in practice these extremes are not available and that will cause some degradation of the power factor.

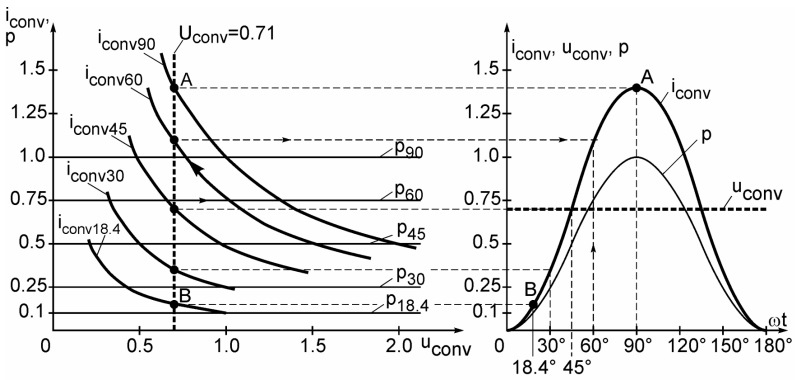


**Figure 4.4 Graphical representation of the required instantaneous power supplied from the mains to the smoothing filter in the case of an ideal PFC**

Figure 4.4 shows how the instantaneous power $p$ is delivered from the mains to the smoothing filter at different time instants. In the left part of Figure 4.4 b, there are curves $i_{conv90}$ to $i_{conv18,4}$ of the inversely proportional dependence between the smoothing filter voltage $u_{conv}$ and its input current $i_{conv}$. Also, the corresponding horizontal lines $p_{90}$ to $p_{18,4}$ of instantaneous power supplied from mains are shown. The voltage on the smoothing filter is chosen 0.71 relative units.

The instantaneous values of the current delivered to the smoothing filter $i_{conv}$ are defined here by the intersection points of current curves $i_{conv18,4}$ to $i_{conv90}$ with dashed line $u_{conv}$=0.71. In the right part of Figure 4.4 b, the curve of the current delivered to the smoothing filter $i_{conv}$ and the abovementioned points A and B on this curve are shown. It also presents the voltage of the smoothing filter $u_{conv}$ (horizontal dashed-line) and the curve of the power $p$ delivered to the smoothing filter. The power curve is defined here by the multiplication of the smoothing filter voltage $u_{conv}$ and current $i_{conv}$ ($p=u_{conv}\cdot i_{conv}$).

The graphics shown in Figure 4.4 describe the ideal characteristics of an "indirect" power factor correcting circuit. In practice, these idealized parameters cannot be achieved, thus, certain distortion occurs in the waveform of the input current. The level of distortion will depend on the selected relation between the output no-load and the nominal operation voltage.

## 4.4 Simulation of PFC SM-PSA

### 4.4.1 Input current and $THD_i$ vs output voltage

The schematic of the power part in the computer model corresponds to that represented in Figure 4.2. To study the dependence of the input current distortion on the load voltage, a model that had a back-emf source with linearly increasing voltage as a load was simulated. Simulation results are shown in Figure 4.5 below.

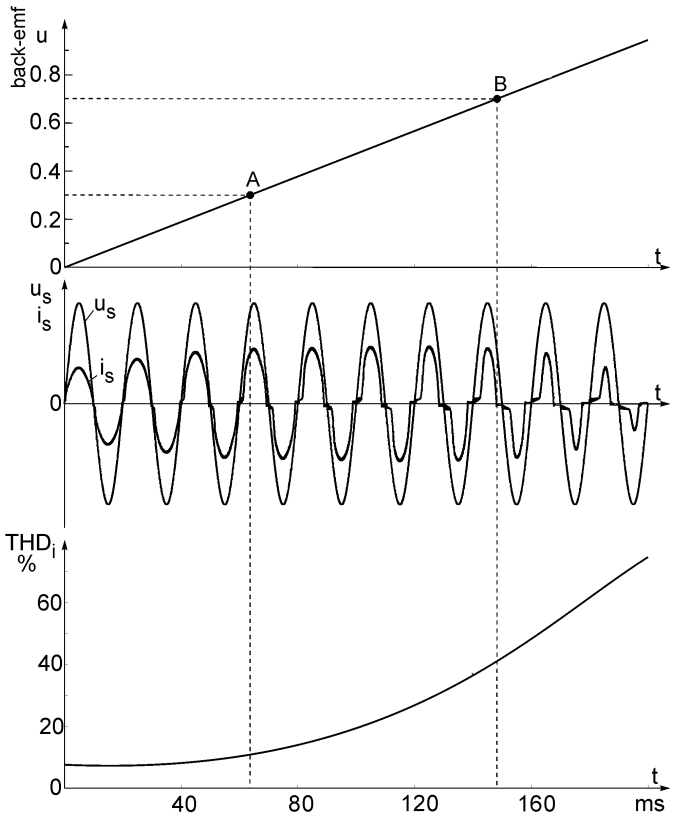


**Figure 4.5 Simulated waveforms of input current $i_s$ and $THD_i$ when the back-emf of load changes from zero to no-load voltage**

As it is seen, the characteristics of the SM-PSA converter enable one to stabilize converter input impedance when the voltage on both secondary windings (see Figure 4.2) is higher than the output voltage. Thus, the range of constant output power independent of the output voltage is relatively narrow for the proposed uncontrolled SM-PSA converter. Consequently, in the range of low instantaneous values of the mains voltage the input impedance of the converter increases and distortion appears in the input current.

It is also seen that at higher values of the load back-emf, the input current (curve $i_s$) appears only when the instantaneous value of the mains voltage (curve $u_s$) reaches a sufficiently high level.

Thus, for the single-phase rectifier with described above correction mains current distortion $THD_i$ was found about 10–40 %, as shown in Figure 4.5. It is about 2–3 times better than for the conventional rectifier with a smoothing capacitor. Also, the phase shift between the voltage and current is not significant in Figure 4.5.

To summarize, input current distortion is the smallest while the load operation range is close to short-circuit and increases with the load back-emf increasing.

Thus, it is unpractical to use a PFC SM-PSA converter in the range close to no-load. The practical operating range is about 0.3 to 0.7 of no-load voltage, as shown between points A and B in Figure 4.5. In the interval 0 to 0.3 of no-load voltage (range close to short-circuit) the operation is possible and input current distortion remains low. But this range is unpractical for permanent operation because of lower power delivered to the load and smaller efficiency of the converter. The decrease in the mains current during the operation near the short-circuit area is caused by the converter automatically switching into the parallel resonance mode. Thus, no short-circuit protection or fast control is needed.

It is possible to reduce distortion by adding an active correction. For this purpose capacitive branch of the PSA converter could be provided with adjustable current by-pass circuit which extends the range of the constant power of the converter. But these topics remain beyond the scope of given thesis.
For the regulation of the output power a simple pulse width control for converter switches could be used. Under such control, the shape of the input current is not changing significantly.

### 4.4.2 Converter operation in a mains cycle

Due to inverter input voltage pulsation, the instantaneous output no-load voltage and power of the converter are changing too, as in Figure 4.6. As it was mentioned, if the inverter has varying input voltage, an instantaneous power $p$ depends on the instantaneous value of the input voltage $u_s$. The right part of Figure 4.6 shows the output power curves $p_{conv}$ constructed as the function of the output capacitor voltage $u_{conv}$. For every instantaneous value of the mains voltage, there is its own output power curve $p_{conv90}$ to $p_{conv18,4}$. By vertical dashed-lines some output voltages on the filter capacitor equal to 0.25, 0.62 and 0.9 p.u are defined. These dashed-lines cross output power curves and the resulting intersection points of instantaneous powers, like $F_{0.25}$ to $F_{0.9}$, define both instantaneous power delivered to the smoothing filter and the instantaneous power supplied from the mains since losses is not taken in account.
The points of maximal instantaneous powers $E_{18.4}$ to $E_{90}$ in the right part of Figure 4.6 are transferred to the left part where the corresponding power curve $p_{PSAmen}(t)$ is constructed in the time domain. The shape of this curve is to some degree different from that of the ideal power curve presented in Figure 4.4. It follows that the shape of the input current is also to some degree different from that of the mains voltage $u_s$ and power factor correction is not perfect. The reason is the zero output power $p_{conv}$ of the SM-PSA converter at no-load and at short-circuit.
Figure 4.6 shows the output current curves $i_{conv}$ as well. In the definition of the output current curves it was taken in account that during short-circuit the output current is changing in the time domain according to the sine waveform of the mains voltage.

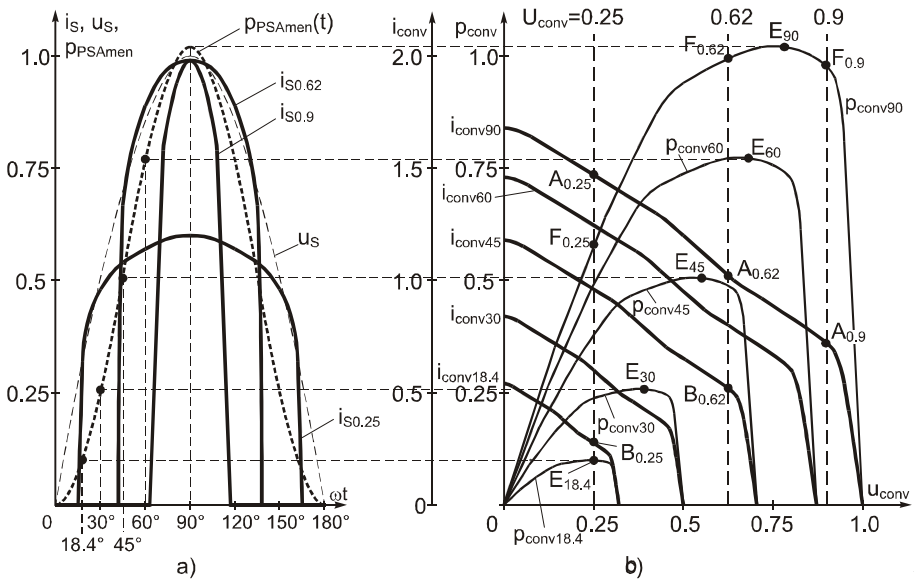


**Fi**

**Figure 4.6 a) Graphical representation of power *p*, mains voltage $u_s$ and input current $i_s$ waveforms and b) operation point in the SM-PSA converter for output voltages 0.25, 0.62 and 0.9 of no-load voltage ($E_{18.4}$–$E_{90}$ – maximal values of power)**

These characteristics of the PSA converter obtained allowed us to analyze the functioning of the power supply given in Figure 4.2. The curves of instant power are not straight lines, but they have starting and ending points at zero power. Consequently, the shape of the input current waveform depends on the output voltage $U_{conv}$ of the converter.

Basically, we can choose the output voltage such that the power curve $p_{conv90}$ and the corresponding straight line of the predefined output voltage have an intersection point in the range close to maximum (e.g. point $F_{0.62}$ at voltage $U_{conv}$=0.62).

But we can also choose another intersection point with some smaller power (e.g. point $F_{0.25}$). Hence, the maximal value of the consumed power (at the amplitude of the mains voltage) depends on the selected output voltage value. At that, with decrease in the power maximal value, the average power and output rectifier powers are also reduced.

When we select another output voltage besides the power changes the shape of input current. The current curves $i_{s0.25}$ to $i_{s0.9}$ in Figure 4.6 a are constructed by dividing the instantaneous powers $p_{conv}$ given in Figure 4.6 b by the instantaneous value of the mains voltage $u_S(t)$. The vertical straight line $U_{conv}$=0.62 crosses the curves of the output current $i_{conv90}$ (point $A_{0.62}$), $i_{conv60}$ ja $i_{conv45}$ (point $B_{0.62}$), but it does not cross the curves $i_{conv30}$ and $i_{conv18.4}$. This means that in the interval 0º–30º there is no input current. Input current appears somewhere between 30º and 45º and there is corresponding distortion in the shape of the input current curve ($i_{S0.62}$ in Figure 4.6 a). If the power curves

$p_{conv30}$ and $p_{conv18.4}$ could have zero power points at a voltage higher than 0.62 (wider power curves), the distortion will not take place.
With an output voltage $U_{conv}$=0.9 the input current does not appear in the range 0º–60º and it occurs only between 60º and 90º. In this case the distortion of the input current becomes even higher ($i_{S0.9}$).
The mode of input current distortion changes at a smaller output voltage. When $U_{conv}$=0.25, the input current appears before 18.4º. But the intersection point $F_{0.25}$ of the power curve $p_{conv90}$ and the corresponding straight line is located far lower from the maximal power (point $E_{90}$). Due to this, at a time of the mains voltage peak value, the instantaneous power is decreased and the current curve $i_{S0.25}$ has a more "flat" top.
In general, the distortion of the input current depends mostly on the relation of the nominal voltage to no-load voltage or on the relative nominal voltage $U^*_{convn}$.
The no-load voltage is equal to the no-load voltage of the PSA converter defined at the amplitude value of the mains voltage $U_{dPSA0/90}$. The relative nominal voltage is

$$U^*_{convn} = U_{convn} / U_{dPSA0/90} \tag{4.5}$$

Based on the information depicted in Figure 4.6 it also could be concluded that to obtain a less distorted shape of the input current in case of a deeply varying load, a conventional (without control) PSA converter has too narrow range of constant power. This range is more times wider in PSA converters that have a controlled current by-passing circuit in the capacitive branch [PT2].

### 4.4.3 Converter operation in a switching cycle

The simulated oscillograms represented in Figure 4.8 describe the processes taking place in the PFC PSA converter having a full-bridge inverter topology, as depicted in Figure 4.7. The box number 7 in Figure 4.7 shows the part of the converter responsible for PFC, which is at the same time a resonant network of SM-PSA.

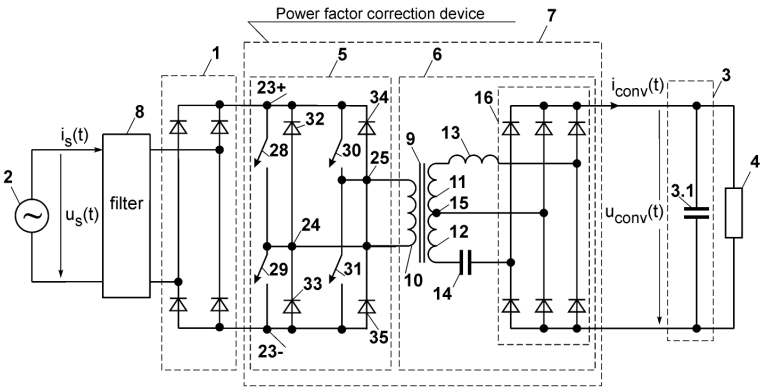


**Figure 4.7 PFC SM-PSA converter topology with elements numbered as in [PT2]**

Figure 4.8 shows current $i_{31}$ through switch 31, current $i_{13}$ through resonant coil, current $i_{15}$ from the common connection terminal (point 15 in Figure 4.7) of the transformer secondary windings, resonant capacitor current $i_{14}$ and voltage $u_{14}$, and also current $i_{conv(t)}$ supplied from the output rectifier bridge to the smoothing filter.

First, we review oscillograms in Figure 4.8 a corresponding to 30 electrical degrees from the beginning of the mains voltage half-cycle (at the half of the mains voltage amplitude).

*Stage 1*: $t=(t_1 \ldots t_2)$ – Control circuit turns on the switches in the inverter diagonal (28 and 31 in Figure 3). Current in the switches and primary winding starts increasing. Current $i_{15}$ is decreasing and the converter is almost in series resonance mode.

*Stage 2*: $t=(t_2 \ldots t_3)$ – Current $i_{15}$ goes through zero and changes its direction.

*Stage 3*: $t=(t_3 \ldots t_4)$ – Current through the resonant capacitor drops to zero since resonant capacitor voltage has increased sufficiently. After that, the current from transformer is delivered to the rectifier bridge mainly through winding 11. Due to this, transformer ratio is higher than it was during the time interval $t_1$ to $t_2$ when windings 11 and 12 were operating in series. Thus, transformer ratio is changing automatically under the influence of circuit voltages and currents.

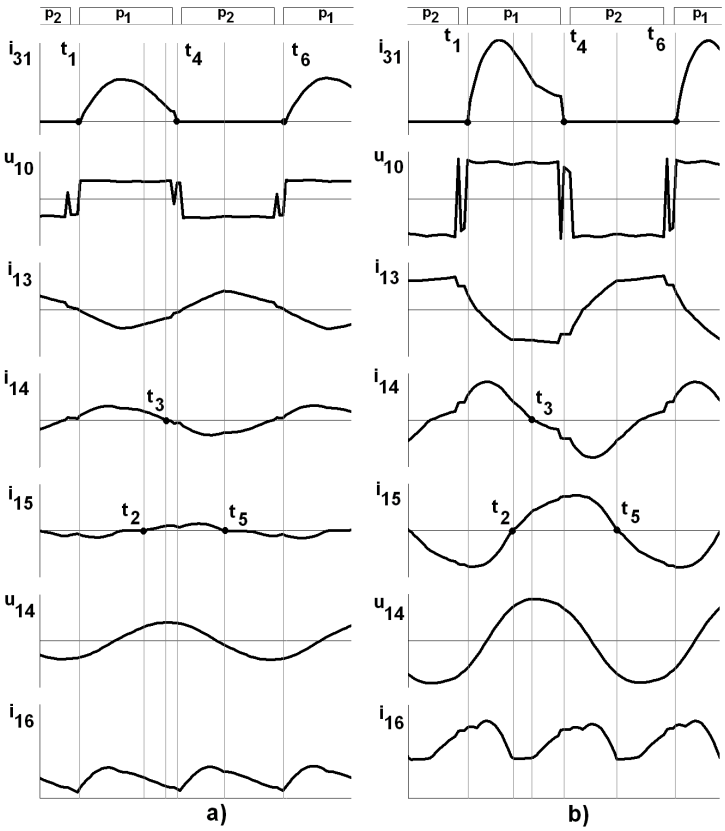

**Figure 4.8 a) Oscillograms of currents and voltages in the PSA converter when the instantaneous value of mains voltage is half and b) peak value**

*Stage 4*: $t=(t_4 \ldots t_6)$ – Control circuit turns off the switches. Current through the capacitor appears in the negative direction and starts to discharge capacitor. After some "dead time" (time between $p_1$ and $p_2$) the control circuit turns on another diagonal (29–30) of the inverter and the primary winding voltage changes to negative. The described processes repeat in the reverse direction.

At the time instant $t_6$, the control circuit turns the diagonal (28–31) again and the described cycle is repeating.

In the oscillograms in Figure 4.8 b, we can see that at the mains voltage amplitude, currents and voltages in the converter have increased. Also, duration and share of current $i_{15}$ ($t_2$ to $t_5$) have increased. Thus, the converter is operating in the parallel resonance mode.

As a result of the analysis of the oscillograms in Figure 4.8 it was found that during low instantaneous values of the mains voltage, the secondary windings of the transformer are connected mainly in series and the converter is in a series resonance mode. Vice versa, during the time intervals when the instantaneous value of the mains voltage is high, the converter operates in the parallel resonance mode that means transformer turns ratio increasing.

It is also seen that turn-off losses at the half of the mains voltage amplitude are relatively low, as current naturally decreases almost to zero at the instant of turn-off. Turn-off current at the mains voltage amplitude value is higher than the previous one, but it is still much lower than the peak switch current. However, if it will be considered necessary, further decrease in the turn-off current that was discussed in the previous chapter is possible.

### 4.4.4 Conclusions

1. The input current of the mains diode rectifier could be transformed to sinusoidal also by the converter placed between the rectifier and the smoothing filter, which is able to keep its transiting power proportional to the instantaneous mains voltage squared and having inverse relation between the output current and voltage (power source). It could be a passive converter without control circuits. The uncontrolled SM-PSA converter can correspond to these conditions only to some extent.
2. The constant power range for the conventional uncontrolled SM-PSA is not sufficiently wide to prevent the distortion of the mains current at low instantaneous values of the mains voltage. The largest distortion is at no-load, while with the output voltage decreasing (accompanied by the output current increasing) distortion decreases. For a single-phase converter the $THD_i$ could be about 25–30% in the nominal operating range.
3. The output voltage of the converter is strongly dependent on the output current value. The short-circuit current is parametrically limited up to 1.2–2 times of the rated current. For example, it could be useful for supplying an electric arc. However, the output voltage of the converter could be

stabilized if a feedbacks circuit implemented to control a PWM in the gating block of inverter.

4. As compared to conventional uncorrected switch-mode hard-switched AC/DC converters, the PFC SM-PSA converter has the following differences: one resonant capacitor and (one to three) resonant inductors added and also, there are six diodes in output rectifier. But this enables about triple decrease in input current distortion. In addition, currents in all the elements of the converter are naturally limited at the level of their rated values while the load can change from no-load to short-circuit.
5. Resonant circuit parameters could be adjusted to have minimal turn-off losses, while turn-on losses minimization techniques for SM-PSA must also be studied in the future.

## 4.5 Experimental results

In order to verify the operation of the proposed converter, an experimental prototype with the MOSFET Full-Bridge inverter topology was built and tested. It contains a high frequency transformer with a center-tapped secondary winding, 10:1:1 turns ratio, operating at 40 kHz. Resonant capacitors with the total capacitance $C$=7 μF and resonant inductor with inductance $L_1$=0.7 μH were installed. The prototype was tested with supply voltage 50 VAC RMS. The relative width of the gating pulses is 0.4. There are three types of loads discussed in this part: resistive load, battery charging and welding process.

### 4.5.1 Resistive load

The output characteristic for this case is presented in Figure 4.9. The resistive load is changing from no-load to short-circuit. It is seen that it has a falling nature that could be an advantage for MMA arc welding. Also, it is evident that short-circuit current is naturally limited. Load voltage value in the further diagrams is the measured true RMS value (no output smoothing capacitor installed).

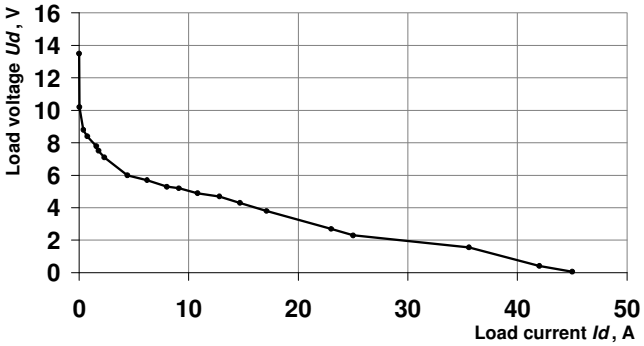


**Figure 4.9 Output characteristic under resistive load variation**

Figure 4.10 shows the input current as a function of load voltage. It is shown that during output short-circuit, the input current becomes even less than the current in the nominal operation mode.

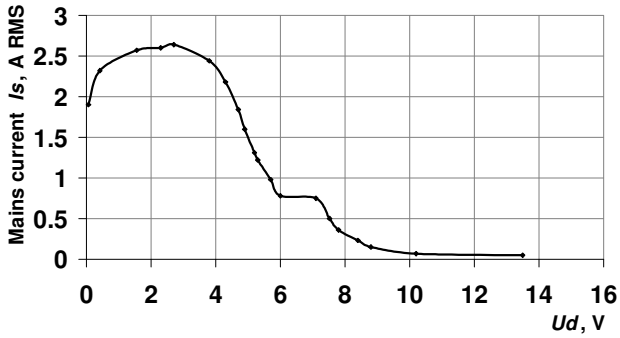


**Figure 4.10 Input current under resistive load voltage variation**

This results from the peculiarity of PSA converter operation (Figures 2.8 and 3.12).

Figure 4.11 presents the input current $THDi_s$ curve at different load voltages. It remains less than 10% up to the load voltage equal to 7 V. Then it increases steeply, but at the same time, the value of the input current has decreased, as shown in Figure 4.10. Thus, the overall impact on the network harmonic pollution is not significant.

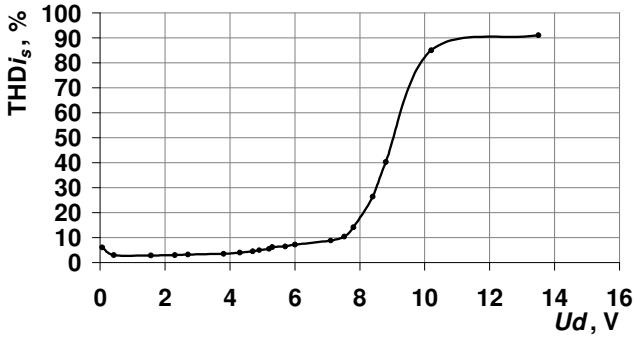


**Figure 4.11 Input current THD under resistive load voltage variation**

Figure 4.12 shows the oscillograms of the filtered input current and voltage while the converter is loaded with a resistive load of 0.3 Ohm. These waveforms show that the mains current is nearly sinusoidal and in phase with the mains voltage. The measured harmonic distortion $THDi_s$ yields 4.5%. However, significant output voltage pulsation could be a drawback for certain loads.

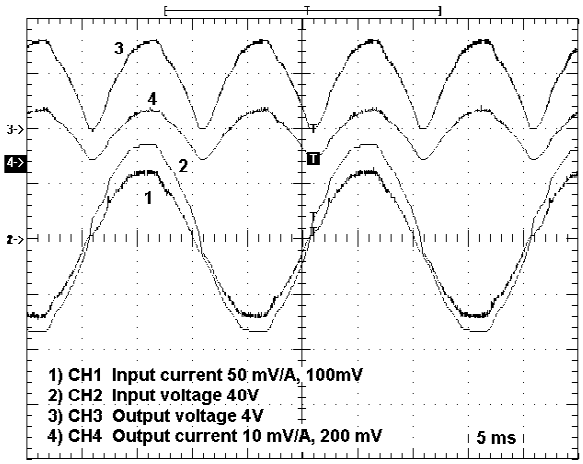


**Figure 4.12 Oscillograms of input current (1) and voltage (2), and output voltage (3), current (4) at a resistive load equal to 0.3 Ohm**

Based on these results it can be concluded that an acceptable operating voltage for the given prototype is from 0 up to 7 V (0 to 50 % of no-load voltage).

### 4.5.2 Battery charging

To validate converter operation for battery charging purposes it was accordingly tested. The 12 V acid battery was almost empty at the beginning of charging, thus battery voltage was only about 5 V. The oscillograms in Figure 4.13 show the filtered mains current and voltage at the beginning of battery charging. The measured harmonic distortion of the mains current $THD_i$ is 26%, PF=0.97.
Then with the battery voltage increasing, charging current is decreasing and the shape of the input current is more distorted. At that, the RMS value of the input current decreases. Thus, the current waveforms and harmonic distortion coincide well with the theory and simulation waveforms shown in Figure 4.5.

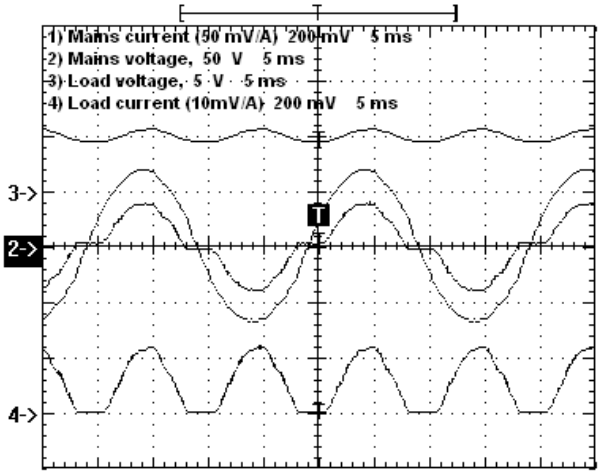


**Figure 4.13 Input current (1) and voltage (2) waveforms, and output voltage (3) and current (4) during battery charging**

The waveforms presented in Figure 4.13 were measured and the results are given in Table 4.1.

**Table 4.1 Measurement results for oscillogram in Figure 4.13**

| Measured value | | | Result |
|---|---|---|---|
| Input voltage, RMS | | | 50 V |
| Input current (True RMS) | | | 1.98 A |
| Harmonics, % of Fund | Fundamental, 100% | | 1.91 A |
| | $3^{th}$ | 24% | 0.46 A |
| | $5^{th}$ | 8% | 0.15 A |
| | $7^{th}$ | 2.6% | 0.05 A |
| | $9^{th}$ | 1.8% | 0.034 A |
| | $11^{th}$ | 2.7% | 0.051 A |
| Load current (measured TRMS value) | | | 12 A |
| Load voltage | | | 5 V |

Measurement results given in Table 4.1 indicate that input current distortion is in the acceptable range according to the international standard IEC61000–3–2 for equipment class A and B.

### 4.5.3 Welding

Another type of a load like an electric arc was investigated. As compared to the previous ones it is characterized by fast and frequent load parameters changing. Electric properties of the converter during testing rather than those of welding will be discussed in this part.

There is a resonant circuit with slightly different parameters used during testing: $L_1$=1.1 μH, $L_2$=0.5 μH, $L_3$=0.2 μH, $C$=6 μF, transformer turns ratio 8:1:1. Other parameters remain the same, full-bridge inverter operating at the switching frequency 80 kHz (inverter output voltage frequency 40 kHz).

The prototype was tested, supplied with full mains voltage 230 VAC RMS. The relative width of the gating pulses for transistors was 0.33.

The figure below shows the output voltage and current during welding.

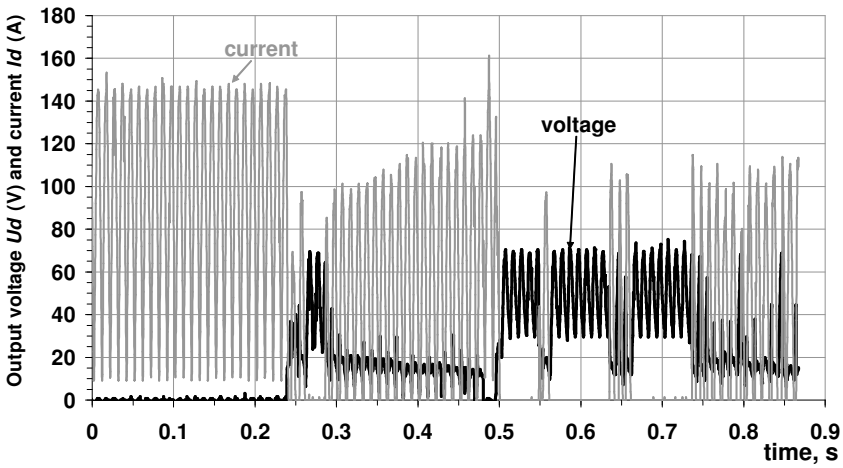


**Figure 4.14 Oscillograms of the welding process for PFC SM-PSA**

During the measuring interval depicted in Figure 4.14, three main conditions of welding appear clearly. In the time interval 0 to 0.2 s, the output voltage is near zero, that indicates output short-circuit. In the interval 0.5 to 0.7 s, there is no output current and voltage is at its maximum (no-load state). The welding process is better represented during the time interval 0.75 to 0.86 s. With the help of the following two pictures (Figures 4.15 and 4.16) the behavior and properties of the tested power supply prototype will be discussed. In Figure 4.15 the averaged output current and voltage are shown. It provides a clear overview of the effective values of current and voltage.

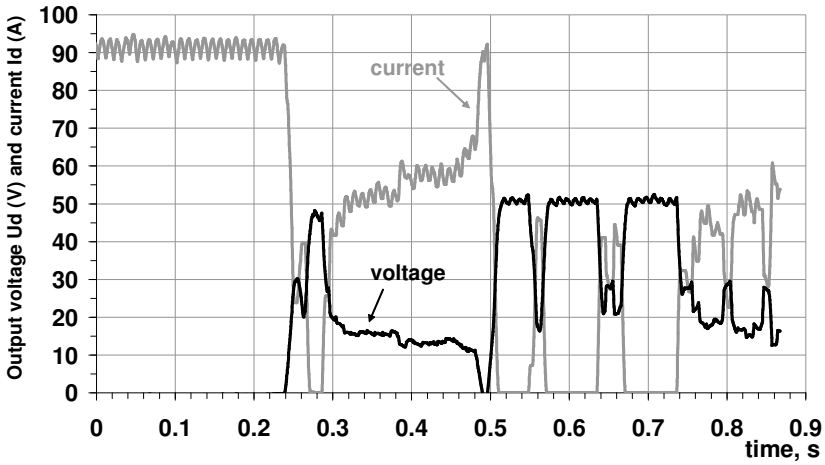


**Figure 4.15 Averaged output current and voltage during the welding process**

The effective welding current is about 40 A and the short-circuit current is near 90 A. As it is evident, a short-circuit current is limited without control, but due to the resonant network of the SM-PSA converter. Mean no-load voltage is 50 V.

In the following figure we can see the "zoomed" waveform of the output voltage and current during the welding process. It is seen that the welding current is pulsating and has zero-current pauses between the pulses in average about 3 ms.

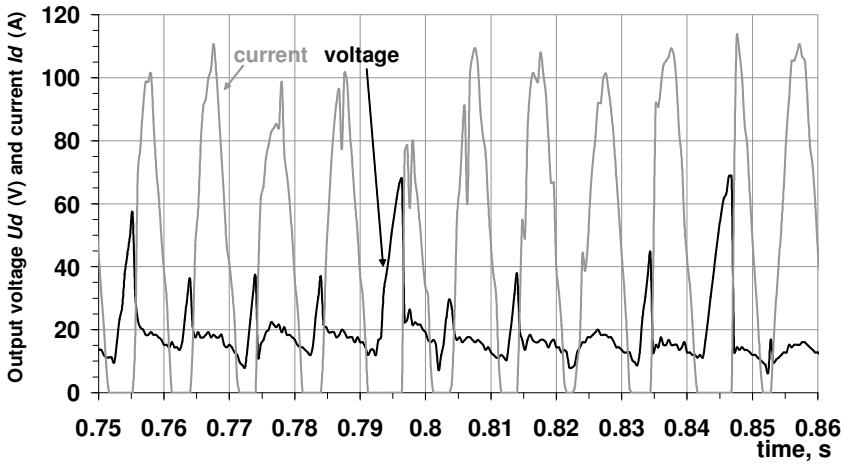


**Figure 4.16 Output current and voltage during welding**

Output voltage is also pulsating with current and, in addition, it has relatively steep spikes during zero-current intervals. This fast increase in the output voltage should in theory assist in the repetitive arc ignition after zero-current

interval. However, the welding properties of such welding current must be studied thoroughly in terms of suitability for different welding techniques.
The following two diagrams describe an input current change while the load current is changing, as depicted in Figure 4.14.

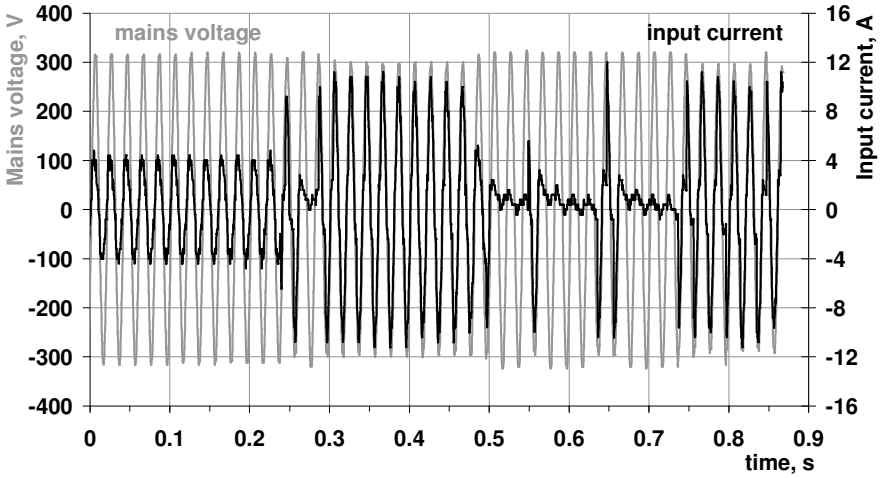


**Figure 4.17 Input current and voltage during whole the welding process**

Figure 4.17 shows that during short-circuit the consumed current is lower than during welding and has a better waveform that corresponds to the simulation results described in Section 4.4. Some input voltage drop during welding is caused by artificially created large-impedance network.

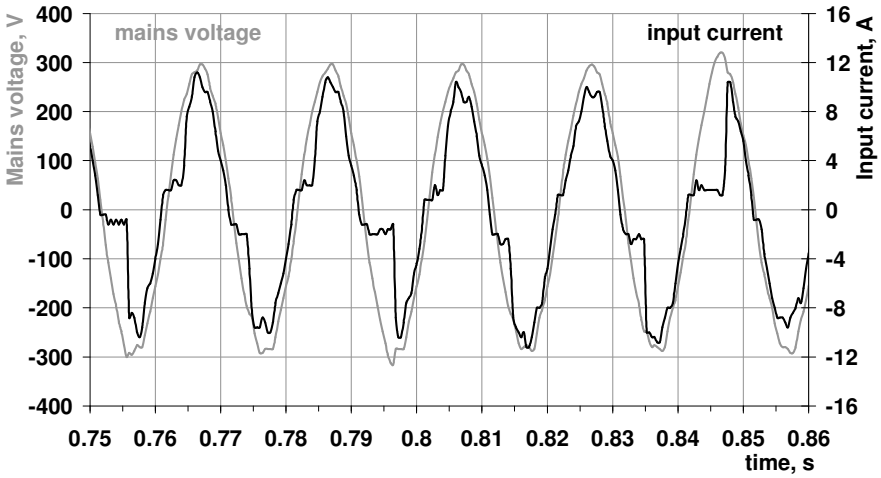


**Figure 4.18 Input current and voltage during welding**

Input current waveform varies in each half-cycle of the mains voltage during welding (Figure 4.18). However, it can be generally classified into two kinds:

1) when the output current has relatively short zero-current intervals – input current changes smoothly and its shape is less distorted (e.g. at $t$=0.81–0.82 s);
2) when the output current has relatively long zero-current intervals as at $t$=0.845 s and the output voltage has time to increase significantly – the input current changes steeply and has more distorted shape.

In conclusion, as a result of the verification, experimental results and simulation ones and showed good coincidence. Some deviations can be explained by differences between the real and computer models. Also, a computer model cannot always consider all the properties of such unstable load, like an electric arc.

## 4.6 Conclusions

In this chapter, a method for indirect power factor correction in a single-phase AC/DC converter was proposed. It comprises rectification of the alternating mains voltage into unidirectional unsmoothed half-waves, transformation of the unidirectional unsmoothed half-waves (by means of switches) into high-frequency voltage and inputting this high-frequency voltage into the power factor correcting circuit with stabilized input impedance.
Stabilization of the input impedance is achieved by keeping an inversely proportional dependence between the instantaneous value of the current supplied to the output smoothing filter and the instantaneous value of voltage on this filter. A comparison of the method with other power factor correction methods is given in Table 4.2.

**Table 4.2 Main outlines of power factor correction methods**

| *Method* | *Passive* | *Active* | *Indirect PFC by SM-PSA* |
|---|---|---|---|
| *Advantages* | Simple topology, no control circuits | Near unity power factor | Uses peculiarities of converter topology, no additional components or control |
| *Disadvantages* | Mostly for linear loads<br>Large weight and size of reactive components | Complex topology and control | Distortion of input current near mains voltage zero crossing |

Maintaining nearly inverse proportional dependence was suggested to be realized by means of the SM-PSA converter. With the proposed topology a partial stabilization of converter input impedance was achieved. This way, power factor correction was obtained.
However, exploiting the natural output characteristics of the SM-PSA converter it is possible to stabilize input impedance only in the time intervals when the instantaneous value of voltage on both secondary windings is higher than the voltage on the smoothing filter capacitor. In the range of low instantaneous

values of the mains voltage, the input impedance of the converter increases and distortion appears in the input current.

The natural characteristics of the proposed passive correction circuit (uncontrolled SM-PSA converter) are used to keep the inverse proportion between the output voltage and current. The nearly constant output power is obtained in such kind of converters. This means that if we increase the load current by decreasing the load resistance, the load voltage is decreasing inversely proportionally to the current. It may be useful in some cases, for example, supplying electric arc or charging batteries.

Although the increased pulsation of the output voltage in the case of high resistive load (small resistance) could be a drawback for some loads, the suggested converter based on the described method provides additional advantages.

Firstly, as the SM-PSA converter includes a transformer, thus, along with the power factor correction, the galvanic separation from the mains and the required voltage level are obtained. Thus, the overall simplicity of the solution is achieved.

Secondly, in the case of the output short-circuit the load current is not increasing more than 2–3 times of the rated current and currents in other circuit elements remain approximately at the level of their rated currents. This limitation of the output current during short-circuit originates from the PSA converter, which turns automatically into the parallel resonance mode. It means that short-circuit protection is not needed. Also, at the output short-circuit, the input current is reduced and less distorted as compared to the current at the nominal operation.

The third advantage for the bridge inverter topology is in the possibility to reduce switching losses by the optimal selection of resonant components in the SM-PSA converter.

The fourth advantage for the single-switch inverter topology, which was not discussed, is the fact that alternating voltage appears in transformer windings due to the resonant capacitor recharging processes. This enables one to reduce the size of the transformer.

# 5. Conclusions

In this thesis a novel switch-mode load-resonant SM-PSA converter was proposed and discussed. It was also revealed that converters of such type could be simply implemented for power factor correction in single-phase AC/DC power supplies. The main results of the research are summarized and reviewed in this part.

## 5.1 Load-resonant switch-mode SM-PSA converter

Resonant switch-mode converters are the solution for modern compact and high-density power supplies. There are three main topologies of switch-mode load-resonant converters: series, parallel and parallel-series. This thesis introduces a new topology. It is a switch-mode load-resonant converter with parametrical parallel and series resonance alternation (SM-PSA). The thesis has covered the following: guidelines of converter design with the calculation of resonant components values and selection criteria, analysis of variations in the resonant network of the SPMSA converter, and converter operational properties. The following results were achieved.

1) As it seen in Figures 3.1 (page 34) and 4.2 (page 80) the SM-PSA converter has a very simple power topology. Control circuit is not even presented as it consists only of a simple PWM block with no feedbacks or special control techniques. Thus, the proposed converter can claim for overall structural simplicity. In addition, the high-frequency transformer ensures galvanic isolation of the load from the network.
2) Analysis of the optimal resonant network topology has shown that in terms of ZCS implementation two variants are acceptable: $L_1L_2C$ and $L_1L_2L_3C$ resonant topologies having $K_Q<1$ and $L_1/(L_2+L_3)<1.2$.
3) Different resonant network topologies have slightly different output characteristics; hence, the most appropriate one should be selected according to load requirements. Thus, for example, topology $L_1L_2L_3C$ with accordingly selected resonant components has the steepest output characteristic or, in other words, the output current is not changing significantly in the range from short-circuit to nominal operation. This property could be valuable for some types of arc welding, as with smaller short-circuit current less spatter occurs [W11].
4) The proposed output regulation by changing the width of the gating pulses is very simple, however, the ZCS will not last long with such regulation and in addition there appears an “unregulated” region in short-circuit current. It could be explained by inverter output quasi-square voltage waveform, which has variable (changing with the width of the gating pulse) higher harmonic content injected into the resonant network (Figure 3.44 page 65).
5) Transient processes in the converter are fast and smooth. It takes only about two cycles of supply voltage to reach a new steady-state for currents and

voltages in the converter elements. At that, the transient process goes smoothly, without voltage spikes or current surges.

6) Voltage on the resonant capacitor is dependent on the values of additional resonant inductors $L_2$ and $L_3$. Higher additional inductances lead to higher operating voltage of the resonant capacitor that must be considered during the design and selection of reactive components.

Comparison of the properties of well-known load-resonant converters and the SM-PSA converter revealed that the SM-PSA is close to parallel-series resonant converters. However, its fundamental difference is in the ability to operate under any load condition without feedbacks or special control circuits due to parametrical output adjusting. Its main drawback is only a larger number of diodes in the output rectifier.

As the main studied load of the proposed converter was a welding arc it would be interesting to compare different "welding inverter" topologies presented below in Table 5.1.

**Table 5.1 Welding inverters with different converter topologies**

| *Type* | *Conventional hard-switched PWM converters* | *Load-resonant switch-mode converters* | *SM-PSA converter* |
|---|---|---|---|
| Output regulation | 1) PWM | 1) PWM<br>2) Frequency<br>3) Others | 1) PWM<br>2) Frequency |
| Advantages | Simple power topology | Low switching losses<br>Short-circuit protection | Simple topology and control<br>Short-circuit proof<br>No circulating current<br>No problems at no-load<br>Parametrical output adjusting to load. |
| Disadvantages | Fast feedback and control circuits<br>High switching losses | Complex control<br>Circulating current problem | Larger number of diodes in the output rectifier |

## 5.2 Power factor correction in the SM-PSA converter

The input impedance of the conventional uncorrected AC/DC power supplies varies in each mains half-cycle. Therefore, the shape of input current differs significantly from the shape of the mains voltage that results in a decreased power factor. Special switch-mode converters like boost or buck-boost converters, which shape the waveform of input current according to the control signals of feedback circuits, are the solution for the problem of poor power factor. Such converters have almost the unity power factor, but they represent usually an additional converter that requires a relatively complicated control circuit.

Another solution proposed in this thesis is a switch-mode PSA converter with an inherent PFC ability. It differs from the abovementioned in the technique of the power factor correction. Here, power factor correction is provided without control, but by keeping converter input impedance constant as much as possible. This "indirect" power factor correction is obtained due to the natural properties inherent to the SM-PSA converter. That means no control circuits are needed and single-stage power conversion is implemented by the same resonant converter since it acts as a power factor correcting device. The best characteristics regarding mains current distortion and converter efficiency are achieved if the load voltage is in the range 0.3 to 0.7 of no-load voltage. The relative drawback of the proposed method is some harmonic distortion of input current, at the average $THD_i$ is 20–30%, however, this harmonic distortion can be in the limits of IEC 60001–3–2 standard. Also, one possible disadvantage is an increased pulsation of the output voltage in the case of low-impedance output. Nevertheless, as compared to conventional AC/DC rectifier with a large smoothing capacitor, the proposed topology allows us to achieve a better power factor and lower distortion by simple techniques. In addition, the proposed converter tolerates any load changes without overloading its components.

### 5.3 Plans for future studies

Further studies concerning the development of the switch-mode PSA converter may include:

1) extending of the ZCS range during output regulation,
2) study on ZVS possibilities,
3) study of other output regulation techniques in SM-PSA,
4) study of output rectifier operation and losses evaluation,
5) comparison of different inverter topologies,
6) development of a planar LCT structure for SM-PSA,
7) improvement of the output current waveform during welding with PFC SM-PSA.

# References

*Power converters*


[H1] **N. Mohan, T. Undeland, W. Robbins.** Power electronics. New York: Wiley. 1995.

[H2] **Б. Ю. Семенов.** Силовая электроника для любителей и профессионалов. Москва: СОЛОН-Р. 2001 (in Russian).

[H3] **Bob Erickson.** Course of lectures: Resonant and Soft-Switching Techniques in Power Electronics ECEN 5817. University of Colorado. USA. 2006. http://ece.colorado.edu/~ecen5817.

[H4] **K. Rajashekara, A. K. Bhat, B. K. Bose.** Power Electronics: The Electrical Engineering Handbook. CRC Press LLC. 2000.

[H5] **J. L. Cour, O. S. Bragtad.** Die Wechselstromtechnik. Berlin: Springer (in German). 1910.

[H6] Switch Mode Power Supply Reference Manual. ON Semiconductor. 2002.

[H7] **L. Wuidart.** Application Note: Topologies for switched mode power supplies. STMicreoelectronics. 1999.

[H8] **Zacharias K. Vachaparambil.** Thesis: Basic Resonant Topologies for switching power supplies. USA: Purdue University School of Electrical Engineering. 1994.

[H9] **Ji Xie.** Thesis: Modeling, Analysis and Design of Fixed Frequency Series-Parallel Resonant DC/DC Converters Using the Extended Describing Function method. Canada; Memorial University of Newfoundland, 1999.

[H10] **Robert L. Steigerwald.** Power Electronic Converter Topology. Proceedings of the IEEE, Vol. 89, No. 6, June 2001.


*PSA Converter*


[PSA1] **Kuno Janson.** Thesis*:* Paralleel- ja järjestikresonantsi parameetrilise vaheldumisega võrgusageduslik resonantsmuundur ja selle rakendamine. Tallinn: TTÜ, (in Estonian). 2001.

[PSA2] **K. Janson** and **J. Järvik.** AC-DC converter with parametric reactive power compensation. IEEE Trans. Ind. Electron., June 1999. Vol. 46, pp. 554-562.

[PSA3] **K. Janson** and **J. Järvik.** Controlled Power Supply. Patent of Europe no. 0575589. 20.10.1998.

[PSA4] **K. Janson** and **J. Järvik.** Controlled Power Supply, United States Patent nr. 5375053/20.12.1994.

[PSA5] **K. Janson, J. Järvik** and **T. Vinnal.** Circuit diagrams of DC-DC line-frequency resonant converters with alternation of parallel and series resonant mode. Proceedings of the 5th International Conference on

Electrical Power Quality and Utilization, 15-17 September 1999. Krakow, Poland. pp. 479–485.

[PSA6] **K. Janson, J. Järvik** and **T. Vinnal.** Commutation Processes in Diode Bridge of Resonant Converter with Alternating Parallel and Series Resonance. Proceedings of the Baltic Electronics Conference, BEC 2000, 8–11 October, 2000. Tallinn, pp. 205–209.

[PSA7] **Jevgeni Shklovski.** Master's thesis: PSA converter and its application for arc welding. Tallinn: Tallinn University of Technology (in Russian). 2002. 90 p.

[PSA8] **K. Janson, J. Järvik and J. Shklovski.** LC Circuit with Alternating Parallel and Series Resonance in Switch-mode Converters. Proceedings of the 3rd International Conference Electric Power Quality and Supply Reliability. Tallinn, Estonia, 2002.

[PSA9] **K. Janson** and **J. Järvik.** Load adapting mains frequency resonant converters for supplying electrical arc – a new way in power electronics. 29th Annual IEEE Power Electronics Specialists Conference Records. PESC 98, Volume 2, 17-22 May 1998, pp. 2090–2096. IEEE Xplore nr. 703468, 1998.

[PSA10] **K. Janson, J. Järvik** and **E. Sepping**. DC current source mode in converter with alternating of parallel and series resonance. Proceedings of the EPE 2003. ISBN: 90–75815–07–7, Toulouse, France. 2003.

*Resonant converters and soft-switching*

[RC1] **TingTing Song and Nianci Huang.** A Novel Zero-Voltage and Zero-Current-Switching Full/Bridge PWM Converter. IEEE Transactions on Power Electronics, March 2005, Vol. 20, No. 2, pp. 286–291.

[RC2] **Yilei Gu, Zhengyu Lu, Lijun Hang, Zhaomong Qian, Guisong Haung.** Three-Level LLC Series Resonant DC/DC converter. IEEE Transactions on Power Electronics, July 2005, Vol. 20, No. 4, pp. 781–789.

[RC3] **Yungtaek Jang, Milan M. Jovanović.** A new family of Full-Bridge ZVS Converters. IEEE Transactions on Power Electronics, May 2004, Vol. 19, No. 3, pp. 701–708.

[RC4] **Robert L. Steigerwald, Rik W. De Doncker, M. H. Kheraluwala.** A Comparison of High-Power DC-DC Soft-Switched Converter Topologies. IEEE Transactions on Industry Applications, Vol. 32, No. 5, September/October 1996, pp. 1139–1145.

[RC5] **Keiki Morimoto, Toshimitsu Doi, Haruhiko Manabe, Nabil A. Ahmed, Hyun-Woo Lee, Mutsuo Nakaoka.** Advanced High Frequency Transformer Linked Soft Switching PWM DC-DC Power Converter with Utility AC Dual Voltage Modes for Low Voltage and Large Current Applications. EPE 2005 Dresden, ISBN: 90–75815–08–5. 2005.

[RC6] **Michael J. Schutten, Robert L. Steigerwald, Mustansir H. Kheral uwala.** Characteristics of load resonant converters operated in a high power factor mode. IEEE Transactions on Power Electronics, April 1992, Vol. 7, No. 2, pp. 304–314.

[RC7] **Pankaj Jain.** M.Eng thesis: Fixed Frequency Series-Parallel DC/DC Resonant Converters. Menzorial University of Newfoundland. 1993.

[RC8] **Ashoka K. S. Bhat**. Fixed Frequency PWM Series-Parallel Resonant Converter. IEEE Transactions on Industry Application, September/October 1992, Volume 28, No 5, pp. 1002–1009.

[RC9] **Richard Farrington, Milan M. Jovanovic, Fred C. Lee.** Analysis of Reactive Power in Resonant Converters. 23th Annual IEEE Power Electronics Specialists Conference Records. PESC 92, Volume 1, 29 June–3 July 1992, pp. 197–205.

[RC10] **M. Marx, D. Schroder.** A Novel Zero-Current-Transition Full-Bridge DC-DC Converter. 27th Annual IEEE Power Electronics Specialists Conference Records. PESC 96, Volume 1, 23-27 June 1996, pp. 664–669.

[RC11] **Mizhi Zhang, T. A. Little.** Evaluation of basic resonant structures and voltage clamping techniques. IEEE 2006, 1–42–44–0136–4/06.

[RC12] **H. Pollock, J. O. Flower.** Design, simulation and testing of a series resonant converter for pulsed applications. IEE 5th International Conference on Power Electronics and Variable Speed Drives. London, October 1994, pp. 256–261.

[RC13] **H. Pollock, J. O. Flower.** Properties and design of series-parallel load-resonant converters: their potential in marine and marine-related applications. Trans IMarE, Vol. 110, Part 2, November 1997, pp. 95–118.

*Power factor correction*

[PF1] **S. Singer.** Power conversion and control with zero AC current harmonics by means of a time-variable transformer. IEEE Proceedings, Vol. 131, Pt. G, No. 4, Aug. 1984, pp. 147–150.

[PF2] **Etsunao Ohtsuji, Osamu Miyashita, Akeshi Maeda.** A high power factor PWM rectifier without voltage sensors. Electrical Engineering in Japan, Vol. 120, No. 4, 1997, pp 90–96.

[PF3] **S. Chattopadhyay, V. Ramanarayanan.** A Single-Reset-Integrator-Based Implementation of Line-Current-Shaping Controller for High-Power-Factor Operation of Flyback Rectifier. IEEE Transactions on Power Electronics, March/Aprill 2002, Vol. 38, No. 2, pp. 490–499.

[PF4] **Takahiro Sonoda, Tamotsu Ninomiya, Satosshi Tamioka, Kei Sato** and **Hiroto Terashi.** A Novel Boost-Input Full-Bridge Converter. Journal of Power Electronics: A Publication of the Korean Institute of power electronics, July 2005, Vol. 5, No. 3, ISSN: 1598–2092, pp. 212–217.

[PF5] **N. K. Poon, Bryan M.H. Pong, Chi K. Tse.** A Constant-Power Battery Charger with Inherent Soft-Switching and Power Factor Correction. IEEE Transactions on Power Electronics, November 2003, Vol. 18, No. 6, pp. 1262–1269.

[PF6] **Sam Ben-Yaakov, Ilya Zeltser.** PWM Converters with Resistive Input. IEEE Transactions on Industrial Electronics, June 1998, Vol. 45, pp. 519–520.

[PF7] **Jung-Bum Kin, Nam-Ju Park, Dong-Yun Lee and Dong-Seok Hyun.** A Control Technique for 120 Hz DC Output Ripple-Voltage Suppression Using BiFRED with a Small-Sized Energy Storage Capacitor. Journal of Power Electronics: A Publication of the Korean Institute of power electronics, July 2005, Vol. 5, No. 3, ISSN: 1598–2092, pp. 190–197.

[PF8] **Jia Wu, Fred C. Lee, Dushan Boroyevich, Heping Dai, Kun Xing and Dengming Ping.** A 100 kW High-Performance PWM Rectifier with a ZCT Soft-Switching Technique. IEEE Transactions on Power Electronics, November 2003, Vol. 18, No. 6, pp. 1302–1307.

[PF9] **Arturo Fernandez, Javier Sebastian, Pedro Alou, Jose A. Cobos, Miguel Rascon.** Low Output Voltage AC/DC Converter with a New Scheme of Synchronous Rectification That Complies With IEC 1000–3–2 Regulations. IEEE Transactions on Power Electronics, July 2003, Vol. 18, No. 4, pp. 966–974.

[PF10] **Shin-Ichi Motegi, Akeshi Maeda, Yasuyuki Nishida.** A New Single-Phase High-Power-Factor Converter with Buck and Buck-Boost Hybrid Operation. Electrical Engineering in Japan, Vol.131, No. 3, 2000, pp 91–100.

[PF11] **H. Pollock, J. O. Flower.** New Method of Power Control for Series-Parallel Load-Resonant Converters Maintaining Zero-Current Switching and Unity Power Factor Operation. IEEE Transactions on Power Electronics, January 1997, Vol. 12, No. 1, pp. 103–115.

[PF12] **Y.-M. Chae, J.-S. Gho, G.-H. Choe, W.-S. Shin, J.-Y. Choi.** PWM Converter-Inverter Arc Welding Machine Using New Type N.C.T. Annual IEEE Power Electronics Specialists Conference Records. PESC 98, Volume 2, 17–22 May 1998, pp. 1636–1641.

[PF13] **Mustansir H. Kheraluwala, Robert L. Steigerwald, Ramachandran Gurumoorthy.** A Fast-Response High Power Factor Converter with a Single Power Stage. 22nd Annual IEEE Power Electronics Specialists Conference Records. PESC 91, Volume 2, 24–27 June 1991, pp. 769–779.

**High-frequency power transformers, inductors and capacitors**

[HT1] **Alex Van den Bossche, Vencislav Cekov Valchev.** Inductors and Transformers for Power Electronics. Taylor & Francis. 2005.

[HT2] **Johan Tjeerd Strydom.** Thesis: Electromagnetic Design of Integrated Resonator-Transformers. Rand Afrikaans University. 2001

[HT3] **Ray Ridley.** Proximity Loss in Magnetics Windings. Designers Series XIII. Switching Power Magazine, 2005.

[HT4] **Reuben Lee, Leo Wilson, Charles E. Carter.** Electronic Transformers and Circuits. Third Edition, Wiley, 1988.

[HT5] **П. Л. Калантаров, Л. А. Цейтлин.** Расчет индуктивностей. Энерго-атомиздат. 1986 (in Russian).

[HT6] **С. С. Вдовин.** Проектирование импульсных трансформаторов, Ленинград: Энергия. 1971 (in Russian).

[HT7] **Ю. С. Русин.** Трансформаторы звуковой и ультразвуковой частоты. Москва: Энергия.1973 (in Russian).

[HT8] **Colonel Wm. T. McLyman.** Transformer and Inductor Design Handbook. Third Edition. Kg Magnetics, Inc. Idyllwild, California, U.S.A. ISBN: 0–8247–5393–3. Marcel Dekker Inc. USA. 2004.

[HT9] Measurement procedures for inductive components. http://www.vacuumschmelze.de. 2006.

[HT10] Catalogue „Film and Paper-Film capacitors" by ЭЛКОД, 2006; available: http://www.elcod.spb.ru/catalogue.pdf (in Russian).

[HT11] Data sheet on polypropylene capacitors for pulse applications: http://www.wima.de/DE/WIMA_FKP_4.pdf

[HT12] **Lloyd H. Dixon, Jr.** Eddy current losses in transformer windings and circuit wiring. Texas Instruments Incorporated. 2003.

[HT13] **M. Stadler, S. Albach.** The Optimization of High Frequency Operated Transformers for Resonant Converters. Proceedings of EPE 2005, Dresden. ISBN: 90–7815–08–5.

[HT14] **Mikka Sippola, Raimo E. Sepponen.** Accurate Prediction of High-Frequency Power-Transformer Losses and Temperature Rise. IEEE Transactions on Power Electronics, September 2005, Vol. 17, No. 5, pp. 835–847.

*Planar structure components*

[L1] **Yves Lembeye, Philippe Goubier, and Jean-Paul Ferrieux.** Integrated Planar L-C-T Component: Design, Characterization and Experimental Efficiency Analysis. IEEE Transactions on Power Electronics, May 2005, Vol. 20, No. 3, pp. 593–599.

[L2] **Johan Tjeerd Strydom, Jacobus Daniel van Wyk.** Electromagnetic modeling for Design and Loss Estimation of Resonant Integrated Spiral Planar Power Passives ($ISP^3$). IEEE Transactions on Power Electronics, May 2004, Vol. 19, No. 3, pp. 603–617.

[L3] **Sriram Ramakrishanan, Robert L. Steigerwald, John A. Mallick.** A Comparison Study of Low-profile Power Magnetics for High-frequency, High-density Switching Converters. Proceedings of 12th

Annual Applied Power Electronics Conference APEC '97, 1997. Vol. 1, 23–27 February 1997 pp. 388–394.

**Welding**

[W1] **Lauri Kärävä.** Inverter technology in welding power sources. Svetsen —Magazine of the Swedish Welding Commission. Special Issue. June 1995, pp. 59–64.

[W2] Справочник по сварке. Том 1. Ленинград. 1960. 556 p. (in Russian).

[W3] **Andres Laansoo.** Keevitustehnika: I osa, Keevitusinverterid. Materjalitehnika-instituut. Tallinna Tehnikaülikool, 1996. 24 p.

[W4] TransPocket 1500 Manual. Fronius. 2005 or available on: http://www.fronius.com/cps/rde/xchg/SID-0AFF0106-7B4AFCC7/fronius_international/hs.xsl/79_5502_ENG_HTML.htm. 2006.

[W5] Invertec V145-S Technical Specification. Lincoln. 2006. Available on: http://content.lincolnelectric.com/en/pdfs/products/literature/V145-Sen.pdf,

[W6] Minarc 150 Technical Specification. Kemppi. 2006. Available on: http://www.kemppi.com/internet/kit.nsf/0/903841007eca7315c2256eb5002e109a/$FILE/Minarc_EN_net.pdf

[W7] Genesis 1500 Technical Specification. Selco. 2006 Available on: http://www.selco.it/index.php?ct=1&sct=3&lang=en&pid=2

[W8] Inverter-based welding power sources help solve maintenance problems, decrease downtime. Available on: http://www.millerwelds.com/education/articles/articles72.html, 2006, by Miller Electric Mfg Co.

[W9] **Jaroslav Dudrik.** Soft-switching PS-PWM DC-DC Converter for Arc Welding. Acta Elektrotechnica et Infoermatica No. 3, Vol. 06, 2006. Technical University of Kosice, Slovak Republic. ISSN 1335–8243. pp. 40–43

[W10] **И. В. Пентегов, С. Н. Мещеряк, М. В. Турты, С. В. Рымар.** Методика расчета дросселей входного и выходного фильтров сварочных инверторных источников питания при использовании стандартных магнитопроводов. Автоматическая сварка. 1997, No. 4 (529), pp. 34–39. (in Russian).

[W11] **H. Pollock, J. O. Flower.** Series-parallel load-resonant converter for controlled-current arc welding power supply. IEE Proceedings online no. 19960257, 1996.

**Patents and intellectual property**

[PT1] **Hubert Aigner / Fronius.** Method for regulating and/or controlling a welding current source with a resonance circuit. Pub. No.: US 6,849,828 B2, Feb 1, 2005.

[PT2] **K. Janson, J. Järvik** and **J. Shklovski / Tallinn University of Technology.** Power Factor Correction Method for AC/DC Converters and Corresponding Converter. Pub. No. WO2006063598 A1, Jun. 22, 2006.

[PT3] **Corticelli Giuliano / Selco SRL** Resonant-load power supply for arc welding.
Patent No. EP0602495. Jun. 22, 1994.

[PT4] **G. Brandli, and M. Dick.** Alternating current FED power supply. U.S. Patent No. 4 084 217, Nov. 04, 1978.

[PT5] **В.И. Серебров.** Двухполупериодный выпрямитель. Авторское св идетельство, СССР 120853, 1959, Б.И. № 13 (in Russian).

[PT6] **Mela Franco, Rossetto Gianni, Taccon Daniele / Selco SRL.** Generator for arc welder with high power factor. DE602004002391D, Oct. 26, 2006.

[PT7] **Mela Franco / Selco SRL.** Generator for unitary power factor arc welders. Patent No. US 7,141,759 B2, Nov. 28, 2006.

**Additional bibliography**

[AD1] **Lazar Rozenblat's** Webpage: SMPS Switching Power Supply Design, available on: http://www.smps.us/, 2006.

# Abstract

The study presented in this thesis describes a novel type of single-phase switch-mode AC/DC load-resonant converters having parametrically (without control action) changing parallel and series resonant LC networks. The converter operation under different load conditions both with help of computer simulation and by experimental verification is discussed. The main practical output of the study is the description of peculiar features inherent to the proposed topology for supplying steeply and deeply varying loads like electric arc.

The study could be divided into two main parts: first, description and analysis of the novel topology of the switch-mode resonant converter during operation from DC voltage source; second, the discussion of the ability of the proposed topology to improve the shape of AC input current without auxiliary power or control circuits. Thus, in addition to a new load-resonant switch-mode converter topology the method for power factor correction inherent to this topology was proposed and discussed.

Different variations in the resonant network topology of the proposed converter were also studied and analyzed to reduce switching losses, especially turn-off losses. Along with that, a calculation procedure and criteria for practical selection of resonant components of the converter were developed.

It is shown that the proposed switch-mode converter topology with parallel and series resonance alternation could be simultaneously applied both for output current limiting and for input current correction while both of the mentioned properties could be obtained parametrically, i.e. without control. Some results of the given research were reported at international conferences and published in refereed databases.

# Kokkuvõte

Käesolevas doktoritöös uuritakse lülitussageduslikke vahelduvvoolu-alalisvoolu resonantsmuundureid, kus järjestikune ja paralleelne LC ahel pidevalt vahelduvad ilma välise juhtimiseta . Uuritakse muunduri talitlust erinevatel koormustel nii arvutimudeli kui praktiliste katsete abil. Uurimise praktilise väljundina nähakse uudse skeemilahenduse eriliste omaduste ärakasutamist järsult ja sügavalt muutlike koormuste toitmisel nagu seda on elektrikaar.

Töö sisu võib jagada kaheks osaks. Esimeses osas kirjeldatakse ja analüüsitakse lülitussagedusliku resonantsmuunduri uue skeemi talitlust alalispingetoitel. Teises osas on uuritud muunduri võimet parandada tarbitava võrguvoolu kuju ilma täiendavate jõu- või juhtimisahelata. Sellega on lisaks uuele resonantsmuunduri skeemile pakutud ning kirjeldatud selle muundurile omase võimsusteguri parenemine

Samuti on uuritud ja analüüsitud selle muunduri erinevad skeemivariante eesmärgiga vähendada lülituskadusid, eriti pooljuhtide väljalülitamisel. Ühtlasi on väljaarendatud ka muunduri resonantselementide arvutusmeetod ja nende elementide valimise kriteeriumid.

Töös on näidatud, et paralleel- ja järjestikresonantsi vaheldumisega muundusskeemi mis töötab lülitussagedusel, saab üheaegselt kasutada nii muunduri väljundvoolu piiramiseks, kui ka võrguvoolu kõvera korrektsiooniks, kusjuures mõlemad efektid saadakse ilma juhttoimeta. Uurimise mõned tulemused on esitatud rahvusvahelistel konverentsidel ja refereeritud andmebaasides.

## List of Publications


1. **Kuno Janson, Jaan Järvik, Heljut Kalda, Jevgeni Shklovski.** Study of Failures with 10 kV and 35 kV Voltage Transformers. In: Proc. of the 3rd International Conference "Electric Power Quality and Supply Reliability", Tallinn, Estonia, 2002. pp. 133–138.
2. **Kuno Janson, Jaan Järvik, Jevgeni Shklovski.** LC Circuit with Alternating Parallel and Series Resonance in Switch-mode Converters. In: Proc. of the 3rd International Conference "Electric Power Quality and Supply Reliability", Tallinn, Estonia, 2002. pp. 91–94.
3. **Kuno Janson, Jaan Järvik, Heljut Kalda, Jevgeni Shklovski, Evald Külm**. Study of transformer overvoltages under single-phase earth faults in 6...35 kV networks with insulated neutral point. In: Proc. of the 5th International Scientific Conference "Electric Power Engineering 2003", Visalaje, Czech Republic, CD-ROM. 2003.
4. **Kuno Janson, Jaan Järvik, Evald Külm, Jevgeni Shklovski, Lauri Kütt.** Study of the Effects of Single Phase Ground Faults to the Voltage Transformers in the 10 kV medium Voltage Power Networks. In: Proc. of the 48. Internationales Wissenschaftliches Kolloquium, Technische Universität Ilmenau, Germany, 2003. pp. 583–584
5. **Kuno Janson, Jaan Järvik, Jevgeni Shklovski, Toomas Vinnal.**. Operation of PSA Converter in Inverter Mode. In: Proc. of the 4th International Conference "Electric Power Quality and Supply Reliability, Pedase, Estonia, Tallinn University of Technology. 2004. pp. 81–86.
6. **Kuno Janson, Jaan Järvik, Jevgeni Shklovski, Toomas Vinnal.** Inverter Mode in Converter with Alternating Parallel and Series Resonance. In: Proceedings of the 11th International Conference on Power Electronics and Motion Control (EPE-PEMC 2004): Riga, Latvia, 2004. Riga Technical University, CD-ROM, A2216. ISBN 9984–32–070–7.
7. **Kuno Janson, Jaan Järvik, Jevgeni Shklovski.** Uninterruptible power supply based on the converter with alternating of parallel and series resonance. In: Proc. of the 4th International Workshop CPE 2005. Gdynia. Poland. ISBN 83–7421–075–3. pp. 44–46.
8. **Kuno Janson, Jaan Järvik, Jevgeni Shklovski.** Method for line current shape forming in ac-dc switch mode power supplies. In: Proc. of the 5th International Conference "Electric Power Quality and Supply Reliability". Viimsi, Estonia, 2006. ISBN: 9985–59–647–1, Tallinn University of Technology, 2006, pp. 27–34.
9. **Kuno Janson, Jaan Järvik, Jevgeni Shklovski.** Novel Power Factor Correction Method and Topology for AC/DC Converters. In: Proceedings of 51st International Scientific Colloquium of Technical University Ilmenau. Sept. 11-15, 2006, ISBN 3–938843–15–2, (CD-ROM) or pp. 349–351.

10. **Jevgeni Shklovski, Kuno Janson, Jaan Järvik.** Indirect Power Factor Correction Method and Corresponding Sensorless Switch-Mode Resonant AC/DC Converter. In: Proc. of the 32nd Annual Conference of the IEEE Industrial Electronics Society IECON 2006, Paris, ISBN: 1–4244–0136–4 2006. IEEE Catalog Number: 06CH37763C.

## Intellectual property

1) Patent "Vahelduvvoolu-alalisvoolu muundurite võimsusteguri korrektsiooni meetod ja muundur meetodi realiseerimiseks"; Estonian Patent Office; Priority date: 14 December 2004; Application nr EE200400124; Application published 15 August 2006; Applicant: Tallinn University of Technology; Authors: K. Janson, J. Järvik, J. Shklovski. Decision on patent issue: 22 December 2006, will be published on the 15 February 2007 in EE Patendileht nr 1/2007.
2) International Patent Application "Power factor correction method for ac/dc converters and corresponding converter". International Application Number: PCT/EE2005/000010, International Publication Number: WO2006/063598 A1, Publication Date 22 June 2006. Applicant: Tallinn University of Technology. Authors: K. Janson, J. Järvik, J. Shklovski. Priority date: 14 December 2004.

**Appendix 1**

**ELULOOKIRJELDUS**

**1. Isikuandmed**

Ees- ja perekonnanimi: Jevgeni Šklovski
Sünniaeg ja -koht: 14.03.1978, Tallinn
Kodakondsus: Eesti
Perekonnaseis: abielus
Lapsed:

**2. Kontaktandmed**

Aadress: Padrkiu tee 1/1–7, 11912, Tallinn
Telefon: (+372) 5276017
E-posti aadress: jevgeni@staff.ttu.ee

**3. Hariduskäik**

| Õppeasutus (nimetus lõpetamise ajal) | Lõpetamise aeg | Haridus (eriala/kraad) |
|---|---|---|
| Tallinna Tehnikaülikool | 2002 | tehnikateaduste magister, elektrotehnika alused ja elektrimasinad |
| Tallinna Tehnikaülikool | 2000 | bakalaureuse kraad, elektriajamid ja jõuelektroonika |
| Tallinna 11. Keskkool | 1996 | keskharidus |

**4. Keelteoskus (alg-, kesk- või kõrgtase)**

| Keel | Tase |
|---|---|
| Vene | Kõrgtase |
| Eesti | Kõrgtase |
| Inglise | Kesktase |
| Saksa | Algtase |

**5. Teenistuskäik**

| Töötamise aeg | Ülikooli, teadusasutuse või muu organisatsiooni nimetus | Ametikoht |
|---|---|---|
| 2000– | Tallinna Tehnikaülikool | Teadur |
| 10–12.2000 | Brandneri Elektroonika AS | Insener |

**6. Täiendõpe**

| Õppimise aeg | Õppeasutuse või muu organisatsiooni nimetus |
|---|---|
| 2005 | TTÜ sisekoolituskursus teemal *"Projektijuhtimine"* |
| 2005 | TTÜ sisekoolituskursus teemal *"Intellektuaalomand teaduses"* |
| 2005 | TTÜ sisekoolituskursus teemal *"Patendiotsing internetis"* |
| 2005 | TTÜ sisekoolituskursus teemal *"Intellektuaalomandi kommertsialiseerimine"* |
| 2001 | HUT kursus teemal *"Innovative design and optimization of electrical machine"* |

**7. Teadustegevus**

| | |
|---|---|
| 2003–2007 | T511 "Muundurite mitteaktiivvõimsuse minimeerimine muutuvate pingenivoode vahelise virtuaaltrafo, kaovaba resistori või kaovaba güraatori realisatsiooni abil" (HM sihtfinantseerimine) |
| 2002–2005 | G5144 "Paralleel- ja järjestikresonantsi vaheldumisega muunduri uurimine aktiiv- ja reaktiivvõimsuse reguleerimise 4-kvadrandilises talitluses" (ETF uurimistoetus) |
| 2004–2006 | G5904 "Parendatud energiakvaliteedi ning kasuteguriga võimsuselektronmuundurite süntees harmoonilistevahelise energiavahetuse optimeerimise ja mitmefunktsionaalsete korrektsioonielementide kasutamisega" (ETF uurimistoetus) |
| 2003–2005 | 380L "Püsimagnetitega sünkroongeneraatorite väljatöötamine" (siseriiklik leping) |

**8. Kaitstud lõputööd**

- "Türistorsagedusmuunduri ETVA modelleerimine" (bakalaureusetöö, 2000)
- "Kõrgsageduslik paralleel- ja järjestikresonantsi vaheldumisega muundur ja selle rakendamine kaarkeevituses" (magistritöö, 2002)

**9. Teadustöö põhisuunad**

- Resonantsmuunduritel põhinevad AC/DC toiteallikad, elektrienergia kvaliteet ja elektromagnetiline ühilduvus

**10. Teised uurimisprojektid**

- Punktkeevituse toiteallika võimsusteguri parendamine.

Kuupäev: 26.11.2006

**CURRICULUM VITAE**

**1. Personal information**

Name: Jevgeni Shklovski
Date and place of birth: 14.03.1978, Tallinn
Citizenship: Estonian
Martial status: married
Children:

**2. Contact information**

Address: Padrkiu tee 1/1–7, 11912, Tallinn
Telephone: (+372) 5276017
E-mail: jevgeni@staff.ttu.ee

**3. Educational history**

| Institution | Graduation date | Education |
|---|---|---|
| Tallinn University of Technology | 2002 | M.Sc., Electrical engineering and electrical machines |
| Tallinn University of Technology | 2000 | B.Sc., Electrical drives and power electronics |
| Tallinn Secondary School No. 11. | 1996 | secondary |

**4. Languages**

| Language | Level |
|---|---|
| Russian | Excellent |
| Estonian | Excellent |
| English | Good |
| German | Beginner |

**5. Professional employment**

| Date | Organization | Position |
|---|---|---|
| 2000– | Tallinn University of Technology | Researcher |
| 10–12.2000 | Brandneri Elektroonika AS | Engineer |

**6. Special courses**

| Date | Organization |
|---|---|
| 2005 | "*Project Management*", Tallinn University of Technology |
| 2005 | "*Intellectual property in since*", Tallinn University of Technology |
| 2005 | "*Patent search in internet*", Tallinn University of Technology |
| 2005 | "*Commercialization of intellectual property*", Tallinn University of Technology |
| 2001 | *"Innovative design and optimization of electrical machine"* Helsinki University of Technology |

**7. Scientific work**

| | |
|---|---|
| 2003–2007 | T511 "Minimization of the non-active power in converters using a virtual time-variable matching transformer, loss free resistor or loss free gyrator" |
| 2002–2005 | G5144 "Research of 4-quadrant active and reactive power regulation for converter with parallel and series resonance alternation" |
| 2004–2006 | G5904 "Synthesis of the power electronic converters with improved power quality and efficiency applying optimum interharmonic energy exchange and multifunctional correction elements" |
| 2003–2005 | 380L "Design of PM synchronous generator" |

**8. Theses**

- "Modeling of thyristor frequency converter ETVA" (B.Sc., 2000)
- "High-frequency PSA converter and its application in welding" (M.Sc., 2002)

**9. Main areas of scientific work**

- AC/DC power supplies based on resonant converters, electric power quality and electromagnetic compatibility

**10. Other research projects**

- Development of power factor correction system for spot welder

Date: 26.11.2006.

# Appendix 2

## Schematic diagram of the SM-PSA prototype converter

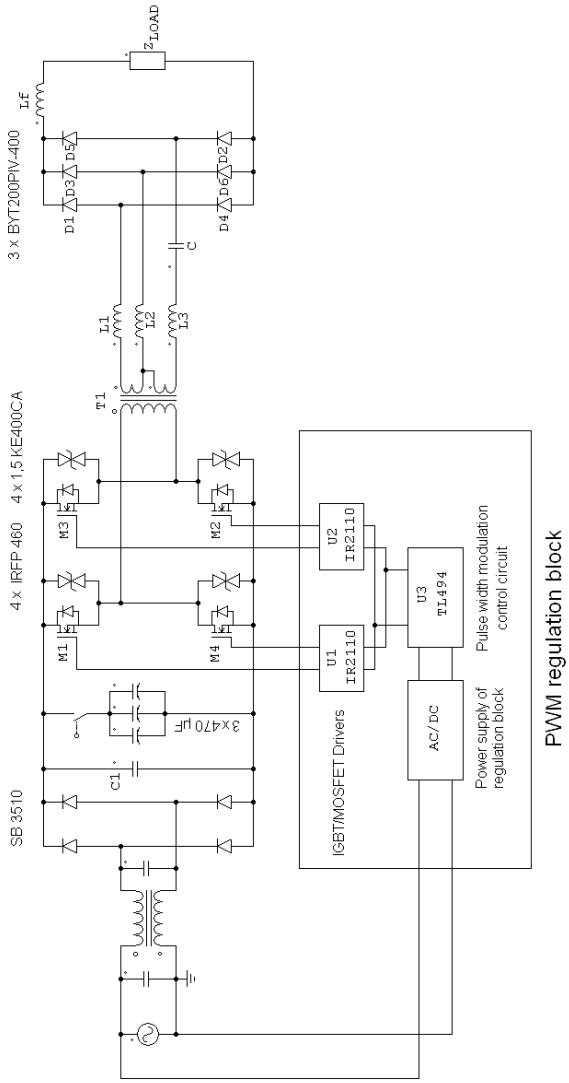


**Figure A 2.1** Schematic of studied SM-PSA prototype converter
(regulation circuit is depicted by its main blocks)

# DISSERTATIONS DEFENDED AT TALLINN UNIVERSITY OF TECHNOLOGY ON *POWER ENGINEERING, ELECTRICAL ENGINEERING, MINING ENGINEERING*

1. **Jaan Tehver**. Boiling on porous surface. 1992.

3. **Endel Risthein.** Electricity supply of industrial plants. 1993.

4. **Tõnu Trump**. Some new aspects of digital filtering. 1993.

5. **Vello Sarv.** Synthesis and design of power converters with reduced distortions using optimal energy exchange control. 1994.

6. **Ivan Klevtsov**. Strained condition diagnosis and fatigue life prediction for metals under cyclic temperature oscillations. 1994.

7. **Ants Meister**. Some phase-sensitive and spectral methods in biomedical engineering. 1994.

8. **Mati Meldorf**. Steady-state monitoring of power system. 1995.

9. **Jüri-Rivaldo Pastarus**. Large cavern stability in the Maardu granite deposit. 1996.

10. **Enn Velmre**. Modeling and simulation of bipolar semiconductor devices. 1996.

11. **Kalju Meigas**. Coherent photodetection with a laser. 1997.

12. **Andres Udal**. Development of numerical semiconductor device models and their application in device theory and design. 1998.

13. **Kuno Janson**. Paralleel- ja järjestikresonantsi parameetrilise vaheldumisega võrgusageduslik resonantsmuundur ja tema rakendamine. 2001.

14. **Jüri Joller**. Research and development of energy saving traction drives for trams. 2001.

15. **Ingo Valgma**. Geographical information system for oil shale mining – MGIS. 2002.

16. **Raik Jansikene**. Research, design and application of magnetohydrodynamical (MHD) devices for automation of casting industry. 2003.

17. **Oleg Nikitin**. Optimization of the room-and-pillar mining technology for oil-shale mines. 2003.

18. **Viktor Bolgov**. Load current stabilization and suppression of flicker in AC arc furnace power supply by series-connected saturable reactor. 2004.

19. **Raine Pajo**. Power system stability monitoring – an approach of electrical load modelling. 2004.

20. **Jelena Shuvalova**. Optimal approximation of input-output characteristics of power units and plants. 2004.

21. **Nikolai Dorovatovski**. Thermographic diagnostics of electrical equipment of Eesti Energia Ltd. 2004.

22. **Katrin Erg**. Groundwater sulphate content changes in Estonian underground oil shale mines. 2005.

23. **Argo Rosin**. Control, supervision and operation diagnostics of light rail electric transport. 2005.

24. **Dmitri Vinnikov**. Research, design and implementation of auxiliary power supplies for the light rail vehicles. 2005.

25. **Madis Lehtla**. Microprocessor control systems of light rail vehicle traction drives. 2006.